COOPERATIVE DISTRIBUTED TRANSMISSION AND RECEPTION

by

Min Ni

A Dissertation

Submitted to the Faculty

of the

WORCESTER POLYTECHNIC INSTITUTE

in partial fulfillment of the requirements for the

Degree of Doctor of Philosophy

in

Electrical and Computer Engineering

by

July 2013

APPROVED:

Professor D. Richard Brown III, WPI, Major Advisor

Professor Andrew G. Klein, WPI

Professor Raghuraman Mudumbai, University of Iowa

To my family.

COOPERATIVE DISTRIBUTED

TRANSMISSION AND RECEPTION

Min Ni, Ph.D.

Worcester Polytechnic Institute 2013

In telecommunications, a cooperative scheme refers to a method where two or more users share or combine their information in order to increase diversity gain or power gain. In contrast to conventional point-to-point communications, cooperative communications allow different users in a wireless network to share resources so that instead of maximizing the performance of its own link, each user collaborates with its neighbours to achieve an overall improvement in performance. In this dissertation, we consider different models for transmission and reception and explore cooperative techniques that increase the reliability and capacity gains in wireless networks, with consideration to practical issues such as channel estimation errors and backhaul constraints.

This dissertation considers the design and performance of cooperative communication techniques. Particularly, the first part of this dissertation focuses on the performance comparison between interference alignment and opportunistic transmission for a 3-user single-input single-output (SISO) interference channel in terms of average sum rate in the presence of channel estimation errors. In the case of interference alignment, channel estimation errors cause interference leakage which consequently results in a loss of achievable rate. In the case of opportunistic transmission, channel estimation errors result in a non-zero probability of incor-

rectly choosing the node with the best channel. The effect of these impairments is quantified in terms of the achievable average sum rate of these transmission techniques. Analysis and numerical examples show that SISO interference alignment can achieve better average sum rate with good channel estimates and at high SNR whereas opportunistic transmission provides better performance at low SNR and/or when the channel estimates are poor.

We next considers the problem of jointly decoding binary phase shift keyed (BPSK) messages from a single distant transmitter to a cooperative receive cluster connected by a local area network (LAN). An approximate distributed receive beamforming algorithm is proposed based on the exchange of coarsely-quantized observations among some or all of the nodes in the receive cluster. By taking into account the differences in channel quality across the receive cluster, the quantized information from other nodes in the receive cluster can be appropriately combined with locally unquantized information to form an approximation of the ideal receive beamformer decision statistic. The LAN throughput requirements of this technique are derived as a function of the number of participating nodes in the receive cluster, the forward link code rate, and the quantization parameters. Using information-theoretic analysis and simulations of an LDPC coded system in fading channels, numerical results show that the performance penalty (in terms of outage probability and block error rate) due to coarse quantization is small in the low SNR regimes enabled by cooperative distributed reception. An upper/lower bound approximation is derived based on a circle approximation in the channel magnitude domain which provides a pretty fast way to compute the outage probability performance for a system with arbitrary number of receivers at a given SNR.

In the final part of this dissertation, we discuss the distributed reception tech-

nique with higher-order modulation schemes in the forward link. The extension from BPSK to QPSK is straightforward and is studied in the second part of this dissertation. The extension to 8PSK, 4PAM and 16QAM forward links, however, is not trivial. For 8PSK, two techniques are proposed: pseudobeamforming and 3-bit belief combining where the first one is intuitive and turns out to be sub-optimal, the latter is optimal in terms of outage probability performance. The idea of belief combining can be applied to the 4PAM and 16QAM and it is shown that better/finer quantizer design can further improve the block error rate performance. Information-theoretic analysis and numerical results are provided to show that significant reliability and SNR gains can be achieved by using the proposed schemes.

ACKNOWLEDGEMENTS

There are so many people I would like to thank, for without their help and accompany, I would never be able to accomplish this dissertation, which is a major milestone in my life.

First, and most importantly, I feel incredibly fortunate to have the most awesome professor Rick Brown as my advisor.

" Give a man a fish, feed him for a day.
Teach a man to fish, feed him for a lifetime."
– Lao Zi, the founder of Taoism.

He is the one that always teaches me how to "fish" so that I can benefit from throughout my life. I am extremely grateful for his vision, guidance and support, not only in my research and academics but also in my life when there are struggles and choices.

Besides my advisor, I am thankful to the rest of my dissertation committee: Andy Klein for always being kind enough to give me valuable comments and organizing the table tennis competition between SPINLAB and ASPECT to remind us the importance of keeping fit; Professor Raghu from University of Iowa for providing me invaluable advice and insights which made my research more fruitful.

I would also like to thank everyone who I interacted with in the PREW and CLASS programs funded by BBN technologies: Professor Madhow for his insightful comments on our paper and unlimited capacity for debate on any topic, Pat for his patience and valuable feedback, Professor Love for the discussions and talks over the weekly teleconference calls. Dzul, Dan, Adam, Matt, Zac and Junil have all provided useful guidance.

Thanks also goes to my current/previous labmates and friends at WPI who all make my experience here special: Qingxiong for her tireless support, Raquel for her warmth, Rui, Radu, Josh and Yizheng for their discussions, Yanjie and Pu for the good time we spent together.

I would also like to take this opportunity to acknowledge the supportive and stimulating environment at Worcester Polytechnic Institute. Particularly, I wish to thank Professor Kaveh Pahlavan for his help and encouragement in many aspects.

I am forever indebted to my mom and dad, Meng Ni and Jiancong Hu for their strong support for my adventure on the other side of the world. My life has also been profoundly affected by my grandparents Qing Ni and Qingyu Yuan. Just like my parents, they always encouraged me to do my best.

Finally, I would like to thank my husband and my best friend, Yunxing, since we were sixteen, for always loving me and supporting me, making life unpredictable and enjoyable no matter at school or at home.

BIOGRAPHICAL SKETCH

Min Ni was born and raised in Chengdu, Sichuan, where is famous for its relaxed and laid-back lifestyle. Being the only child of Jiancong Hu and Meng Ni, she lived a carefree childhood of fun and indulgence. As Min grew up in the 1990's, her parents bought her a Yamaha electronic keyboard in hopes of teaching her discipline as well as improving concentration. However, Min showed little interest in playing keyboard. After a series of struggles, her parents finally gave up and Min happily joined a youth chorus of a local TV station where she later became the leading singer just before she went to middle school. Though Min loved singing and missed her little friends in the chorus group, she had to quit since she attended a boarding school which is one of the most prestigious schools in Chengdu. This is perhaps the most important decision in Min's life since this is where she met her significant other, Yunxing, before she realized it several years later.

After taking the national higher education entrance exam, Min successfully completed high school in 2003 and was accepted by Sichuan University (SCU) which is the top university in the southwest of China. Influenced by her father who has worked as a staff in the ECE department for many years, Min decided to enroll in the Electrical Engineering program. Thanks to the years of boarding school experience, Min was well disciplined and her performance stood out from her contemporaries. Ranked No.1 in the department, she was exempted from standardized exams and directly got accepted to the grad school.

Maybe the path ahead of her was too straight and smooth, or maybe she stayed in one place too long, Min did not feel that excited when she started her grad school at SCU. She felt that there was much more out there for her to explore. For the first time, she started to think about her choices and future. When her mom

first heard of this decision, she thought her daughter went crazy since she never truly left this city for her entire 23 years of life. Her dad, on the other hand, was more supportive and helped convincing mom to trust their daughter. To show her determination and avoid putting extra financial burden on her parents, Min found a home tutor position to teach high school kids English, math and physics at $6.00 per hour. Luckily, one of the kids' father offered her a translation job at $10.00 per hour which she later used for taking TOEFL, GRE and applying for grad schools.

It was the year 2008 that Min started the email conversation with Professor D. Richard Brown III, an associate professor at Worcester Polytechnic Institute. Min was so lucky that she impressed Professor Brown by her carefulness when she read one of his publications, and even more luckily, she was informed by Professor Brown that she won the WPI Parks fellowship a month after she got an offer from WPI. Although Min also got offers from UMass Amherst, UMass Lowell and University of Delaware, she decided to go to WPI without any hesitation. She began her studies and reunited with her boyfriend at WPI in August of 2009.

As Min completes her studies at WPI this summer, she is actively looking for jobs in industry. Though got rejected by Qualcomm after two phone interviews, Min believed that good things happen to those who wait and who are prepared. She will continue to be positive in times of uncertainty and enjoy what life offers her.

TABLE OF CONTENTS

LIST OF TABLES

LIST OF FIGURES

LIST OF ABBREVIATIONS

Table 1: Abbreviations used in this dissertation.

Abbreviation	Meaning
AWGN	Additive white Gaussian noise
BC	Belief combining
BER	Bit error rate
BLER	Block error rate
BPSK	Binary phase shift keying
CJ	Joint original Cadambe-Jafar SISO IA solution from [1] with SHV orthonormalization from [2] and with perfect CSI
{CJ,KT,OT}-est	average sum rates with channel estimation error of the corresponding scheme
CSI	Channel state information
DoF	Degrees of freedom
DR	Distributed reception
IA	Interference alignment
KT	Joint improved SISO IA suboptimal subspace optimization solution from [3] with SHV orthonormalization from [2] and with perfect CSI
LLR	Log-likelihood ratio
LMMSE	Linear minimum mean square error
MIMO	Multiple-input multiple-ouput
MMSE	Minimum mean square error
OT	Opportunistic transmission [4] with perfect CSI
PAM	Pulse amplitude modulation
PDF	Probability density function
QAM	Quadrature amplitude modulation
RND	Random time-division channel access scheme
SHV	Orthornormalization scheme proposed by Shen, Host-Madsen and Vidal
SIMO	Single-input multiple-output
SISO	Single-input single-output
SNR	Signal-to-noise ratio
ZF	Zero-forcing

LIST OF SYMBOLS

Symbol	Meaning
$\mathbf{0}_{m\times n}$	$m \times n$ matrix of all 0's
$\mathbf{1}_{m\times n}$	$m \times n$ matrix of all 1's
$\boldsymbol{I}_n$	$n \times n$ identity matrix
$(\cdot)^\top$	matrix transpose
$(\cdot)^\dagger$	matrix conjugate transpose
$[\boldsymbol{S}]_{i,j}$	i,jth entry of matrix $\boldsymbol{S}$
$\text{sgn}(\cdot)$	sign function
det	determination of matrix
$\text{diag}(\boldsymbol{x})$	square diagonal matrix with vector $\boldsymbol{x}$ along diagonal
$\text{diag}(\boldsymbol{A})$	vector resulting from extraction of diagonal elements of $\boldsymbol{A}$
$\lceil\cdot\rceil, \lfloor\cdot\rfloor$	round up, down to nearest integer
$\text{tr}(\cdot)$	matrix trace
$\text{Re}(\cdot)$	extraction of real-valued component
$\text{Im}(\cdot)$	extraction of imaginary-valued component
$\|\|\boldsymbol{x}\|\|_p$	ℓ_p norm
$E[\cdot]$	expectation
$\hat{\boldsymbol{A}}$	estimate of a matrix $\boldsymbol{A}$

Chapter 1

Introduction

The purpose of a communications network is to enable the exchange of messages between its nodes. With the surging demand for wireless services such as HD video streaming, real-time gaming, etc., the conventional point-to-point communication can no longer meet the needs for such a large variety of high-data-rate multimedia services. Therefore, an intense research effort on more diversified communication technologies has been made to maximize the system performance under the respective resource constraints. However, due to the uneven resource distribution or the diverse channel quality among users, the effectiveness of some solutions could be limited. Interestingly, some of these problems can be alleviated or resolved if users are willing to share their local resources and cooperative in exchanging messages among their neighbours. This is the essence of cooperative communication.

1.1 Motivation

It has been understood in the information theory community for over three decades that wireless communication, such as cellular network, sensor networks, and ad-hoc networks can benefit from the cooperation of nodes that overhear the transmission [5–9]. Different from conventional point-to-point communications, cooperative communication and networking allows different users or nodes in a wireless network to share resources to create collaboration through distributed transmission/reception where each user's information is transmitted not only by its lo-

cal user, but also by its neighbours. It presents a new communication paradigm promising significant improvement in system capacity and reliability.

Since wireless networks are becoming denser with the deployment of small and low-power cellular base stations such as femto, pico and micro cells [10–12], neighbouring base stations have to operate on the same or overlapping pieces of spectrum. Naturally, it leads to interference, which if not properly managed, can significantly harm network performance and eliminates the gain of moving to smaller cells. Figure 1.1 shows an example of interference in a relay-aided cellular system.

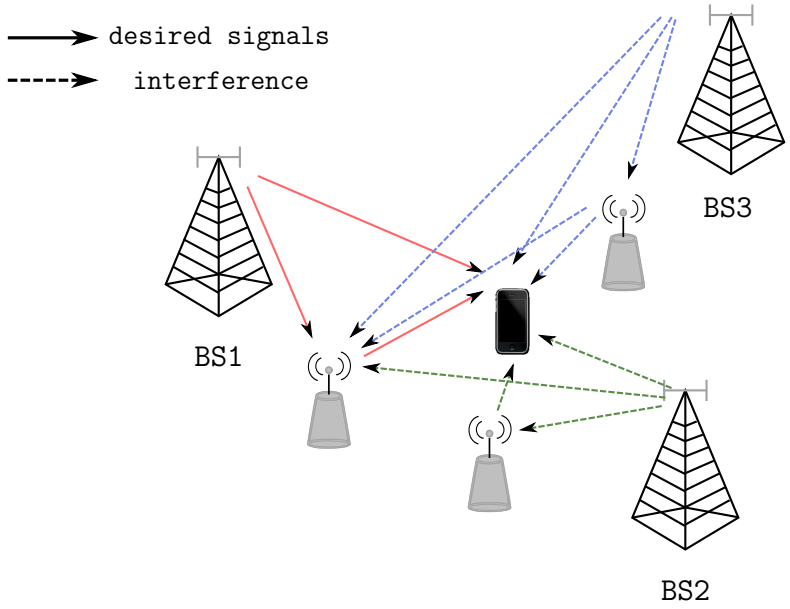

Figure 1.1: A typical relay-aided cellular system. In addition to the desired signal from the home base station, each relay or user receives interference from other-cell base stations or relays.

In conventional multiuser systems, it is often assumed that each user is only interested in retrieving information from its own sources, thus competing for the channel resources. As summarized in [1], current wireless system designs either treat interference as noise [13,14], which degrades system performance when the in-

terference becomes strong, or orthogonalize interferences from desired signals [15], which might cause shortage of resources when the number of interferers grows. The latter approach which assigns users orthogonal subchannels of the available spectrum turns out to be the most commonly adopted in practice, for example, TDMA, FDMA, CDMA etc. By using this approach each user gets a slice of the pie. As can be expected, when the density of users in the system increases, the spectral efficiency of each user diminishes quickly since each user gets a smaller slice of pie.

Despite the enormous amount of research on interference-aware receivers in the past twenty years and the large performance improvements promised by the multiuser techniques, traditional wireless system still generally treat interference as background noise [16–18]. This is mainly due to the lack of fundamental understanding of interference channel. To understand the performance limit of interference channels, the simplest information-theoretic model–a two-user interference system is studied in 1961 [19]. However, except for some special cases [20, 21], the capacity region for a two-user interference channel has remained an open question for 50 years. The largest achievable rate region we know so far was published in [22] 1981 and a generalized degrees of freedom characterization that identifies different operational regimes for such channels is provided in [13] in 2006. However, for interference channels with more than two users, even the degrees of freedom characterizations remains unknown.

Recently, it has been shown that the sum capacity per user for the K user interference channel is

$$\frac{1}{2}\log_2(SNR) + o(\log_2(SNR))$$

which means that "everyone gets half of the cake" [1]. The mechanism that approaches this capacity is referred as interference alignment (IA). In general, IA is a technique that aligns the interference into a reduced dimensional subspace by linear precoding so that simultaneous communications among many users over a small signal space can be achieved while keeping the desired signal separable from the interference [23]. This idea was first crystallized by Jafar and Shamai in [24] and later a general principle was established in [1].

To illustrate the idea of IA, we borrowed the toy example from [1]. In the 3-user interference network shown Figure 1.2, each channel has a propagation delay associated with it where the propagation delay equals to 1 symbol duration for each desired transmit-receive pair and it equals to 2 symbol durations for all interference pairs. At time n, the channel output at receiver k is defined as

$$y_k[n] = \sum_{j \neq k} x_j[n-2] + x_k[n-1] + z_k[n]$$

where $z_k[n]$ is i.i.d zero mean unit variance Gaussian noise. If no interference is present, each user would achieve a capacity of $C = \log_2(1+P)$ where $\mathrm{E}[|x_k[n]|^2] \leq P$. Now if the transmitter only transmits according to the schedule shown in the figure, which is only half the time, with power $2P$. The desired signal can be received free from interference half of the timeslots. Hence the rate achieved at each user is $R = \frac{1}{2}\log_2(1+2P)$ where the pre-log factor $1/2$ denotes the degrees of freedom.

The example shown above aligns the signals in time. Actually IA can align signals in any dimension, including time, frequency or space. It is a linear precoding technique that can compact interfering signals into small dimensional subspaces at each receiver leaving the desired signal interference free, if properly designed. IA

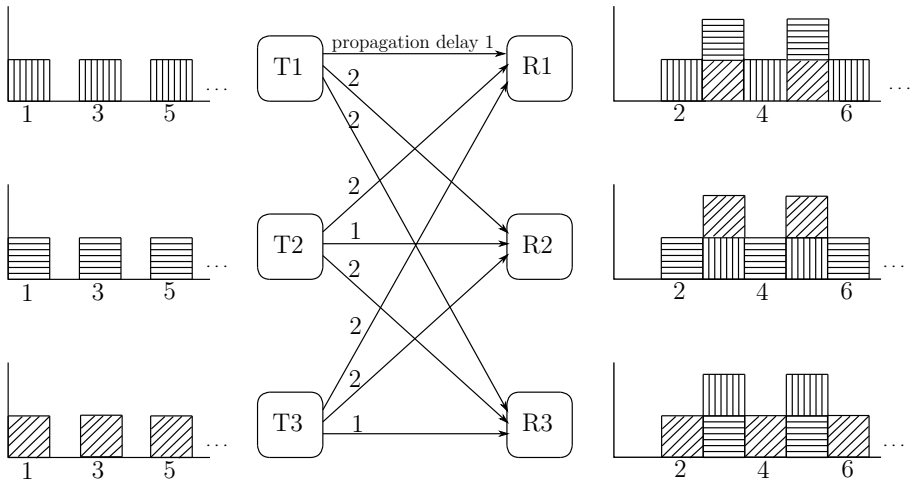

Figure 1.2: Illustration of interference alignment: Everyone gets half the cake [1].

can be viewed as a cooperative approach since the transmitters neglect the performance of their own link to allow other users to perfectly cancel interference [25].

While IA promises substantial theoretical gain in wireless networks, it comes with challenges in implementation. First, it requires extensive channel state information to be exchanged over the backhaul between the transmitters. From a practical point of view, obtaining CSI at the receivers is an estimation problem which in general is not error-free. Hence, it is crucial to understand the effect of channel estimation error on the capacity region [26–29]. Also, the integration of IA with other system issues such as scheduling needs to be addressed [30, 31]. Therefore it is necessary to compare the traditional interference avoidance approaches with IA in more practical scenarios and thus get a better understanding of the challenges that stand in the way of realizing such systems in real world.

If no cooperative transmission techniques can be employed, it is still possible to improve the system performance and combat fading by reducing the fluctuations in the power gain seen by the transmitted signal. Since for different receive antenna

elements spaced widely enough apart, it is unlikely for all of them to fade badly at the same time. The idea, in which the receiver gets multiple versions of the transmitted signal that has low probability of experiencing severe fading at the same time is referred as receive diversity [32, 33]. In [34–38], diversity reception is shown to be a powerful technique for reducing the effects of delay spread as well as for reducing the effects of AWGN, co-channel interference and random FM noise, if the rms delay spread is small compared to the symbol duration.

Cooperative reception is a technique where multiple receivers in a wireless network combine their observations to increase diversity and power gain and, consequently, improve the probability of successfully decoding noisy transmissions. The idea of cooperative reception can be dated back to 1983 where it was applied in the context of aperture synthesis for radio astronomy, e.g. the Very Large Array [39]. Results show that better resolution and SNR gains can be achieved by forwarding observations over a high-speed optical backhaul network to a processing center for subsequence alignment and combining.

More recently, cooperative reception has been used for wireless networks with limited backhaul capabilities. For example, soft handoff [40, 41] has been successfully used in the cellular systems in 1990s. Recent information-theoretic studies [42–45] have shown that more sophisticated cooperative reception techniques have significant potential to increase diversity, improve capacity, and improve interference rejection, even with tight backhaul constraint. Several techniques have been proposed to achieve these gains including link-layer iterative cooperation [46–48], distributed iterative receiver message-passing [49], and most-reliable/least-reliable bit exchange iterative decoding [50–55].

In general, all these techniques considered a scenario where multiple nodes receive independent copies of the same message. Since the nodes in a receive cluster are fully-connected, if any node in the cluster successfully decodes the message from the distant transmitter, it broadcasts the decoded message to other receive nodes. A more interesting case is that none of the receive nodes is able to decode the broadcasted message and this is where the cooperative reception comes into play. For example, in [53], an iterative distributed decoding method is introduced where each nodes requests additional information from other nodes for the decoded bits whose soft outputs magnitudes are the lowest $x\%$. This later is referred as the least reliable bits (LRB)-based scheme and a simple extension of it is to broadcast the soft information to all the receive nodes so that each of the node can make use of this a priori in the next iteration of soft-input and soft-output decoding. By using the LRB-based collaborative decoding schemes, more than 5 dB can be achieved over conventional maximal rate combining (MRC) for a packet of 900 bits and a cluster size of 8 nodes. Since the overhead per receiver grows linearly with the size of the cluster, the overhead soon exceeds MRC with large N. To make the overhead independent of the number of receivers, a most reliable bits (MRB) exchange scheme is presented in [53] where each node sends out the most reliable bits only once. Improvements of the MRB-based collaborative decoding such as adding memory to the node and sending hard-decisions of MRBs are proven to achieve 7 dB antenna gain while maintaining a fixed per-receiver overhead. Performance analysis of the LRB/MRB-based collaborative decoding schemes are studied in [55] and an upper bound for the error performance is developed based on a density-evolution model. Another stream of work based on belief propagation (BP) algorithm is proposed in [43, 56]. In both papers, BP is employed for an

inference problem which involves the choice of the graphical representation and the order of activation of nodes and message passings on the graph. It is shown that near single user performance can be achieved with moderate amount of message passing between the nodes.

A limitation of all of these techniques is that they are based on iterative transmissions and decoding. As such, the backhaul requirements are variable and the decoding latency can be significant if the number of iterations is large. The focus of these studies is also often on achieving diversity gains, rather than SNR gains. SNR gains through distributed receive beamforming are particularly appealing since they can be linear in the number of receivers and allow for longer-range and/or higher-data rate communication as well a reduction in the size, weight, power and cost of the transmitter.

This dissertation focuses on particular distributed transmission and reception techniques for cooperative networks. The simplest form of distributed transmission is opportunistic transmission [4, 57, 58] where the transmit nodes send messages opportunistically at each instant in time based on the feedback of the channel quality from the receive nodes. An advantage of opportunistic transmission is that it can be implemented with moderate computational complexity and only a small amount of feedback is required from the receive nodes. We compare opportunistic transmission and the more recent approach, i.e. interference alignment for a 3-user single-input and single-output interference channel in terms of average sum rate in the presence of channel estimation errors. In addition to the study on distributed transmission, this dissertation also addresses the problem of jointly decoding messages from a single distant transmitter to a cooperative receive cluster

with a conventional LAN comprising the backhaul and we extend the results to more spectrally efficient forward link modulation schemes.

1.2 Dissertation Overview

The main body of this dissertation is organized into three chapters:

- A performance comparison of opportunistic transmission and interference alignment with channel estimation errors (Chapter 2)
- Distributed reception with coarsely-quantized observation exchanges (Chapter 3)
- Distributed reception with higher-order forward link modulation (Chapter 4)

and is followed by a conclusion and a discussion of potential research directions.

The contents of these chapters are described in more detail below.

Chapter 2 mainly compares the average sum rate performance between opportunistic transmission and interference alignment with channel estimation errors. Since recent analysis on IA showing that the sum rate of a SISO interference channel can scale linearly with the number of users in the system, it is of interest to study its performance under imperfect CSI assumption. Starting with a brief review of interference management approaches, we present a 3-user SISO interference channel model that will be used throughout this chapter. Due to its simplicity,

opportunistic transmission is discussed in the first place where the average sum rate performance with perfect/imperfect CSI is given explicitly. Then the IA is discussed in detail. In addition to the closed-form solution we found for SISO IA which is originally introduced in [1], we present the simulation results of several modified IA solutions with perfect CSI. Then a causal implementation procedure for the SISO IA is developed and the performance is evaluated with imperfect CSI. Finally, we present the simulation results of opportunistic transmission and SISO IA which suggest that SISO IA can achieve better average sum rate with good channel at high SNR whereas opportunistic transmission tends to provide better performance at low SNR and/or when the channel estimates are poor which is more robust to estimation errors.

Chapter 3 of this dissertation considers methods to improve the probability of successfully decoding binary phase shift keyed (BPSK) messages from a single distant transmitter to a cooperative receive cluster connected by a local area network (LAN). Although much has been written recently on distributed decoding method that requires only small amount of information exchange between the receive nodes while getting huge diversity gains, most of these methods are iterative which makes the backhaul requirements variable and thus result in significant decoding latency if the number of iterations is large. In this chapter, we develop an approximate distributed receive beamforming algorithm based on the exchange of coarsely-quantized observations among some or all of the nodes in the receive cluster. We show that for BPSK, summing unquantized LLRs is equivalent to beamforming which sheds some light on exchanging quantized LLRs. Information theoretic analysis and simulation results show that the performance penalty (in terms of outage probability and block error rate) due to coarse quantization is

small in the low SNR regimes enabled by cooperative distributed reception. We also demonstrate via bound analysis and simulations that the gap between the beamforming and the proposed technique is no more than 2.1483 dB for any number of receive nodes.

Chapter 4 of this dissertation applies the idea in chapter 3 with more spectrally efficient forward link modulation schemes. Though similar to the BPSK, direct application of exchanging quantized LLRs among the receive nodes does not seem to be the optimal approach for MPSK in general. An intuitive cooperative distributed reception method, i.e., pseudobeamforming is developed based on exchanging hard decisions of the observations and fed it to a customerized demodulator according to the statistics of the aggregate quantization error. Then we introduce the belief combining which is shown to be the optimal distributed reception technique based on exchanging coarsely quantized observations. Both information-theoretic analysis and simulation results demonstrate that the belief combining with 8PSK forward link modulation can preserve the merits we have seen for the BPSK case i.e., significant reduction in LAN throughput requirement can be achieved while the performance penalty due to coarse quantization is small in the low SNR regime. Similar idea is applied to the 4PAM and 16QAM forward link modulations with minor modifications due to the different types of symmetry of the constellations. Since quantizer designs have great influence on outage probability performance for 4PAM and 16QAM, optimal quantizer design is discussed in this chapter where we show that the optimal quantizer amplitude threshold can be found by numerical maximization of the mutual information between the channel input and the quantized channel output. The results of LDPC code are also demonstrated which suggests that the achievable performance with real block codes can be close to the

information-theoretic predictions.

Chapter 5 of this dissertation summarizes the results from the prior chapters and concludes with a discussion of potential problems stemming from this work for future research.

1.3 Dissertation Contributions

The main contributions of this dissertation are listed as follows:

- Chapter 2

  – Exact expressions for computing the average sum rate of the opportunistic transmission under the 3-user SISO interference system model.

  – Exact and approximate expressions for computing the average interference leakage and the average sum rate of the 3-user SISO interference system model.

  – Development of a causal implementation procedure of SISO IA together with a circularly symmetric and a non-i.i.d amplitude/phase channel estimation error model.

  – A numerical average sum rate performance comparison between opportunistic transmission and SISO IA for the 3-user SISO interference system with channel estimation errors showing that SISO IA can achieve better average sum rate with good channel at high SNR whereas opportunistic transmission tends to provide better performance at low SNR and/or when the channel estimates are poor which means more robust to estimation errors [59].

- Chapter 3

  – Development of a distributed reception protocol [60] based on the exchange of coarsely-quantized observations among some or all of the nodes in the receive cluster with BPSK forward link modulation.

  – Explicit estimates of backhaul throughput requirements as a function the forward link information rate, and demonstrating the efficacy of the technique with full and limited receiver participation.

  – An information-theoretic analysis of the corresponding distributed reception system, an exact expressions for the mutual information with observations arbitrarily quantized or unquantized.

  – Simulations of information-theoretic analysis and an LDPC coded system in fading channels demonstrating that the performance penalty in terms of outage probability due to coarse quantization is small in the low SNR regimes enabled by cooperative distributed reception.

  – An analysis of a conjectured upper and lower bound on the distributed reception technique with BPSK forward link modulation which offers a fast way of predicting the outage probability performance for a given rate r. The gap between the ideal beamforming and 1-bit belief combining is at most 2.1483 dB for any number of receive nodes N.

- Chapter 4

  – Development of a general framework for distributed reception with higher order forward link modulations (8PSK, 4PAM and 16QAM).

  – Development of pseudobeamforming which is an intuitive distributed reception technique for 8PSK forward link modulation.

– Simulations of an LDPC coded system in fading channels demonstrating the pseudobeamforming is suboptimal compared with the belief combining in terms of outage probability.

– Optimal quantizer designs for 4PAM with 2-bit/3-bit per observation and 16QAM with 4-bit/6-bit per observation showing that improvement in the outage probability performance can be achieved by maximizing the mutual information between the channel input and the quantized channel output via numerical simulations.

Chapter 2

A Performance Comparison of Opportunistic Transmission and Interference Alignment with Channel Estimation Errors

This chapter compares interference alignment and opportunistic transmission for a 3-user single-input single-output (SISO) interference channel in terms of average sum rate in the presence of channel estimation errors. In the case of interference alignment, channel estimation errors cause interference leakage which consequently results in a loss of achievable rate. In the case of opportunistic transmission, channel estimation errors result in a non-zero probability of incorrectly choosing the node with the best channel. The effect of these impairments is quantified in terms of the achievable average sum rate of these transmission techniques. Analysis and numerical examples for independent and identically distributed fading channels show that SISO interference alignment can achieve better average sum rate with good channel estimates and at high SNR whereas opportunistic transmission provides better performance at low SNR and/or when the channel estimates are poor.

2.1 Background

Wireless networks are interference-limited due to the increasing number of users that need to share the spectrum to achieve the high-rate communication. The problem of achieving efficient communication in an interference channel has attracted much research activity in recent years. The growing demands on wireless networks, for example, 4G networks including WiMAX and 3GPP Long Term Evolution (LTE), to support high data rates and high capacity has driven the need to develop efficient interference management techniques [16, 61].

Conventional interference management approaches such as interference avoidance divide the channel resources among the transmitters, e.g. using time division such that only one node transmits at a time [62–64]. When the receive nodes can measure and feedback the channel quality, the transmit nodes can transmit opportunistically by using the best available channel at each instant in time [4]. An advantage of opportunistic transmission is that this technique can be implemented with moderate computational complexity and only a small amount of feedback is required from the receive nodes.

Another more recent interference management approach is to use interference alignment (IA). It is shown in [1] that by using IA, the capacity of a K-user single-input and single-output interference channel with frequency selective or time-varying channel coefficients is

$$C(SNR) = \frac{K}{2}\log_2(SNR) + o(\log_2(SNR))$$

which approaches the Shannon capacity of interference networks at high SNR. The main idea of IA is to align the interference into a reduced dimensional subspace by

linear precoding so that simultaneous communications among many users over a small signal space can be achieved while keeping the desired signal separable from the interference [23].

Since both opportunistic transmission and IA require feedback, and this feedback is typically based on noisy estimates and is often coarsely quantized, it is of interest to understand how these systems perform in the presence of channel estimation or quantization errors. For example, an opportunistic transmission scheduling policy is proposed in [65] which is shown to be robust to estimation errors from both stochastic approximation algorithm and imperfect measurement of channel conditions. However, no explicit expression is given to evaluate the average sum rate performance for the SISO interference channel by using opportunistic transmission. Another study [66] considers a broadcast channel with estimation errors where the transmit node sends to the user with the highest estimated SNR but backs off on the transmit rate based on the variance of the estimation error. However, the performance of such scheme relies heavily on the duration of training period and the effects of channel estimation error is not explicitly quantified. Compared with opportunistic transmission, finding a closed-form SISO IA solution is non-trivial in the first place. The majority of recent IA-inspired solutions are either non-unique [67–70] or initialization dependent due to iterative nature of the algorithm [71–79]. Besides, most of the aforementioned work focuses on MIMO interference channels with full knowledge of CSI whereas our work mainly focuses on the performance of SISO channels and non-iterative solutions in the presence of channel estimation errors. Hence, the study on the simplest case would provide insights on IA prototyping [80–82].

In this chapter, the performance of opportunistic transmission and IA with channel estimation errors is compared for a 3-user SISO interference system. A simple opportunistic transmission strategy is employed where only the transmit-receive pair with the largest channel magnitude estimate can communicate at each instant in time. For IA, a closed-form solution of a suboptimal subspace design [3] is used which avoids the initialization considerations inherent in iterative IA algorithms [25, 72]. Our analysis and simulation results for independent identically fading channels show that IA can achieve higher average sum rate only at high SNR and with accurate channel information whereas opportunistic transmission can provide better performance at low SNR and/or with relatively bad channel estimates.

2.2 System Model

We assume a system with $K = 3$ single-antenna transmitters and 3 single-antenna receivers where each transmitter wishes to send messages only to its associated receiver as shown in Figure 2.1. Let $h_{kj}(t) \overset{\text{i.i.d.}}{\sim} \mathcal{CN}(0, I)$ denote the channel from transmitter j to receiver k at time t where $j, k \in \{1, 2, 3\}$. We assume that all channels are additive and that there is no intersymbol interference. A coarse level synchronization is assumed among the transmitters and receivers so that symbols arrive at the same time at the receivers.

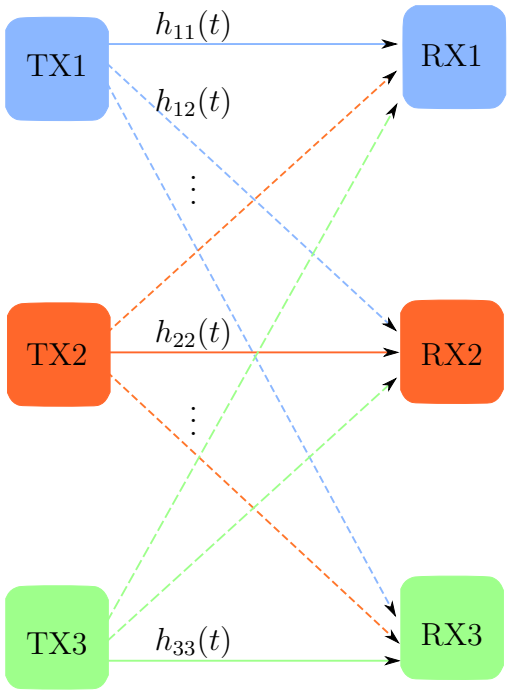

Figure 2.1: A 3-user interference channel.

2.3 Opportunistic Transmission

Opportunistic transmission is a simple strategy that can improve average rate through by selecting the best available channel for transmission and only using this channel while the other transmitters remain silent. In the context of the system model in Section 2.2, this means that only the transmitter with the maximum $|h_{kk}(t)|$ transmits at time t. Unlike interference alignment, as discussed in Section 2.4, opportunistic transmission only requires feedback of three channel states. We consider a scenario here with only spatial opportunism and no temporal opportunism. The transmitter with the best channel to its receiver transmits with fixed energy $\mathcal{E}$ in that timeslot. Under our i.i.d channel assumption, note that the *average transmit energy* for each transmitter is $\mathcal{E}/K$ in opportunistic transmission.

For all $j, k \in \{1, 2, 3\}$, we have

$$f_{|h_{kj}(t)|}(x) = \frac{x}{\sigma^2} e^{\frac{-x^2}{2\sigma^2}}, \text{ and}$$
$$F_{|h_{kj}(t)|}(x) = 1 - e^{-\frac{x^2}{2\sigma^2}}$$

where $\sigma^2 = 0.5$. Figure 2.2 shows an example of histogram of the absolute value of complex Gaussian random variables and its theoretical Rayleigh pdf with $\sigma^2 = 0.5$.

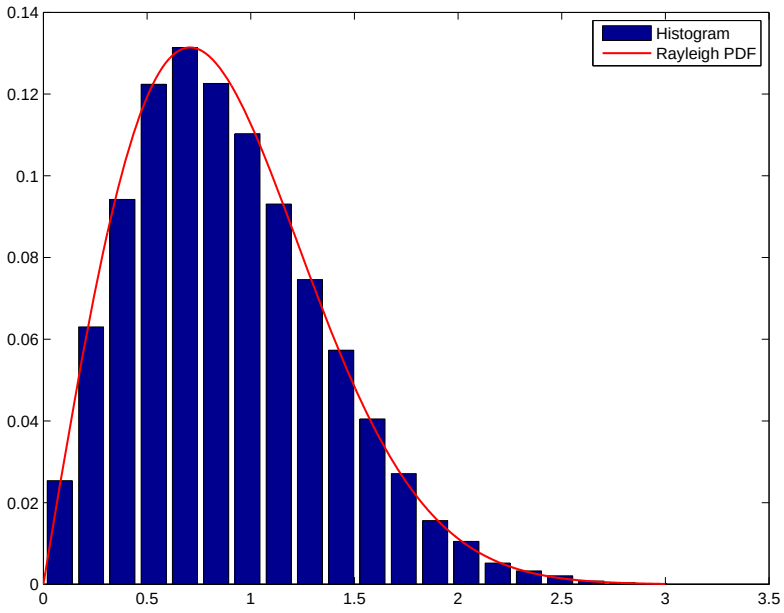

Figure 2.2: An example of histogram of the absolute value of complex Gaussian random variables and its theoretical Rayleigh pdf with $\sigma^2 = 0.5$.

Letting

$$\lambda(t) = \max(|h_{11}(t)|, |h_{22}(t)|, |h_{33}(t)|),$$

we can write the distribution of the best channel as [83]

$$f_{\lambda(t)}(x) = \frac{3x}{\sigma^2} e^{-\frac{x^2}{2\sigma^2}} \left(1 - e^{-\frac{-x^2}{2\sigma^2}}\right)^2. \tag{2.1}$$

Figure 2.3 shows an example of histogram of the absolute value of complex Gaussian random variables and its theoretical Rayleigh pdf with $\sigma^2 = 0.5$.

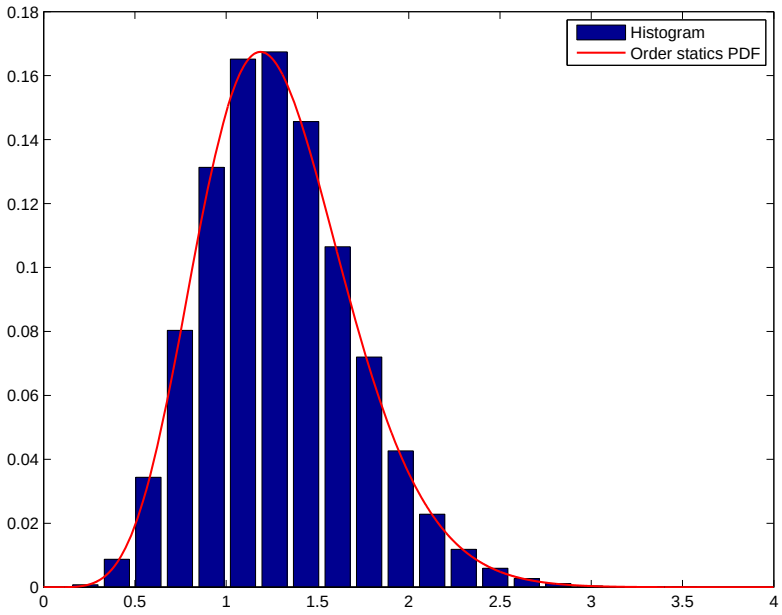

Figure 2.3: An example of histogram of the order statistic random variables and its theoretical pdf with $\sigma^2 = 0.5$.

Under our fixed transmit energy assumption, the average sum rate of the opportunistic transmission with perfect CSI can then be written as

$$R_{\text{ave}-\text{OT}} = \text{E}\left[\log_2\left(1 + \mathcal{E}\lambda^2(t)\right)\right] \tag{2.2}$$

$$= \int_0^{+\infty} f_{\lambda(t)}(x) \log_2\left(1 + \mathcal{E}x^2\right) dx. \tag{2.3}$$

Note that $R_{\text{ave}-\text{OT}}$ corresponds to the average sum rate of opportunistic transmission with perfect CSI.

When CSI is imperfect, there is a non-zero probability that the transmitter with the best channel is not selected for transmission. Let $\hat{h}_{kk}(t)$ denote the channel

estimates from transmitter k to receiver k where $k \in \{1, 2, 3\}$. Define

$$\hat{k} = \arg \max_{k \in \{1,2,3\}} |\hat{h}_{kk}(t)|$$

and $\hat{\lambda}(t) = |h_{\hat{k}\hat{k}}(t)|$. Note that $\hat{\lambda}(t) \leq \lambda(t)$ for all t. Then the average sum rate of the opportunistic transmission with imperfect CSI can be written as

$$\hat{R}_{\text{ave}-\text{OT}-\text{est}} = \text{E}\left[\log_2\left(1 + \mathcal{E}\hat{\lambda}^2(t)\right)\right]. \tag{2.4}$$

2.4 Three-user SISO Interference Alignment

This section describes the symbol extended channel model used for a 3-user SISO IA scheme, the associated performance metrics, and a closed-form solution for SISO IA precoding vectors. It is worth mentioning here that SISO IA requires feedback of all nine of the channels to all of the transmitters to allow computation of the precoding vectors. Channel estimation error can result in interference leakage. We also point out that, unlike opportunistic transmission where the transmit energy was fixed in each timeslot, the IA scheme described below is based on an average energy constraint for each symbol-extended block transmission.

2.4.1 Symbol extended channel model

To provide the required dimensionality for aligning interference subspaces in the SISO IA context, it is necessary to consider a symbol extended channel model in which each transmitter sends a block of precoded symbols over the channel. Let X_j denote the N-symbol extension of the transmitted symbol $\boldsymbol{x}_j = \begin{bmatrix} x_j(t+1) & \cdots & x_j(t+l_j) \end{bmatrix}^\top$

from transmitter j where l_j represents the number of independent streams at the j^{th} transmitter. It has been shown in [1] that $(l_1, l_2, l_3) = (n+1, n, n)$ is achievable on the N-symbol extended channel when $N = 2n + 1$. The elements of $\boldsymbol{x}_j$ are assumed to be i.i.d zero mean complex circularly symmetric Gaussian with variance $\frac{\mathcal{E}}{K}$, i.e., $\boldsymbol{x}_j \sim \mathcal{CN}(0, \frac{\mathcal{E}}{K} I_{l_j})$. Hence, X_j can be written as

$$X_j = V_j \boldsymbol{x}_j = \begin{bmatrix} \boldsymbol{v}_j^{[1]} & \boldsymbol{v}_j^{[2]} & \cdots & \boldsymbol{v}_j^{[l_j]} \end{bmatrix} \boldsymbol{x}_j \tag{2.5}$$

where V_j is a $N \times l_j$ precoding matrix and $\boldsymbol{v}_j^{[i]}$ represents the i^{th} column of V_j, $i \in \{1, 2, \cdots, l_j\}$. Let $V_j^\dagger V_j = \frac{N}{l_j} I_{l_j}$. Since each transmitter access the channel N times in a block transmission, the transmit energy at transmitter j is constrained such that $\mathrm{E}[\|X_j\|^2] = \frac{N\mathcal{E}}{K}$.

Since the symbols from each transmitter are transmitted over N time slots as a "supersymbol", the extended channel H_{kj} (note that H_{kj} is not MIMO channel) is defined as

$$H_{kj} := \begin{bmatrix} h_{kj}(t+1) & 0 & \cdots & 0 \\ 0 & h_{kj}(t+2) & \cdots & 0 \\ 0 & 0 & \cdots & h_{kj}(t+N) \end{bmatrix} \tag{2.6}$$

where h_{kj} is a scalar at each channel use and $h_{kj}(t)$ and $h_{kj}(s)$ are independent for all $t \neq s$. The received signal vector at receiver k is then

$$\begin{aligned} \boldsymbol{y}_k &:= H_{kk} X_k + \sum_{j \neq k}^{K} H_{kj} X_j + \boldsymbol{w}_k \\ &= H_{kk} V_k \boldsymbol{x}_k + \sum_{j \neq k}^{K} H_{kj} V_j \boldsymbol{x}_j + \boldsymbol{w}_k \end{aligned} \tag{2.7}$$

where $\boldsymbol{y}_k$ is the $N \times 1$ received signal vector and $\boldsymbol{w}_k$ is the additive white Gaussian noise at receiver k distributed as $\boldsymbol{w}_k \sim \mathcal{CN}(0, I_N)$ at receiver k.

At the receiver side, we assume zero-forcing decoders. Let U_k be an $N \times l_k$ matrix whose columns are orthogonal to the interference signal subspace at the k^{th} receiver. The filtered received signals can then be written as

$$\begin{aligned} \boldsymbol{z}_k &= U_k^{\dagger} \boldsymbol{y}_k \\ &= U_k^{\dagger} H_{kk} V_k \boldsymbol{x}_k + \sum_{j \neq k}^{K} U_k^{\dagger} H_{kj} V_j \boldsymbol{x}_j + U_k^{\dagger} \boldsymbol{w}_k. \end{aligned} \tag{2.8}$$

2.4.2 Performance metrics

The formula for computing average sum rate can be of different forms based on the types of receivers employed in the system and for different purposes. For example, zero forcing decoders are deployed in [2, 71, 78] whereas MMSE receivers are used in [3].

If perfect knowledge of CSI is assumed at the transmitter and receiver, the individual sum rate at user k derived with receivers deploying zero-forcing decoders can be written as

$$R_k = \log_2 \left| I_{l_k} + \frac{\mathcal{E}}{K} \bar{H}_{kk} \bar{H}_{kk}^{\dagger} \left(\sum_{k \neq j} \frac{\mathcal{E}}{K} \bar{H}_{kj} \bar{H}_{kj}^{\dagger} + I_{l_k} \right)^{-1} \right|$$

in units of bits per block, where $\bar{H}_{kj} = U_k^{\dagger} H_{kj} V_j, \forall (k, j)$. The average sum rate with perfect CSI is then

$$R_{\text{ave-IA}} = \frac{1}{N} \mathrm{E} \left[\sum_{k=1}^{K} R_k \right]$$

in units of bits per channel use.

When MMSE receivers are deployed, the individual rate for user k is defined

as

$$R_k := \log_2 \frac{\left| I_N + \sum_j \frac{\mathcal{E}}{K} H_{kj} V_j V_j^\dagger H_{kj}^\dagger \right|}{\left| I_N + \sum_{j \neq k} \frac{\mathcal{E}}{K} H_{kj} V_j V_j^\dagger H_{kj}^\dagger \right|} \tag{2.9}$$

for $j = \{1, 2, \cdots, K\}$. Simulations in section 2.4.4 show that these two type of receivers give close performance for the given system. Hence unless otherwise stated, zero forcing decoders are applied through the entire dissertation.

When CSI is imperfect, we can denote the channel estimate as $\hat{H}_{kj}$. Then the precoding and decoding matrices $\hat{V}_j$ and $\hat{U}_k$, respectively, are computed based on the estimated CSI rather than the actual CSI. Hence the resulting individual sum rate will be

$$\hat{R}_k = \log_2 \left| I_{l_k} + \frac{\mathcal{E}}{K} \hat{\bar{H}}_{kk} \hat{\bar{H}}_{kk}^\dagger \left(\sum_{k \neq j} \frac{\mathcal{E}}{K} \hat{\bar{H}}_{kj} \hat{\bar{H}}_{kj}^\dagger + I_{l_k} \right)^{-1} \right| \tag{2.10}$$

in units of bits per block, where $\hat{\bar{H}}_{kj} = \hat{U}_k^\dagger H_{kj} \hat{V}_j, \forall (k, j)$. The corresponding average sum rate with imperfect CSI is then

$$\hat{R}_{\text{ave}-\text{IA}-\text{est}} = \frac{1}{N} \mathrm{E} \left[\sum_{k=1}^{K} \hat{R}_k \right] \tag{2.11}$$

in units of bits per channel use.

Another metric to evaluate the quality of alignment is the average interference leakage [77]. Unlike sum rate, the average interference leakage reveals more details about how well the interference is aligned and suppressed at each receiver. It measures the power in the leakage interference at each receiver, i.e., the interference power remaining in the filtered received signal and thus serves as a better indicator of the quality of interference alignment.

Introduced in [77], the average interference leakage is defined as

$$I_{\text{ave}-\text{IA}} = \frac{1}{N}\text{E}\left[\sum_{k=1}^{K} I_k\right] \tag{2.12}$$

where the individual interference leakage at the k^{th} receiver is

$$I_k = \text{Tr}\left[U_k^{\dagger} Q_k U_k\right] \tag{2.13}$$

where

$$Q_k = \sum_{j=1,k\neq j}^{K} \frac{\mathcal{E}}{K} H_{kj} V_j V_j^{\dagger} H_{kj}^{\dagger} \tag{2.14}$$

is the interference covariance matrix at receiver k. The decoding vectors U_k can usually be obtained by using Gram-Schmidt process. Details can be found in Appendix A. When interference is perfectly aligned and suppressed the leakage will be zero. Hence the average interference leakage can be written as

$$\begin{aligned} I_{\text{ave}-\text{IA}} &= \frac{1}{N}\text{E}\left[\sum_{k=1}^{K} I_k\right] \\ &= \frac{1}{N}\text{E}\left[\sum_{k=1}^{K} \text{Tr}\left[U_k^{\dagger} Q_k U_k\right]\right] \\ &= \frac{1}{N}\text{E}\left[\sum_{k=1}^{K} \text{Tr}\left[U_k^{\dagger}\left(\sum_{j=1,j\neq k}^{K} \frac{\mathcal{E}}{K} H_{kj} V_j V_j^{\dagger} H_{kj}^{\dagger}\right) U_k\right]\right] \\ &= \frac{1}{N}\text{E}\left[\sum_{k=1}^{K}\sum_{j=1,j\neq k}^{K} \frac{\mathcal{E}}{K} \text{Tr}\left[\left(U_k^{\dagger} H_{kj} V_j\right)\left(U_k^{\dagger} H_{kj} V_j\right)^{\dagger}\right]\right]. \end{aligned} \tag{2.15}$$

When imperfect CSI is assumed, the precoding matrices $\hat{V}_j$ and the decoding matrices $\hat{U}_k$ are computed based on $\hat{H}_{kj}$. The estimated interference leakage at user k are computed as

$$\hat{I}_k = \text{Tr}\left[\hat{U}_k^{\dagger} \hat{Q}_k \hat{U}_k\right] \tag{2.16}$$

where

$$\hat{Q}_k = \sum_{j=1,j\neq k}^{K} \frac{\mathcal{E}}{K} H_{kj} \hat{V}_j \hat{V}_j^{\dagger} H_{kj}^{\dagger}.$$

Hence the average interference leakage can be obtained by

$$\hat{I}_{\text{ave-IA}} = \frac{1}{N}\mathrm{E}\left[\sum_{k=0}^{K}\hat{I}_k\right]. \tag{2.17}$$

2.4.3 Closed-form solutions for SISO IA

Many algorithms for computing optimal IA precoding matrices are iterative and, since convergence depends on the initialization, this makes them unattractive when it comes to studying the performance of IA with imperfect CSI. In this section, a handful of non-iterative IA algorithms with closed-form solutions will be discussed and used as a basis for our comparison with opportunistic transmission in the sequel.

SISO interference alignment with l_k streams from transmitter k requires

$$\begin{aligned} U_k^{\dagger}H_{kj}V_j &= 0 \quad \text{for } j \neq k \\ \operatorname{rank}(U_k^{\dagger}H_{kk}V_k) &= l_k. \end{aligned} \tag{2.18}$$

The first closed-form solution for the precoding vectors in a 3-user SISO interference channel was given in [1] in which the precoding vectors are defined as

$$\left.\begin{aligned} H_{12}V_2 &= H_{13}V_3 \\ H_{23}V_3 &\prec H_{21}V_1 \\ H_{32}V_2 &\prec H_{31}V_1 \end{aligned}\right\} \Rightarrow \begin{aligned} V_1 &= A \\ V_2 &= (H_{32})^{-1}H_{31}C \\ V_3 &= (H_{23})^{-1}H_{21}B \end{aligned} \tag{2.19}$$

where

$$\begin{aligned} T: &= H_{12}(H_{21})^{-1}H_{23}(H_{32})^{-1}H_{31}(H_{13})^{-1} \\ A: &= \begin{bmatrix} \boldsymbol{\omega} & T\boldsymbol{\omega} & \cdots T^n\boldsymbol{\omega} \end{bmatrix}_{N\times(n+1)} \\ B: &= \begin{bmatrix} T\boldsymbol{\omega} & T^2\boldsymbol{\omega} & \cdots & T^n\boldsymbol{\omega} \end{bmatrix}_{N\times n} \\ C: &= \begin{bmatrix} \boldsymbol{\omega} & T\boldsymbol{\omega} & \cdots & T^{n-1}\boldsymbol{\omega} \end{bmatrix}_{N\times n}. \end{aligned} \tag{2.20}$$

In [1], $\boldsymbol{\omega} = \begin{bmatrix} 1 & 1 & \cdots & 1 \end{bmatrix}^\top$.

The idea of the IA scheme for three-user interference alignment can be extended for K-user cases and details of the solutions and examples can be found in Appendix B. As stated in [23], this scheme is primarily of theoretical interest because of its strong asymptotic character which limits its practical use. However, it is one of the most powerful theoretical IA constructions that can be applied to many scenarios.

Based on this scheme, it is showed in [84] that a global optimal solution $\tilde{\boldsymbol{\omega}}^*$ exists which maximizes the sum rate while preserving the achievable degrees of freedom. An alternative suboptimal improved subspace design is proposed in [3] where the suboptimal precoding vector is

$$\begin{aligned} V_k(\boldsymbol{\omega}) &= W(\boldsymbol{\omega})\Gamma_k \\ \tilde{\omega}_i &= 3\left(\sum_k \gamma_{ki}\gamma_{ki}^\dagger\right)^{-1} \end{aligned} \tag{2.21}$$

where $\tilde{W} := W^\dagger W$, $\tilde{\omega}_i = |\omega_i|^2$ which is the ith element of the $N\times N$ diagonal matrix $\tilde{W}$ and γ_{ki} is the ith row vector of matrix Γ_k (which is defined in [84]). Both CJ and KT schemes can be further improved by SHV orthonormalization [67].

2.4.4 Performance of SISO IA with perfect CSI

In this section, we compare the average sum rates obtained by the SISO IA schemes with perfect CSI. The SNR in these numerical results is defined as SNR $= \frac{\mathcal{E}}{K}$.

In the first example, we compare the average sum rates by using different receivers discussed in section 2.4.2. The channel is assumed to have i.i.d complex Gaussian distribution, i.e., $H_{kj} \overset{\text{i.i.d.}}{\sim} \mathcal{CN}(0, I_N)$ where each transmitter has $N = 3$ symbol extensions.

Figure 2.4 shows the average sum rate comparison between the CJ scheme with ZF decoder and MMSE decoder after 1000 channel realizations. The ideal average sum rate curve $D_n \log_2(snr)$ is plotted as reference where in case $D_1 = \frac{4}{3}$. It is shown in this figure that the average sum rates with these two decoders are very close to each other at high SNRs. Both decoders achieve almost 10 bits/sec/Hz gain at 50 dB compared with the random precoding vectors scheme. Hence ZF decoder is deployed in the rest of the simulations.

The next example compares the performance of CJ scheme and the suboptimal improved subspace schemes, i.e., KT for a three-user SISO interference channel with $N = 3$. Figure 2.5 shows the average sum rates of various IA schemes after 1000 channel realizations. Observations from this figure show that the KT scheme outperforms the CJ around 1.33 bits/sec/Hz at high SNRs. The gap between the ideal average sum rate curve and KT is around 1.23 bits/sec/Hz.

Then we extended the number of symbol extensions from $N = 3$ to $N = 5$ and $N = 11$. The simulation results are shown in Figure 2.6 and 2.7 where $D_2 \log 2(snr)$

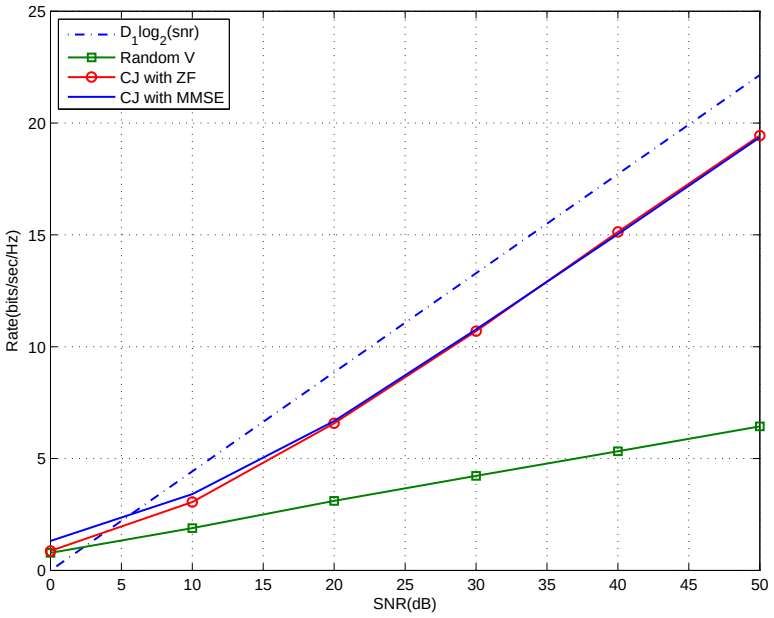

Figure 2.4: Average sum rates of a three-user SISO system with $N = 3$ by using IA schemes with ZF decoders and MMSE decoders.

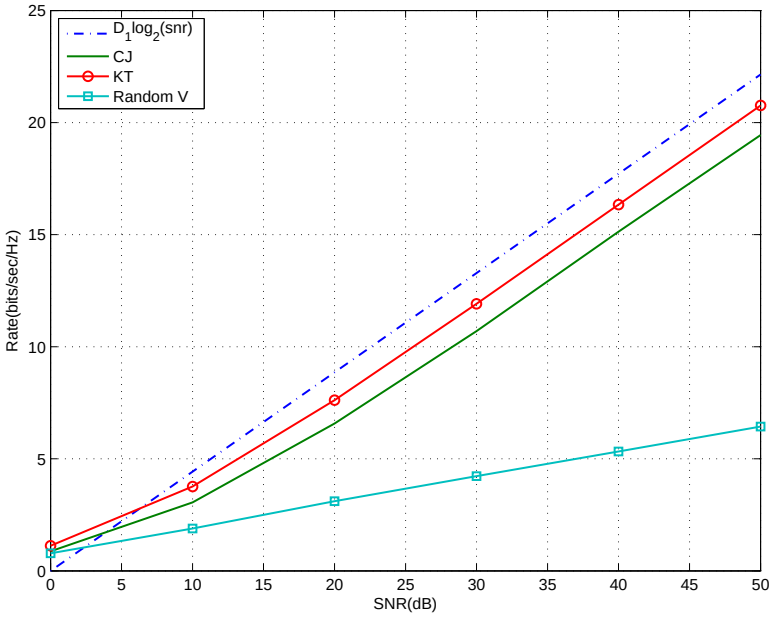

Figure 2.5: Average sum rates of a three-user SISO system with $N = 3$ by using various IA schemes.

and $D_5 \log_2(snr)$ are plotted as references and $D_2 = \frac{7}{5}, D_5 = \frac{16}{11}$. When ZF decoder is deployed, the average sum rate of the KT schemes with $N = 5$ increases by 0.4981 bits/sec/Hz whereas it decreases by 0.0497 bits/sec/Hz with $N = 11$ case compared with $N = 3$. It means that the average sum rate does not increase monotonically with N. In fact, there is an optimal size $N^\star$ for the signal dimension which is $\arg\min_{\lfloor N \rfloor} |(n+1)^L + n^L - K(K-1)|$, where $L = (K-1)(K-2) - 1, N = (n+1)^L + n^L$ and $n \in \mathbb{N}$. In this case, $N = 5$. This optimal signal dimension size is implicit in the proof that for a fixed tolerance δ around the target value of 1/2 DoF per user, as the number of users, K, grows, the logarithm of the size of the signal space needed by the CJ scheme expands as $\Theta(K^2)$. For the details of the proof, we refer the reader to [23]. The performance of the CJ scheme drops significantly compared with the previous case. There is more than 5 bits/sec/Hz loss at 50 dB compared with the CJ in Figure 2.5. Hence for a three-user SISO interference channel, the KT-based schemes are proved to be near-optimal in the average sum rate sense.

The last example in this section shows the performance of a four-user SISO interference channel by using the CJ-based interference alignment schemes. Since the suboptimal subspace optimal solutions proposed in [84] are derived only for three-user SISO interference channels, these solutions cannot be used for the cases where $K > 3$. Figure 2.8 shows the average sum rate for a four-user SISO interference channel with $N = 33$ by using the original CJ (without SHV orthonormalization) and CJ schemes. In this case, the slope of the ideal average sum rate is $D_1 = \sum_i^4 d_i = \frac{35}{33}$ where $\begin{bmatrix} d_1 & d_2 & d_3 & d_4 \end{bmatrix} = \begin{bmatrix} \frac{32}{33} & \frac{1}{33} & \frac{1}{33} & \frac{1}{33} \end{bmatrix}$. It seems to be surprising that the performance of the original CJ scheme is very close to the random precoding vector cases while the CJ still provides significant gain in average

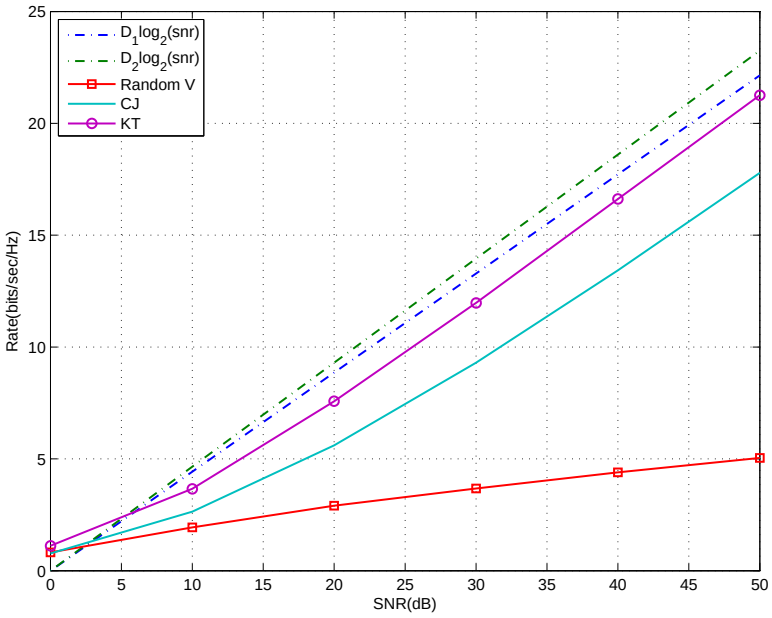

Figure 2.6: Average sum rates of a three-user SISO system with $N = 5$ by using various IA schemes.

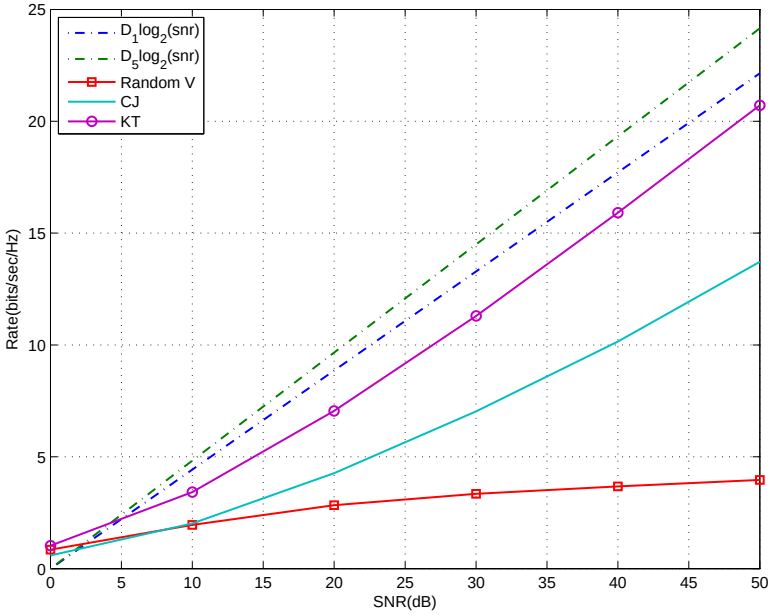

Figure 2.7: Average sum rates of a three-user SISO system with $N = 11$ by using various IA schemes.

sum rate performance. This can be explained by the structure of the solution. For example, V_1 is a 33×32 matrix. Even though the interference from other users can be cancelled at receiver 1, the 32 columns of V_1 will end up interfering with each other when they arrive at receiver 1. The CJ scheme solves this problem by apply SHV orthonormalization and therefore results in significant improvement in the performance.

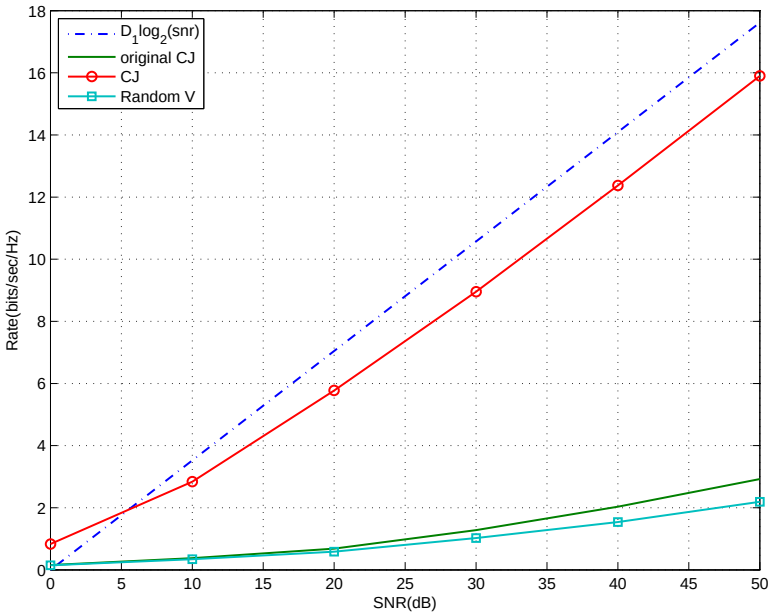

Figure 2.8: Average sum rates of a four-user SISO system with $N = 33$ by using various CJ-based IA schemes.

2.4.5 A causal implementation procedure of SISO IA

Since all discussions so far are under the assumption that global channel state information is known, it is natural to question the feasibility and robustness of the suboptimal schemes in the previous sections with imperfect channel information, for example, imperfect phase estimates and amplitude estimates.

Starting from a causal implementation procedure of SISO IA and the simplest channel estimation error model, i.e., circularly symmetric channel estimation errors, we will first compare its average interference leakage performance and the average sum rate performance with the perfect channel estimation. Then we will extend the model to have non-i.i.d. amplitude/phase estimation errors.

Recall equation (2.6). It indicates that the closed-form solution for SISO IA requires the knowledge of the current and the future CSI. The non-causality property of this solution makes the implementation impossible. Thus this SISO IA technique becomes unattractive to many engineers.

In this section, a causal implementation of a three-user SISO IA system with N symbol extensions will be discussed by using the closed-form solution. Although only $\frac{1}{N}$ of the precoding vectors can be obtained per feedback based on the current channel estimates, the system is able to compute all the precoding vectors after the feedback stage and then transmit the symbol.

In order to keep the analysis simple, we assume $N = 3$ and thus V_1 is 3×2, V_2 and V_3 are 3×1 matrices. Figure 2.9 illustrates the three-stage procedure of the causal implementation:

1. At the TDMA training stage, each transmit node sends channel tones separately to the receivers in order to avoid interference and get better channel estimates. All receive nodes have the corresponding channel estimates at the end of the training stage.

2. The receivers start to broadcast the estimated CSI back to the transmit nodes separately. By the end of the feedback stage, all three transmit nodes

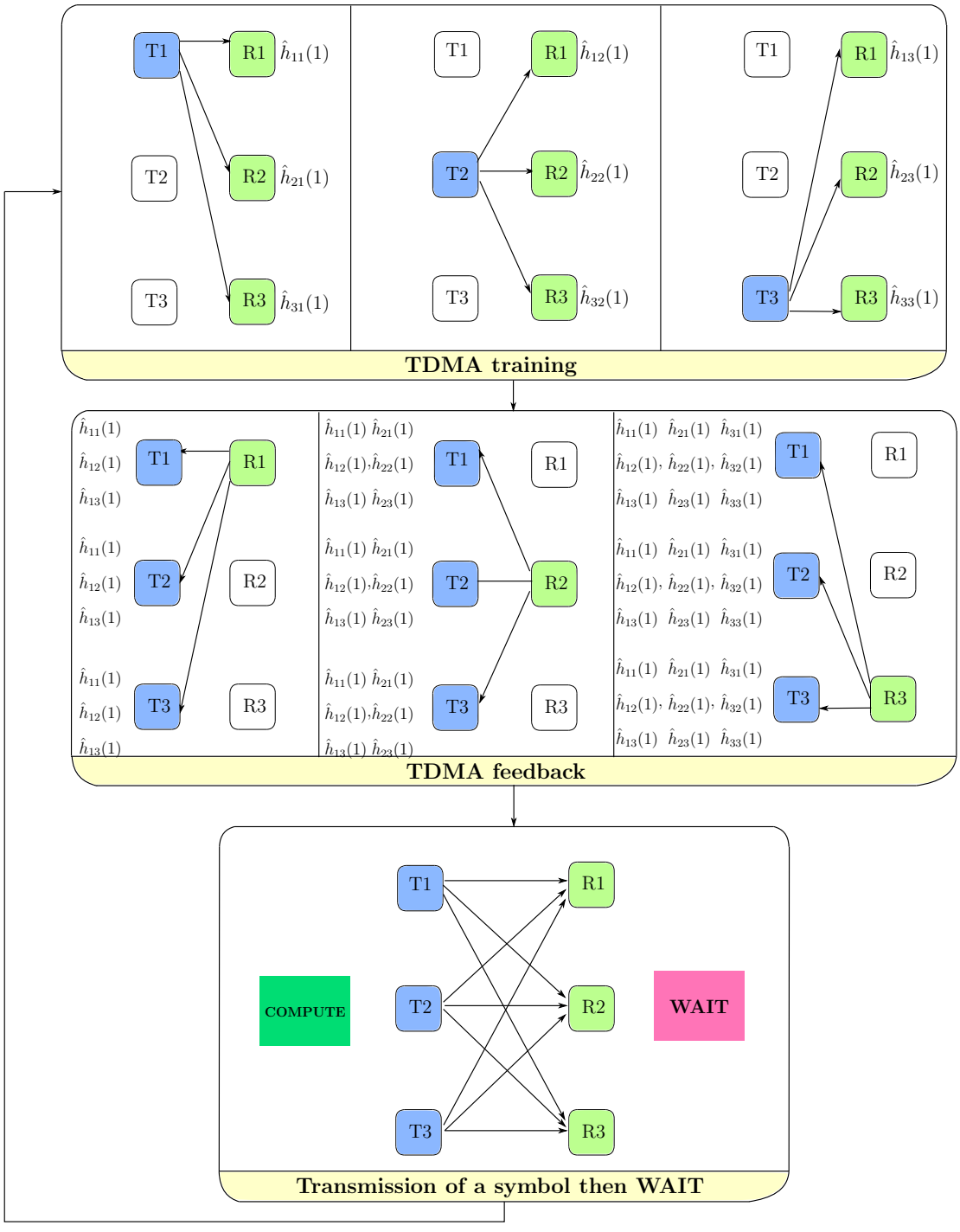

Figure 2.9: A three-stage procedure of the causal three-user SISO IA implementation.

have the channel estimates.

3. Based on the feedback CSI, the first row of precoding vectors can be computed according to the closed-form solution. Hence part of the symbol can be transmitted. After the transmission is complete, the system waits for a sufficient long period and then repeats stage 1 to 3 to compute the next row of the precoding vectors until the whole precoding vectors are obtained by the transmit nodes.

Figure 2.9 helps to explain this procedure in more details. With perfect CSI, the precoding solutions proposed by CJ for a three-user SISO IA with $N = 3$ are as follows

$$V_1 := A$$
$$V_2 := (H_{32})^{-1} H_{31} C$$
$$V_3 := (H_{23})^{-1} H_{21} B$$

where

$$T := H_{12}(H_{21})^{-1} H_{23}(H_{32})^{-1} H_{31}(H_{13})^{-1}$$
$$A := \Big[\boldsymbol{\omega} \quad T\boldsymbol{\omega}\Big]_{3\times 2},$$
$$B := \Big[T\boldsymbol{\omega}\Big]_{3\times 1},$$
$$C := \Big[\boldsymbol{\omega}\Big]_{3\times 1}$$
$$\boldsymbol{\omega} = \begin{bmatrix} 1 & 1 & 1 \end{bmatrix}^{\top}.$$

Since H_{kj} are 3×3 diagonal matrices, let $T = \texttt{diag}(t_i)$ where $i \in \{1, 2, 3\}$. V_k

can be further simplified as

$$V_1 = \begin{bmatrix} 1 & t_1 \\ 1 & t_2 \\ 1 & t_3 \end{bmatrix}, V_2 = \begin{bmatrix} \frac{h_{31}(1)}{h_{32}(1)} \\ \frac{h_{31}(2)}{h_{32}(2)} \\ \frac{h_{31}(3)}{h_{32}(3)} \end{bmatrix}, V_3 = \begin{bmatrix} t_1 \frac{h_{23}(1)}{h_{23}(1)} \\ t_2 \frac{h_{23}(2)}{h_{23}(2)} \\ t_3 \frac{h_{23}(3)}{h_{23}(3)} \end{bmatrix} \tag{2.22}$$

where $H_{kj} = \texttt{diag}(h_{kj}(i))$ and $t_i = \frac{h_{12}(i)h_{23}(i)h_{31}(i)}{h_{21}(i)h_{32}(i)h_{13}(i)}, i \in \{1, 2, 3\}$.

Observation of equation (2.22) suggests that the i^{th} row of the precoding vectors is only relevant to the i^{th} row of the estimated CSI. So after the TDMA training and the feedback stage, the precoding vectors are

$$\hat{V}_1 = \begin{bmatrix} 1 & \hat{t}_1 \\ 1 & * \\ 1 & * \end{bmatrix}, \hat{V}_2 = \begin{bmatrix} \frac{\hat{h}_{31}(1)}{\hat{h}_{32}(1)} \\ * \\ * \end{bmatrix}, \hat{V}_3 = \begin{bmatrix} \hat{t}_1 \frac{\hat{h}_{23}(1)}{\hat{h}_{23}(1)} \\ * \\ * \end{bmatrix}, \tag{2.23}$$

$$\hat{t}_1 = \frac{\hat{h}_{12}(1)\hat{h}_{23}(1)\hat{h}_{31}(1)}{\hat{h}_{21}(1)\hat{h}_{32}(1)\hat{h}_{13}(1)} \tag{2.24}$$

where $\hat{(\cdot)}$ denotes the estimates or quantities computed based on the estimates and $*$ denotes the terms that are temporarily unavailable. But it is clear that all these precoding vectors can be obtained by repeating the three-stage procedure.

Since after the feedback stage, each transmitter only knows $\hat{H}_{kj}$. The precoding vectors $\hat{V}_j$ and the decoding vectors $\hat{U}_k$ are computed based on $\hat{H}_{kj}$. The estimated average sum rate can be computed by equations (2.10),(2.11) and the estimated average interference leakage can be obtained by equations (2.16), (2.17).

2.4.6 Performance of SISO IA with imperfect CSI

Two channel estimation error models are discussed in this section and simulation results of SISO IA systems with different channel estimation errors are provided.

Circularly symmetric channel estimation error model

Consider the CSI estimation error follows the circularly symmetric Gaussian distribution. The estimated channel is

$$\hat{H}_{kj} = H_{kj} + W_{kj} \tag{2.25}$$

where $W_{kj} \overset{\text{i.i.d}}{\sim} \mathcal{CN}(0, \sigma_W^2 I_N)$.

The average interference leakage can be written as

$$\hat{I}_{\text{ave-IA}} = \frac{1}{N}\mathrm{E}\left[\sum_{k=1}^{K}\sum_{j=1,j\neq k}^{K}\frac{\mathcal{E}}{K}\mathrm{Tr}\left[\hat{U}_k^{\dagger}W_{kj}\hat{V}_j\hat{V}_j^{\dagger}W_{kj}^{\dagger}\hat{U}_k\right]\right] \tag{2.26}$$

$$= \frac{1}{N}\mathrm{E}\left[\sum_{k=1}^{K}\mathrm{Tr}\left[\hat{U}_k^{\dagger}\hat{Q}_{Wk}\hat{U}_k\right]\right] \tag{2.27}$$

where

$$\hat{Q}_{Wk} = \sum_{j=1,j\neq k}^{K}\frac{\mathcal{E}}{K}W_{kj}\hat{V}_j\hat{V}_j^{\dagger}W_{kj}^{\dagger}.$$

Suppose $\hat{U}_k$ does not suppress the interference at all. The maximum estimated

average interference leakage is

$$\begin{aligned}\hat{I}_{\text{ave}-\text{IA}-\max} &= \frac{1}{N}\mathrm{E}\left[\sum_{k=1}^{K}\mathrm{Tr}\left[\hat{Q}_{Wk}\right]\right] \\ &= \frac{1}{N}\mathrm{E}\left[\sum_{k=1}^{K}\mathrm{Tr}\left[\sum_{j=1,j\neq k}^{K}\frac{\mathcal{E}}{K}W_{kj}\hat{V}_j\hat{V}_j^{\dagger}W_{kj}^{\dagger}\right]\right] \\ &= \frac{\mathcal{E}}{KN}\sum_{k=1}^{K}\mathrm{E}\left[\mathrm{Tr}\left[\sum_{j=1,j\neq k}^{K}\hat{V}_j^{\dagger}W_{kj}^{\dagger}W_{kj}\hat{V}_j\right]\right] \\ &= \frac{\mathcal{E}}{KN}KN\sigma_W^2 \\ &= \mathcal{E}\sigma_W^2.\end{aligned}$$

Hence the approximation for average interference leakage in dBm/sec/Hz is

$$\hat{I}_{\text{ave}-\text{IA}-\max} = 10\log\left(\mathcal{E}\sigma_W^2\right) + 30 \tag{2.28}$$

and it is linear affine with σ_W^2.

Non-i.i.d. amplitude/phase estimation error model

Unlike the simple CSI estimation error in (2.25), the new channel estimate is modelled as

$$\hat{h}_{kj}(i) = \left(|h_{kj}(i)| + W_a(i)\right)e^{j\left(\measuredangle h_{kj}(i)+W_\phi(i)\right)} \tag{2.29}$$

where $W_a(i) \overset{\text{i.i.d.}}{\sim} \mathcal{N}(0,\sigma_{W_a}^2)$ and $W_\phi(i) \overset{\text{i.i.d.}}{\sim} \mathcal{N}(0,\sigma_{W_\phi}^2)$, $i \in \{1,2,\cdots,N\}$.

The rest of this section provides several simulation results of SISO IA systems with different channel estimation errors.

In the first example, the circularly symmetric channel estimation error model is considered for a three-user interference system. The channels are assumed to be

$H_{kj} \overset{\text{i.i.d.}}{\sim} \mathcal{CN}(0, I_N)$ where the symbol extensions $N = 3$. After 1000 channel/noise realizations, the average interference leakage and the average sum rate are plotted in Figure 2.10 at 40 dB.

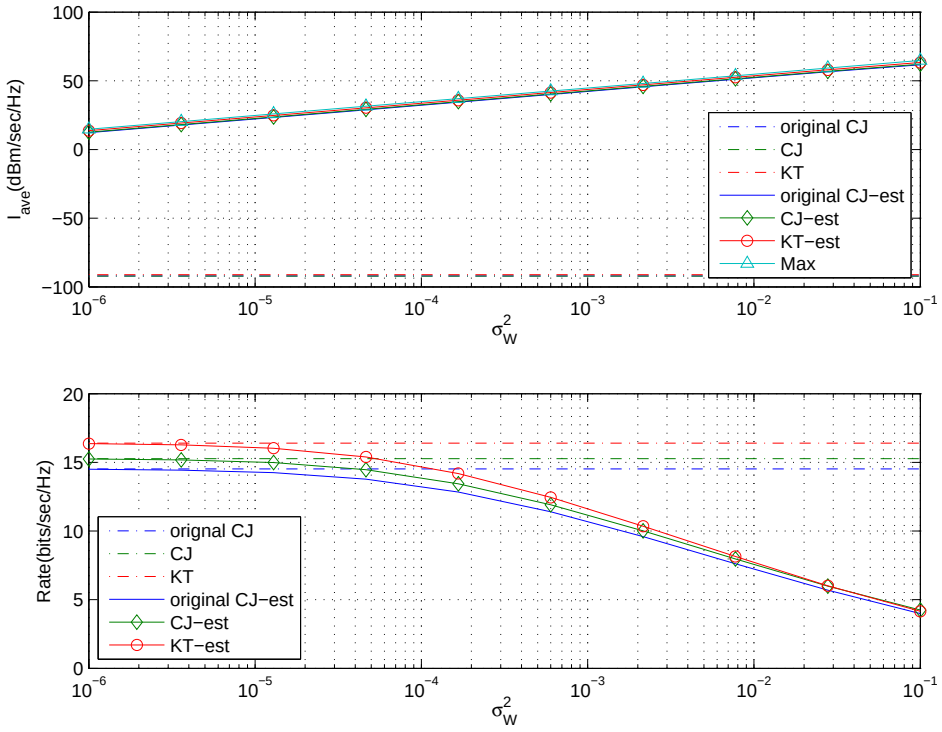

Figure 2.10: The average interference leakage and average sum rate of a three-user SISO system with $N = 3$ at 40 dB.

Observation of the average interference leakage curves show that when perfect CSI is assumed, all the schemes achieve almost zero interference leakages. The maximum estimated average interference leakages with channel estimation errors are shown to have the greatest leakage compared with other schemes.

In the average sum rate plot, noticeable improvements can be observed by using CJ scheme rather than using the original CJ scheme. These improvements can be found in both perfect CSI case and the imperfect CSI case. Further improve-

ments are made by using the KT scheme. The gap between the KT-est and the original CJ-est is approximately 0.2129 bits/sec/Hz at $\sigma_W^2 = 0.1$. The difference between KT and KT-est is about 10.0185 bits/sec/Hz at $\sigma_W^2 = 0.1$. The sum rate performance of all three schemes decrease with increasing σ_W^2.

Like that of the previous figure, plots in Figure 2.11 show the average interference leakage and the average sum rate performance of the $N = 3$ SISO IA system at SNR=15 dB. It can be seen that the maximum estimated average interference leakages preserves the linear affine feature at lower SNR and the leakage is around 30 dBm/sec/Hz less than that of the 40 dB case. The average sum rate performance seems to be 10 bits/sec/Hz worse than the 40 dB case. Hence better sum rate performance can be achieved at higher SNR. We can also conclude that the average sum rate is more sensitive to the estimation error at high SNR. Among the three IA schemes, the $\hat{R}_{\text{ave}}$ of KT-est outperforms the other two schemes by approximately 0.3615 bits/sec/Hz and 0.6738 bits/sec/Hz respectively at $\sigma_W^2 = 0.1$.

Next, we examine the average interference leakage and average sum rate performance of KT scheme with different number of symbol extensions $N = 3, 5, 11$. The results in Figure 2.12 show that the interference leakage curves increase with growing σ_W^2 and gradually flatten out. The interference leakages with $N = 3, 5, 11$ are almost the same. The average sum rate plots suggest that the KT with $N = 5$ yields the best performance while $N = 3$ outperforms $N = 11$. For $N = 5$, the gap between the KT and KT-est at $\sigma_W^2 = 0.1$ is 12.7158 bits/sec/Hz.

Now consider non-i.i.d. amplitude/phase estimation error model for a three-user SISO system with $N = 3$ and the variances of the estimation errors are generated as

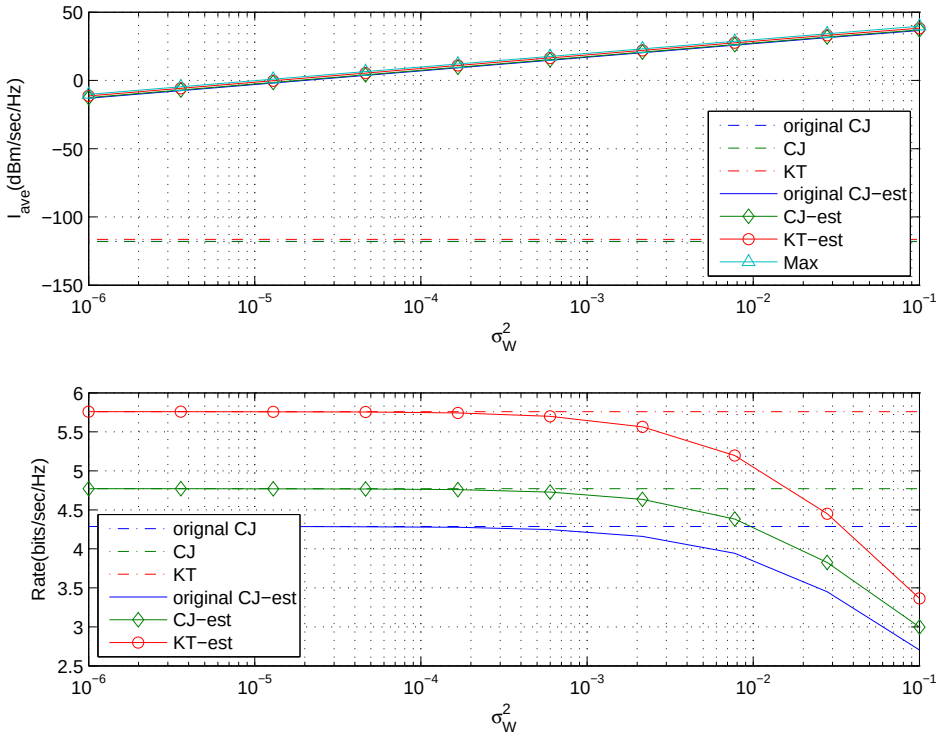

Figure 2.11: The average interference leakage and average sum rate of a three-user SISO system with $N = 3$ at 15 dB.

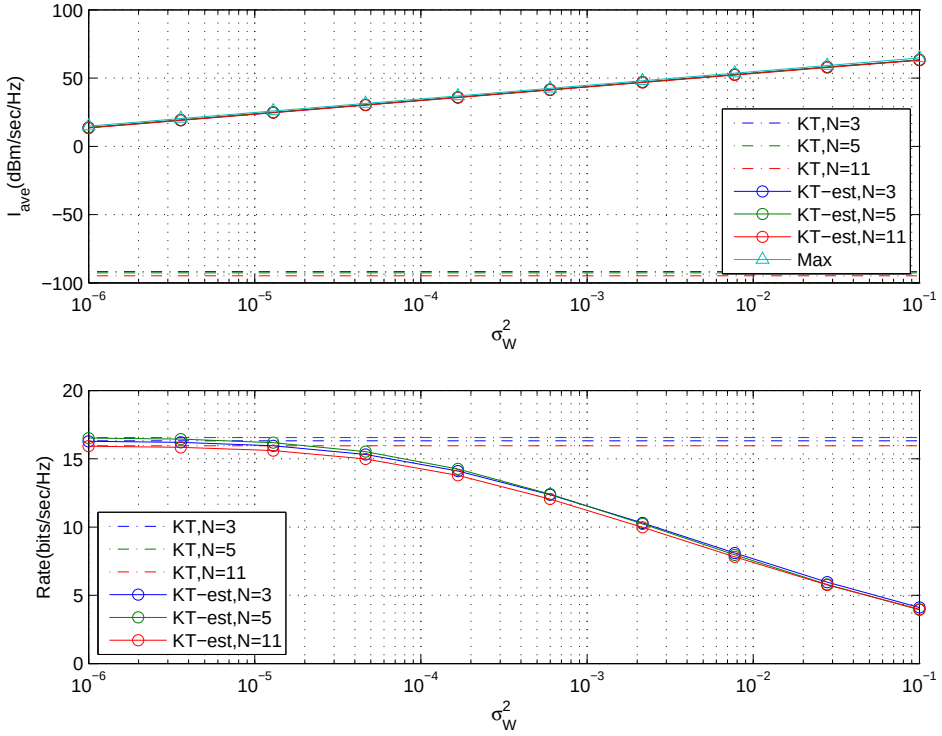

Figure 2.12: The average interference leakage and average sum rate of a three-user SISO system with $N = 3, 5, 11$ at 40 dB.

1. 30 equally logspaced $\sigma^2_{W_a}(i) \in [0.5 \times 10^{-6}, 0.05]$,

2. 30 equally logspaced $\sigma^2_{W_\phi}(i) \in [0.5 \times 10^{-6}, 0.05]$.

After 100 iterations are performed for each $\left(\sigma^2_{W_a}(i), \sigma^2_{W_\phi}(i)\right)$ pair, the contours of the average interference leakage and the sum rates by using the KT scheme are shown in Figure 2.13. While $\hat{I}_{\text{ave}}$ grows with increasing $\left(\sigma^2_{W_a}(i), \sigma^2_{W_\phi}(i)\right)$, $\hat{R}_{\text{ave}}$ decreases. It seems that $W_a(i)$ and $W_\phi(i)$ have similar effects on the IA performance and the worse of $W_a(i), W_\phi(i)$ dominates the performance.

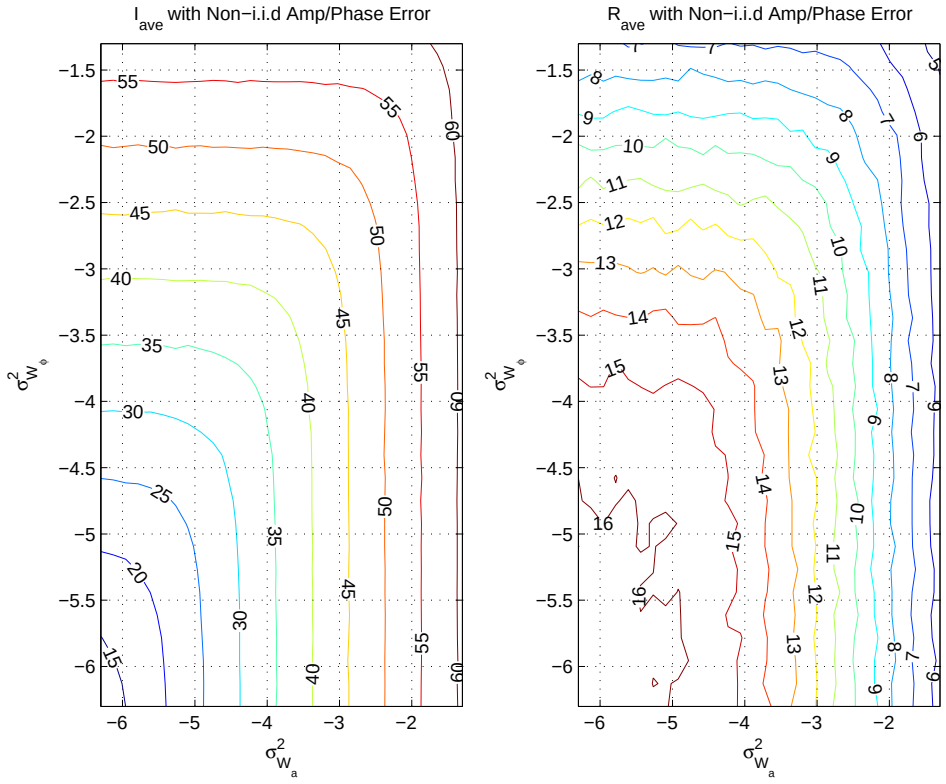

Figure 2.13: The contour plot of the average interference leakage and the average sum rate of KT-est with $N = 3$ and 40 dB.

To confirm that the performance of IA depends on the worse of $\sigma^2_{W_a}(i), \sigma^2_{W_\phi}(i)$, we check two cases: $\sigma^2_{W_a} \gg \sigma^2_{W_\phi}$ and $\sigma^2_{W_a} \ll \sigma^2_{W_\phi}$. Therefore, with the same

simulation setup, the following parameters are used:

1. When $\sigma^2_{W_a} \gg \sigma^2_{W_\phi}$: 30 equally logspaced $\sigma^2_{W_a}(i) \in [0.1, 0.5]$; 30 equally logspaced $\sigma^2_{W_\phi}(i) \in [10^{-6}, 10^{-4}]$.

2. When $\sigma^2_{W_a} \ll \sigma^2_{W_\phi}$: 30 equally logspaced $\sigma^2_{W_\phi}(i) \in [0.1, 0.5]$; 30 equally logspaced $\sigma^2_{W_a}(i) \in [10^{-6}, 10^{-4}]$.

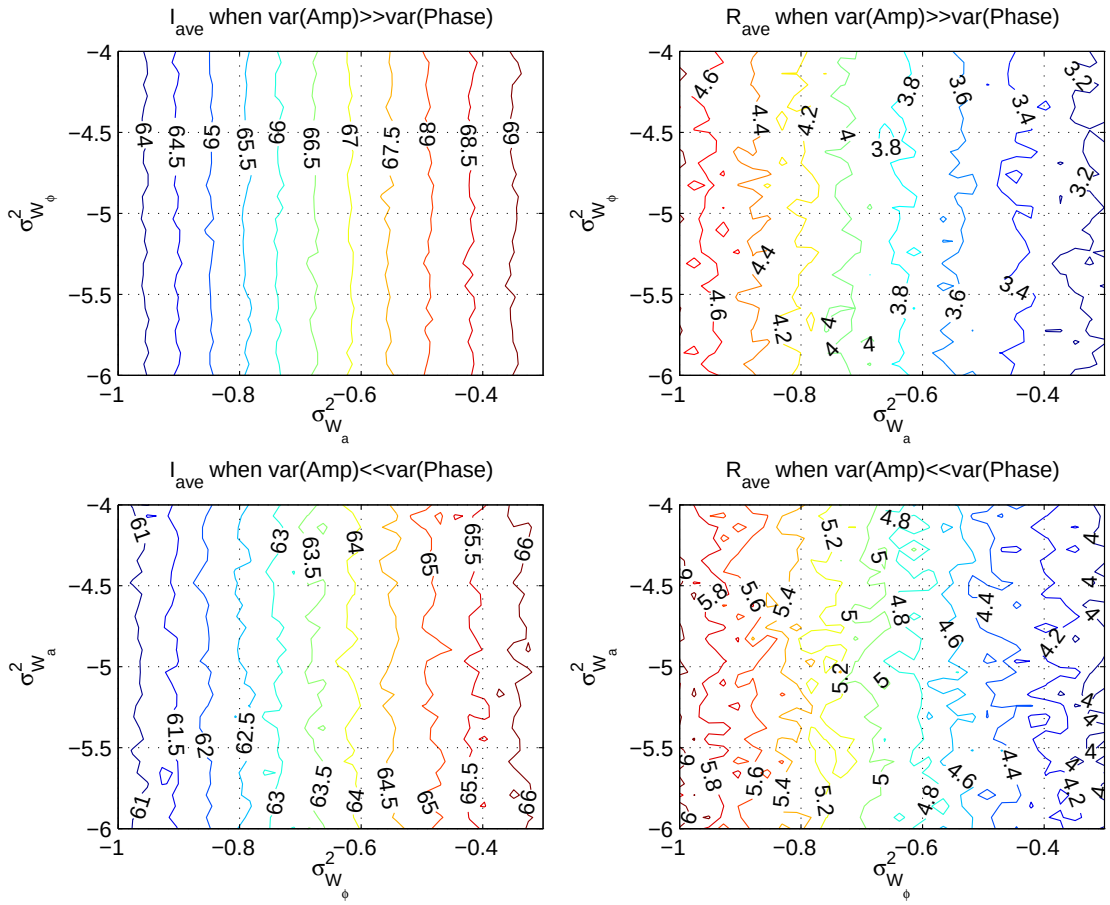

Figure 2.14: The contour plots of the average interference leakage and the average sum rate by using KT scheme. (Notice that the x-axis and the y-axis are switched for the top and bottom plots.)

Figure 2.14 shows the average interference leakage and the average sum rate

of KT scheme. The interference leakage plots on the left-hand side suggest that the worse error variance dominates the leakage performance since almost the same performance can be achieved on the y-axis and the leakage curves mainly vary along the x-axis. We can see that the greater the error variance, the greater the interference leakage is. A similar trend can be observed in the average sum rate plots but the rate grows in a reverse way. Comparing the top and bottom cases in the same range, we can conclude that the error variance of the amplitude $\sigma^2_{W_a}$ has more impact on the IA performance than the phase σ^2_{ϕ}.

2.5 Comparison between Opportunistic Transmission and the SISO IA

In this section, we compare the average sum rates obtained by opportunistic transmission and the SISO IA schemes by using ZF decoders with imperfect CSI. The SNR in these numerical results is defined as SNR $= \frac{\mathcal{E}}{K}$ with $K = 3$ in all of the tested cases.

In the first example, a 3-user SISO interference channel is assumed in the system where each transmitter has $N = 3$ symbol extensions. Channel coefficients are drawn temporarily and spatially i.i.d. from a complex Gaussian distribution, i.e., $h_{kj}(t) \overset{\text{i.i.d.}}{\sim} \mathcal{CN}(0, I_N)$. Independent circularly symmetric complex channel estimation errors denoted $w_{kj}(t) \overset{\text{i.i.d.}}{\sim} \mathcal{CN}(0, \sigma^2_W)$ as are assumed. 1000 channel realizations are generated and 1000 noise realizations are generated for each σ^2_W value.

As shown in Figure 2.15 for $N = 3$, the KT SISO IA scheme achieves the highest average sum rate as 16.03 bits/sec/Hz which has a gain of 0.57 bits/sec/Hz over the OT and a gain of 1.35 bits/sec/Hz over CJ respectively at 40 dB SNR. When channel estimation error is considered, the average data rate performance decreases as expected. Compared with KT-est, OT-est is about 1 bits/sec/Hz worse when $\sigma_W^2 \leq 10^{-4}$. However, the OT-est outperforms KT-est when the channel estimates get worse. When $\sigma^2 > 10^{-4}$, OT-est starts to outperform KT-est and is also robust to the bad channel estimates. As σ_W^2 increases, OT-est converges to the RND scheme which picks a random user to transmit at full energy. The two SISO IA schemes shown in Figure 2.15 perform worse than RND when $\sigma_W^2 > 0.1$.

Figure 2.16 shows the same simulation as Figure 2.15 except the SNR is now set to 15 dB. Here we see opportunistic transmission performing better than both SISO IA schemes. The average sum rate for KT is almost 1.76 bits/sec/Hz worse than the OT. This gain maintains for the imperfect CSI cases, i.e., OT-est always at least 1 bits/sec/Hz better than KT-est. Again, OT-est converges to RND as σ_W^2 increases.

Figure 2.17 shows the average sum rate performance for the 3-user SISO IA with $N = 5$ symbol extensions at 40 dB. Compared with Figure 2.15, KT is about 0.45 bits/sec/Hz better than the $N = 3$ case and OT-est starts to outperform KT-est around $\sigma_W^2 = 10^{-4}$. The CJ, however, is 1.47 bits/sec/Hz worse than that in the $N = 3$ case. Hence increasing the number of symbol extensions N does not always improve the average sum rate performance. Even for the KT scheme, the average sum rate will drop when N is greater than the number of sources of interference, i.e. $K(K-1)$.

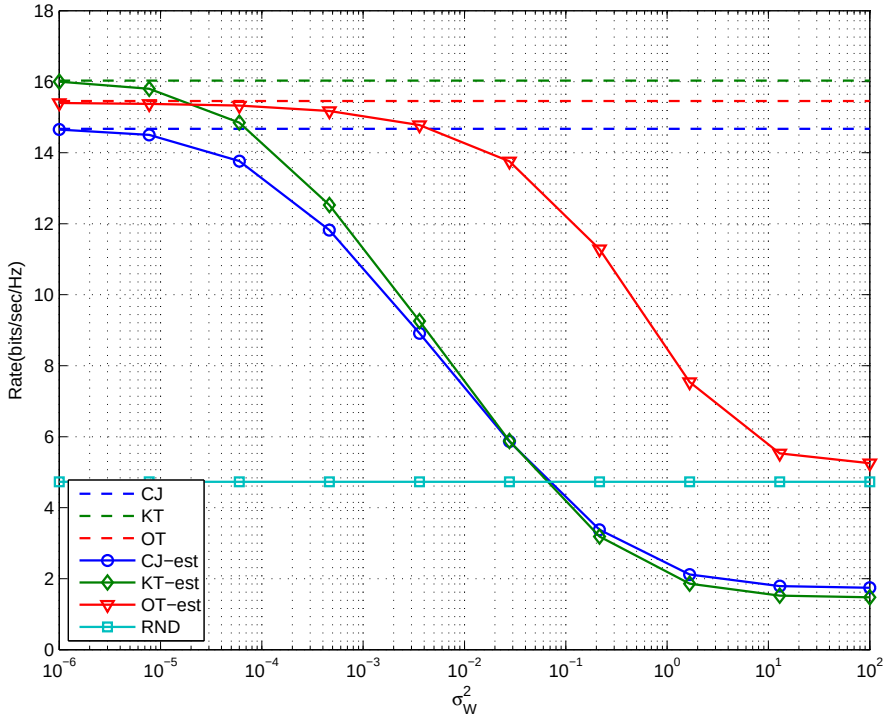

Figure 2.15: Average sum rate versus channel estimation error variance for 3-user opportunistic transmission and SISO IA with $N = 3$ symbol extensions at 40 dB SNR.

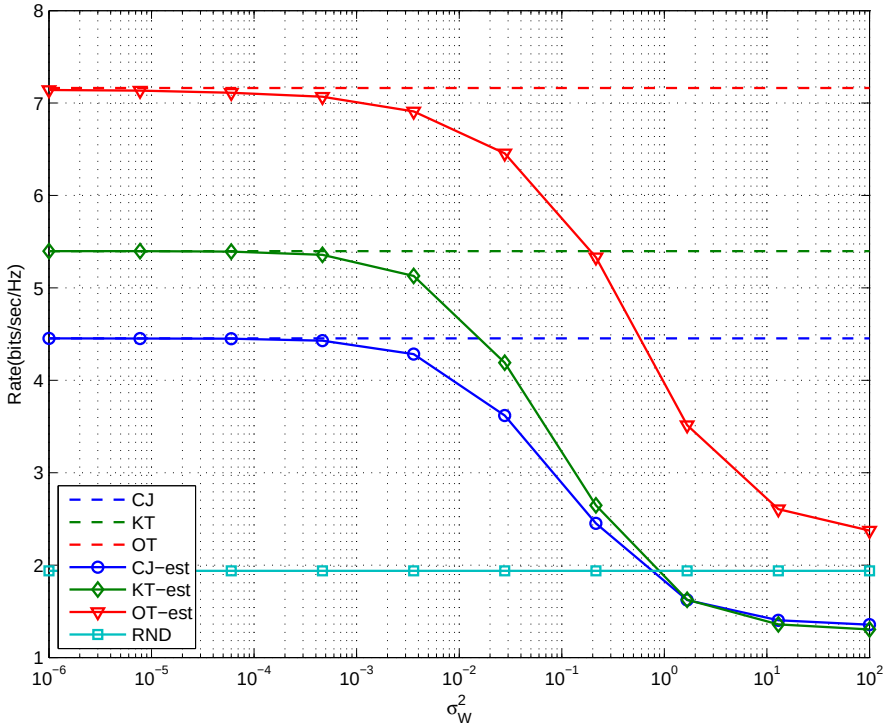

Figure 2.16: Average sum rate versus channel estimation error variance for 3-user opportunistic transmission and SISO IA with $N = 3$ symbol extensions at 15 dB SNR.

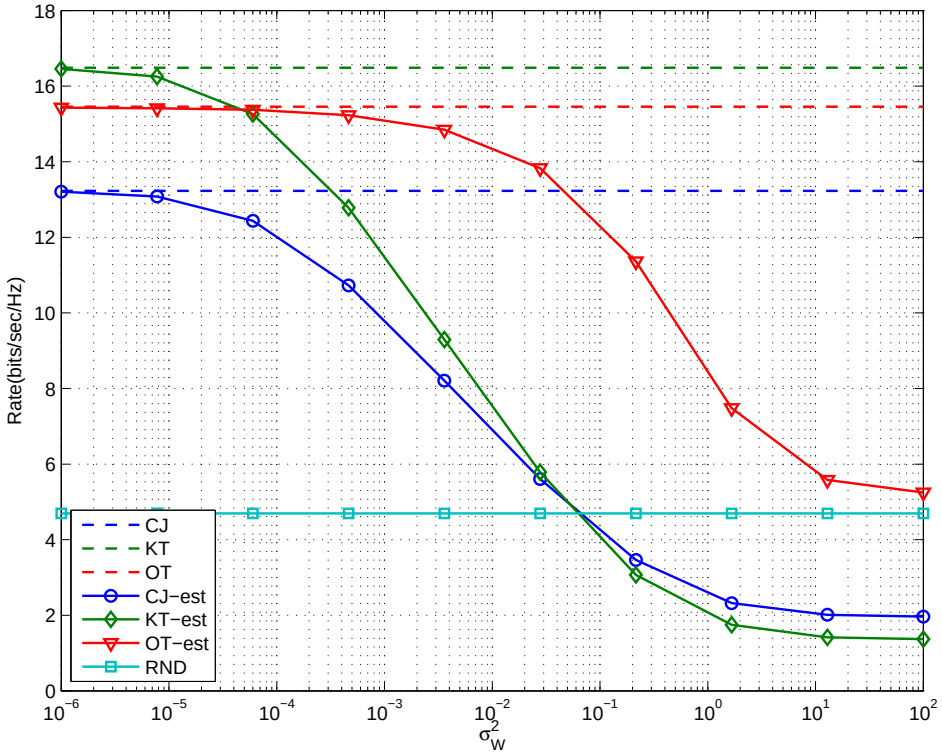

Figure 2.17: Average sum rate versus channel estimation error variance for 3-user opportunistic transmission and SISO IA with $N = 5$ symbol extensions at 40 dB SNR.

In the remaining results, we directly compare the sum rate of different schemes by varying SNR from 0 to 40 dB and channel estimation error variance $\sigma_W^2 \in \left[10^{-6}, 1\right]$. 1000 channel/noise realizations are performed for each (SNR, σ_W^2) pair. For $N = 3$ symbol extensions, the difference of the average sum rate between OT and CJ and OT and KT are compared in Figure 2.18 and 2.19, respectively. A positive contour indicates that the OT outperforms IA techniques in terms of average sum rate, whereas a negative contour indicates that IA is better. Between the two IA schemes, KT achieves slightly larger performance advantage area over OT in the regime of good channel estimates and high SNR, i.e., $\sigma_W^2 < 10^{-4}$ and SNR>30 dB. With low SNR and/or poor channel estimates, i.e., SNR<30 dB and/or $\sigma_W^2 > 10^{-4}$, OT has the best sum rate performance amongst all schemes considered here. Figure 2.20 shows the difference of the average sum rate between OT and KT for the case with $N = 5$ symbol extensions. As can be seen, KT has slightly better performance than the $N = 3$ case at high SNR and in the low σ_W^2 regime. Otherwise, the results are similar to those seen in the $N = 3$ case. When the SNR is low or the channel estimates are bad, opportunistic transmission achieves better sum rate performance than either SISO IA scheme.

2.6 Conclusions

In this chapter, we have compared opportunistic transmission with a low complexity subspace suboptimal IA technique based on the 3-user SISO IA scheme proposed in [1]. In the case of interference alignment, channel estimation errors cause interference leakage which consequently results in a loss of achievable rate whereas in the case of opportunistic transmission, channel estimation errors result

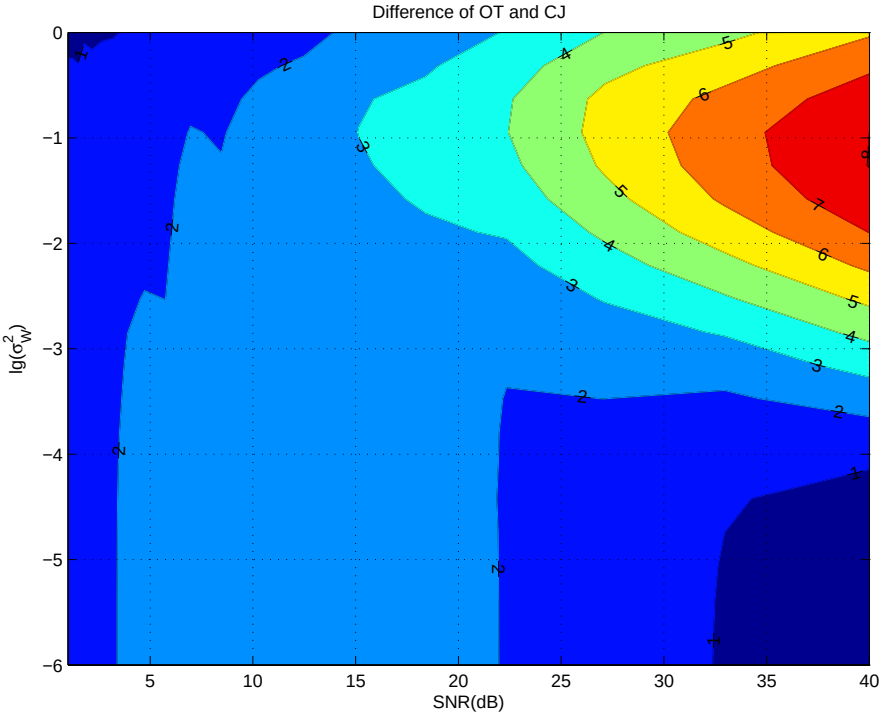

Figure 2.18: The difference of the average sum rate between OT and CJ with $N = 3$ symbol extensions.

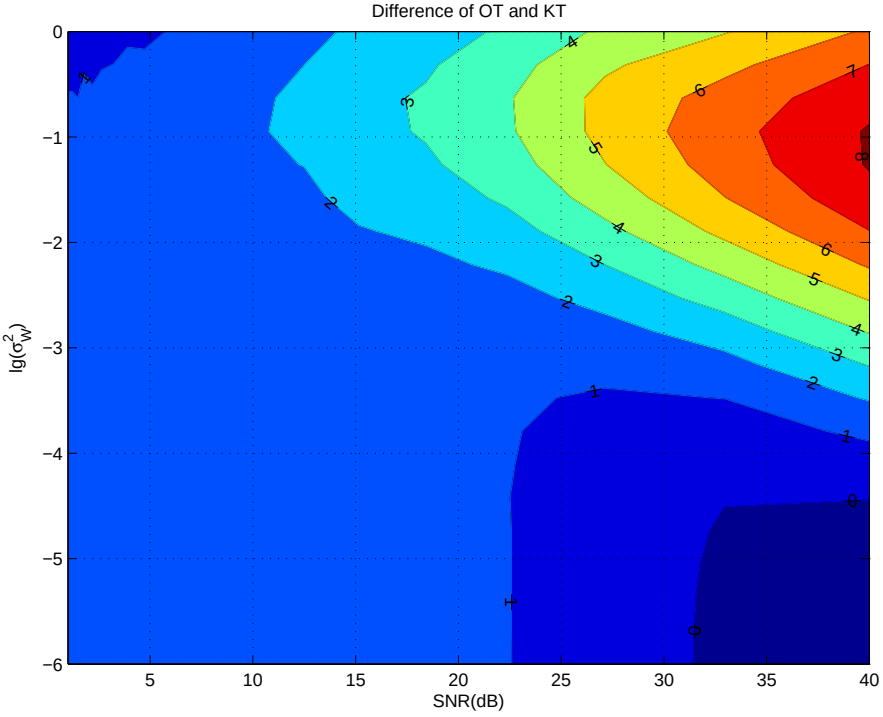

Figure 2.19: The difference of the average sum rate between OT and KT with $N = 3$ symbol extensions.

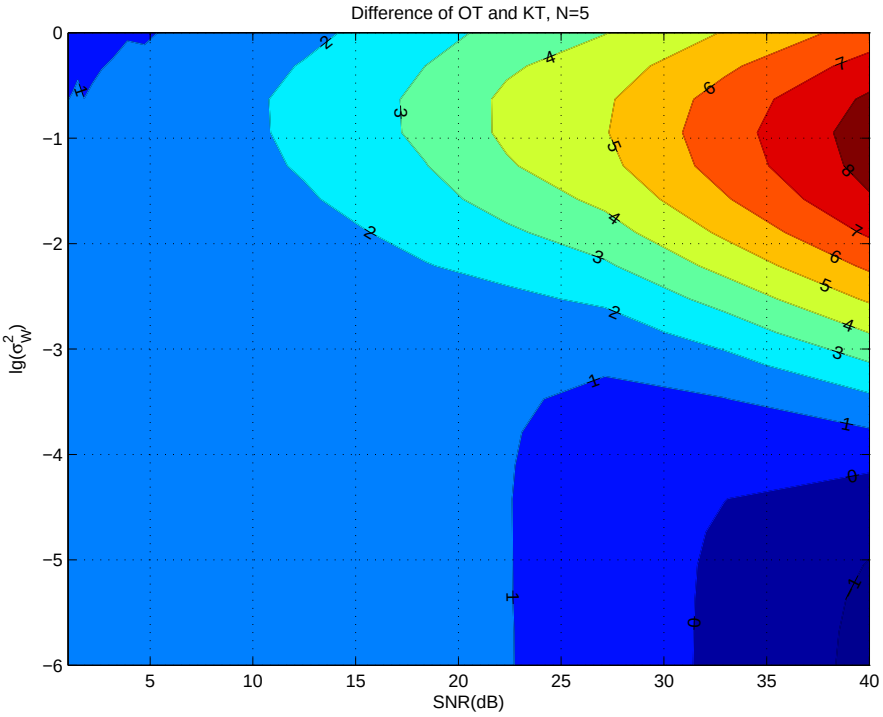

Figure 2.20: The difference of the average sum rate between OT and KT with $N = 5$ symbol extensions.

in a non-zero probability of incorrectly choosing the node with the best channel.

Simulation results show that opportunistic transmission outperforms SISO IA in low SNR conditions and when channel estimates are poor. SISO IA based on [1] or [3] with SHV orthonormalization tends to perform better at high SNR with good channel estimates.

Chapter 3

Distributed Reception with Coarsely-Quantized Observation Exchanges

This chapter considers the problem of jointly decoding binary phase shift keyed (BPSK) messages from a single distant transmitter to a cooperative receive cluster connected by a local area network (LAN). An approximate distributed receive beamforming algorithm is proposed based on the exchange of coarsely-quantized observations among some or all of the nodes in the receive cluster. By taking into account the differences in channel quality across the receive cluster, the quantized information from other nodes in the receive cluster can be appropriately combined with locally unquantized information to form an approximation of the ideal receive beamformer decision statistic. The LAN throughput requirements of this technique are derived as a function of the number of participating nodes in the receive cluster, the forward link code rate, and the quantization parameters. Using information-theoretic analysis and simulations of an LDPC coded system in fading channels, numerical results show that the performance penalty (in terms of outage probability and block error rate) due to coarse quantization is small in the low SNR regimes enabled by cooperative distributed reception. An analytical approximation of upper/lower bound for the outage probability are discussed which provide a pretty fast way to compute the outage probability for a system with arbitrary number of receive nodes at given SNR value.

3.1 Background

Originated from the idea of diversity reception [32,85–87], distributed reception is a technique where multiple receivers in a wireless network combine their observations to increase diversity and power gain and, consequently, improve the probability of successfully decoding noisy transmissions. Distributed reception has been used historically in the context of aperture synthesis for radio astronomy, e.g. the Very Large Array [39], where each antenna typically forwards observations over a high-speed optical backhaul network to a processing center for subsequent alignment and combining. The advantages of this approach are well-documented and include improved resolution as well as signal-to-noise (SNR) gains.

More recently, the idea of distributed reception has been considered for wireless networks with limited backhaul capabilities. A simple form of distributed reception, i.e. soft handoff [40], has been successfully used in cellular systems since the 1990s. Recent information-theoretic studies [42–45] have shown that more sophisticated distributed reception techniques have potential to increase diversity, improve capacity, and improve interference rejection, even with tight backhaul constraints. Several techniques have been proposed to achieve these gains including link-layer iterative cooperation [46,47,88], distributed iterative receiver message-passing [49], and most-reliable/least-reliable bit exchange iterative decoding [50–55]. A limitation of all of these techniques is that they are based on iterative transmissions and decoding. As such, the backhaul requirements are variable and the decoding latency can be significant if the number of iterations is large. The focus of these studies is also often on achieving diversity gains, rather than SNR gains. SNR gains through distributed receive beamforming are particularly appealing since they can

be linear in the number of receivers and allow for longer-range and/or higher-data rate communication as well a reduction in the size, weight, power and cost of the transmitter.

In this dissertation, we consider the problem jointly decoding binary phase shift keyed (BPSK) messages from a single distant transmitter to a cooperative receive cluster with a conventional LAN comprising the backhaul. We show that exchanging quantized observations among the nodes in the receive cluster can provide a simple but powerful approach for non-iterative, fully-distributed reception over a LAN with limited capacity. Unlike most-reliable/least-reliable bit exchange techniques in which information is transmitted over the backhaul/LAN based on requests from other receivers, our approach is for receivers to quantize each demodulated bit (prior to decoding) and broadcast all of these quantized values to the other receivers in the cluster. A naive implementation with fine-grained quantization of the observations at each receiver can generate large amounts of LAN traffic. For example, in a 10 node cluster with a rate $r = 1/2$ forward link code and $b = 16$ bits per observation, the LAN would need to support a normalized throughput of approximately 320 bits per forward link information bit. Our approach is based on *coarse* quantization and adapts to LAN throughput constraints by allowing for different quantization parameters as well as allowing a subset of the receivers in the cluster to participate in the broadcast of quantized observations.

The numerical results from information-theoretic analysis, as well as simulations of an LDPC-coded system, show that exchanging just one bit per forward-link coded bit (i.e., hard decisions based on the sign of the observation) typically results in outage probability performance within 1.5 dB of ideal receive beamform-

ing, while two bits per coded bit (one sign bit and one amplitude bit) performs within 0.5 dB of ideal receive beamforming. Our results lead to the intuitively pleasing observation that the low (per node) SNR regimes enabled by cooperative distributed reception limit the performance loss caused by coarse quantization. We also provide explicit estimates of backhaul throughput requirements as a function of the forward link information rate, and demonstrate the efficacy of the technique with full and limited receiver participation.

3.2 System Model

We consider the scenario shown in Figure 3.1 where we have a single transmitter and a cluster of N receive nodes. The goal is to communicate common broadcast messages over the forward link from the distant transmitter to all of the receive nodes. As one example, the scenario in Figure 3.1 could correspond to a long-range downlink in which the receive cluster jointly processes messages from a distant base station.

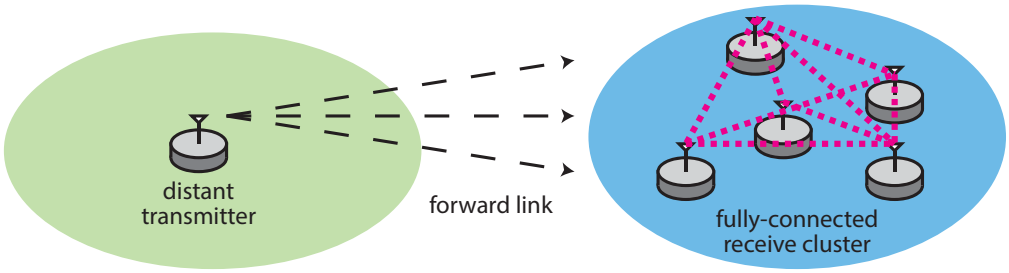

Figure 3.1: Distributed reception scenario.

The forward link complex channel from the distant transmitter to receive node i is denoted as h_i for $i = 1, \ldots, N$ and we denote the vector channel $\boldsymbol{h} =$

$[h_1, \ldots, h_N]^\top$. It is assumed that the receive cluster has already established a LAN backhaul, either ad-hoc or through infrastructure such as an access point, and that LAN transmissions are reliable. The LAN is also assumed to support broadcast transmission in which any single node can send a message to all other nodes simultaneously. The LAN and the forward link are assumed to operate on different frequencies so that the receive cluster can transmit/receive on the LAN while also receiving signals from the distant transmitter over the forward link. The LAN is also assumed to support a larger throughput than the coded bitrate of the forward link.

For ease of exposition, we assume the distant transmitter uses binary phase shift keying (BPSK) modulation and that messages are (n, k) block coded where n and k correspond to the block length the message length, both in bits, respectively. The forward link code rate is denoted as $r = k/n$. A mechanism for detecting a correctly decoded block, e.g. a CRC check, is assumed. The forward link channels are assumed to be block fading, where each h_i is constant over a block and is independent and identically distributed (i.i.d.) in each block. The channels are also assumed to be spatially i.i.d.

Given a channel input of $X = \pm 1$, the phase-corrected signal received at the i^{th} receive node is given as

$$Y_i = \sqrt{\rho}_i X + W_i \tag{3.1}$$

where $\rho_i = 2|h_i|^2 \mathcal{E}_s / N_0$, $\mathcal{E}_s$ is the energy per coded forward link bit, $N_0/2$ is the additive white Gaussian noise power spectral density, and $W_i \sim \mathcal{N}(0, 1)$. The noise realizations are assumed to be spatially and temporally i.i.d. The quantity ρ_i corresponds to the signal-to-noise ratio (SNR) of the coded forward link bits at

receive node i.

3.3 Distributed Reception Protocol

This section first provides an overview of the main idea behind the proposed distributed reception protocol, followed by additional details pertaining to a specific implementation.

In the low per-node SNR regimes of interest for large receive clusters, individual nodes are typically unable to successfully decode messages from the distant transmitter. Thus, while receiving a block over the forward link, each node in the receive cluster locally demodulates the transmission and generates LLRs for each of the n coded bits in the current block. These LLRs are not immediately used for decoding. Rather, all of the receive nodes (or a subset of nodes with better channel quality) quantize their soft demodulator outputs and broadcast *all* of their quantized values, along with quantized SNR estimates, over the LAN to the other receive nodes in the cluster. Each receive node then combines the information received over the LAN with their locally unquantized LLRs and passes these results to their local block decoder for decoding. If any receive node successfully decodes the message, it then forwards the decoded message over the LAN to the other receive nodes in the cluster. If two or more nodes successfully decode the message and attempt to broadcast the successfully decoded block, it is assumed the LAN has a mechanism for contention resolution.

An important constraint is that the LAN has limited capacity. If the LAN had unlimited capacity, all of the nodes in the receive cluster could effectively forward

unquantized LLRs to the other receive nodes in the cluster and each node could simply sum these LLRs to realize an ideal receive beamformer, as shown in the Appendix C. While this case serves as an important benchmark, this chapter considers the achievable performance of distributed reception with limited LAN capacity.

As a specific example of how distributed reception can be performed with limited LAN capacity, consider the timeline shown in Figure 3.2. After receiving and locally demodulating a block, the following steps are performed by the receive cluster over the LAN:

1. All N nodes exchange estimates of their channel magnitudes $|h_i|$ or received SNRs ρ_i.

2. The $M \leq N$ nodes with the strongest channel magnitudes or SNRs participate[1] by forwarding all of their quantized observations over the LAN. As quantized messages are received over the LAN, each receive node (including those that do not participate) scale this quantized information (based on the previously exchanged channel magnitudes/SNRs, as discussed in Section 3.5) and combine it with their locally unquantized LLRs.

3. If any receive node successfully decodes the message, it broadcasts the decoded message over the LAN to the other receive nodes in the cluster.

[1]A "participating" node is a node that broadcasts its quantized observations over the LAN to the other nodes in the receive cluster. We consider the general case where, due to poor channel conditions or LAN capacity constraints, some nodes in the receive cluster may not broadcast quantized observations.

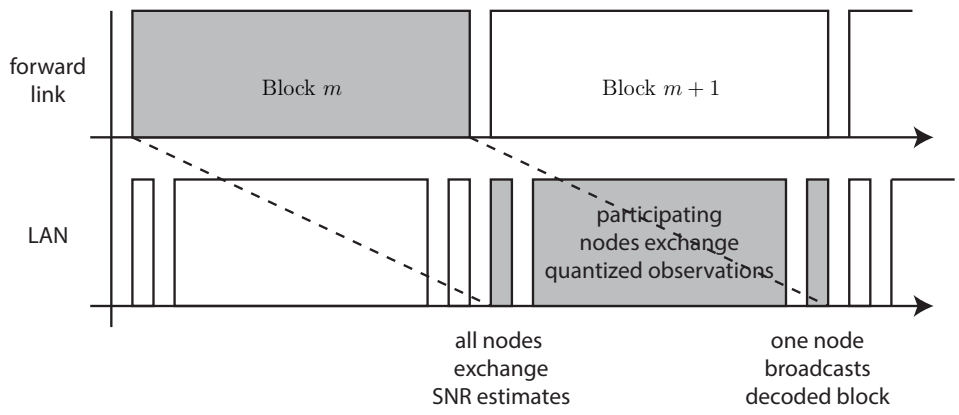

Figure 3.2: Distributed reception protocol timeline example.

The number of participating nodes M can be selected to satisfy a LAN throughput constraint. To determine M, we assume the number of quantization bits per coded bit is fixed for all receive nodes and is denoted as b. The normalized LAN throughput, in units of LAN bits per forward link information bit, can be calculated as

$$\eta_{\mathsf{LAN}} = \frac{No_1 + Mbn + k + o_2}{k} \approx \frac{Mb}{r} + 1 \leq C_{\mathsf{LAN}} \tag{3.2}$$

where No_1 is the overhead of exchanging SNR estimates and determining which nodes will participate, o_2 is the contention overhead in disseminating the successfully decoded block, and C_{LAN} is the maximum normalized LAN throughput. It is assumed that n and k are sufficiently large such that the overheads are negligible. Given r, b, and C_{LAN}, it follows that selecting $M \leq \min\{N, r(C_{\mathsf{LAN}} - 1)/b\}$ satisfies (3.2).

3.3.1 Distant transmitter functionality

Figure 3.3 shows a block diagram of the distant transmitter. The base functionality of the distant transmitter is to encode messages and modulate encoded blocks for

wireless transmission to the receive cluster. Encoding must include provisions for error correction and error detection. To support the error detection functionality, each forward link message includes some number of checksum bits for detecting incorrectly decoded messages. This could be, for example, a CRC check or an MD5 hash. The number of information bits plus checksum bits is k, with the number of checksum bits typically being a very small fraction of k. To support

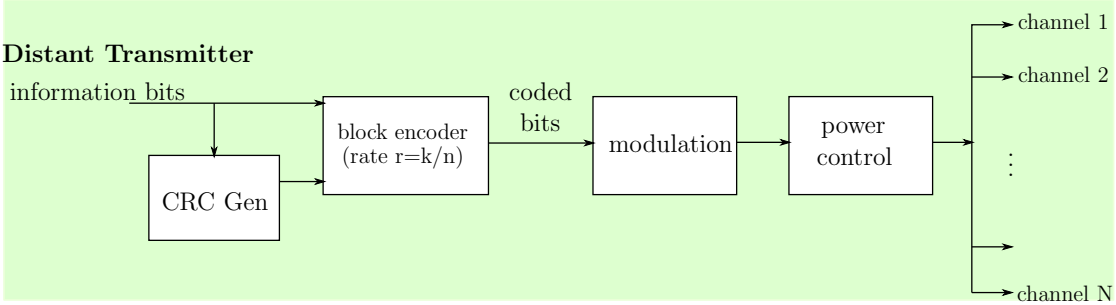

Figure 3.3: Distant transmitter functional block diagram. Upper layer functions such as addressing, packet sequencing, and encryption are not shown.

the error correction functionality, a rate $r = k/n$ block code is employed at the transmitter. The number of message bits (k) and the number of codeword bits (n) are both assumed to be large (at least a few thousand bits). Additionally, the distant transmitter may employ power control if feedback from the receive cluster is available.

3.3.2 Receive node functionality

It is assumed that the receive cluster has already established a LAN, either ad-hoc or through infrastructure such as an access point, such that each node in the receive cluster has a unique address, knows the addresses of the other nodes in the

receive cluster, and can communicate directly with all other nodes in the receive cluster. LAN transmissions are assumed to be reliable. The LAN is assumed to support broadcast transmission in which any single node can send a message to all other nodes simultaneously.

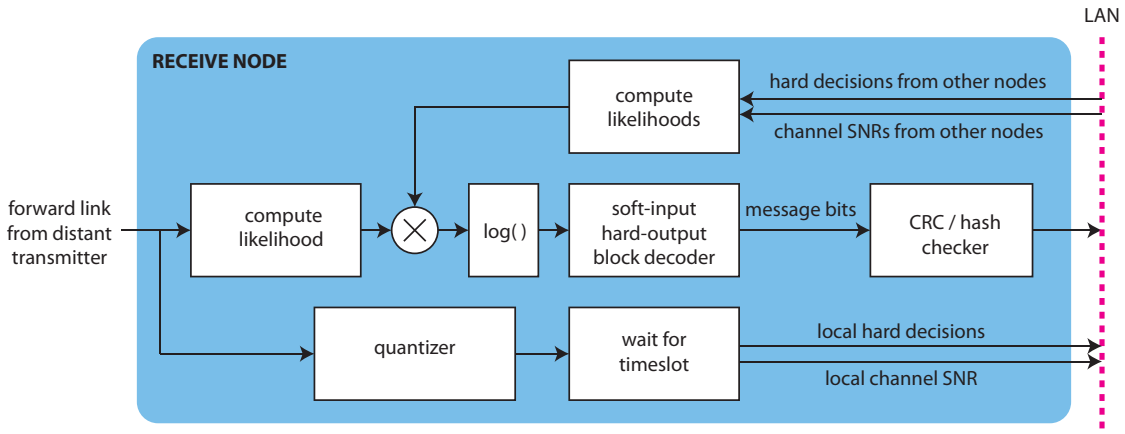

Figure 3.4: Receive node functional block diagram.

After receiving a block over the forward link, each node in the receive cluster quantizes and forwards its n coded bit hard decisions over the LAN. As quantized coded-bit hard decision messages are received over the LAN, each receive node computes the likelihoods based on the hard decisions from other nodes and combine these likelihoods with the one generated based on the locally unquantized observations to form the aggregate likelihoods. After receiving and combining all of the likelihood messages, each receive node attempts to decode the block based on the LLRs. The CRC/hash checker is used to determine if the block was successfully decoded. Any node that successfully decodes the block then broadcasts the decoded k-bit message over the LAN via a successfully decoded block message. If two or more nodes successfully decode the packet and attempt to send successfully decoded block messages, it is assumed the LAN has a mechanism for contention

resolution.

Figure 3.4 shows a functional block diagram of a receive node. The functional blocks include the forward link soft-input soft-output demodulator, the LLR quantizer and codebook generator, the quantized LLR scaler and combiner, the soft-input hard-output decoder, and the block error detector (CRC/hash checker).

3.3.3 Advantages

Since each receive node in the system has identical functionality as shown in Figure 3.4, no single receive node is designated as a collection point. There are a few advantages of this distributed approach including:

1. less overhead (no electing and maintaining the best collection point).
2. all receive nodes can run identical firmware.
3. diversity gain from slightly different decoder inputs at each receive node.
4. robustness to node failure.
5. robustness to LAN unreliability.
6. Average LAN traffic could be potentially reduced by having each receive node attempt to first decode the block using only the local unquantized LLRs and then only forward quantized LLRs if the decoded message has errors. Decoding latency for large block codes may be high, however, hence the proposed technique reduces latency by only performing decoding after all of the quantized LLRs have been exchanged over the LAN.

3.4 Information Theoretic Analysis

This section develops an information-theoretic framework for quantifying the performance of the proposed distributed reception scheme where each node in the receive cluster combines their local unquantized LLRs with quantized observations from other nodes in the receive cluster. Figure 3.5 shows an example of an information-theoretic model for a three-node cluster with full participation using one-bit quantization. This model corresponds to the situation at node 3 since it combines the quantized observations from nodes 1 and 2 with the unquantized information at node 3.

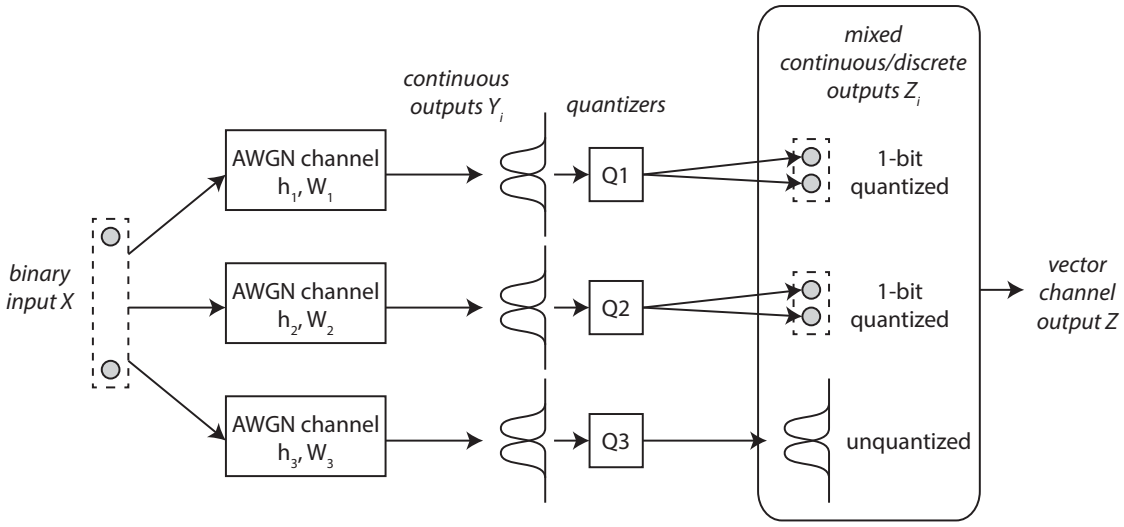

Figure 3.5: $N = 3$ node information-theoretic model example.

Given equiprobable binary channel inputs X drawn from $\{x_0, x_1\}$, the channel realization $\boldsymbol{h}$, the vector channel output $\boldsymbol{Z} = [Z_1, \ldots, Z_N]^\top$ with elements arbitrarily quantized or unquantized, and denoting $p(\boldsymbol{z}|k) = p_{\boldsymbol{Z}|X}(\boldsymbol{z}|X = x_k)$, the mutual

information $I_{\boldsymbol{h}}(X;\boldsymbol{Z})$ can be expressed as

$$\begin{aligned} I_{\boldsymbol{h}}(X;\boldsymbol{Z}) &= H(X) - H_{\boldsymbol{h}}(X|\boldsymbol{Z}) \\ &= 1 + \frac{1}{2}\sum_{k=0}^{1}\int_{-\infty}^{\infty} p(\boldsymbol{z}|k)\log_2\left\{\frac{p(\boldsymbol{z}|k)\frac{1}{2}}{p_{\boldsymbol{Z}}(\boldsymbol{z})}\right\} d\boldsymbol{z} \\ &= 1 - \frac{1}{2}\sum_{k=0}^{1}\int_{-\infty}^{\infty} p(\boldsymbol{z}|k)\log_2\left\{\frac{\sum_{\ell=0}^{1} p(\boldsymbol{z}|\ell)}{p(\boldsymbol{z}|k)}\right\} d\boldsymbol{z} \\ &= 1 - \frac{1}{2}\sum_{k=0}^{1}\mathrm{E}\left[\log_2\left\{\frac{\sum_{\ell=0}^{1} p(\boldsymbol{z}|\ell)}{p(\boldsymbol{z}|k)}\right\}\,\Big|\, X = x_k\right] \end{aligned}$$

where all distributions are conditioned on $\boldsymbol{h}$ and the conditional expectation is over the quantized vector channel output $\boldsymbol{Z}$ given a scalar channel input $X = x_k$. Based on the symmetry of the input constellation and the noise, this conditional expectation is identical for $X = x_0$ and $X = x_1$, hence we can write

$$\begin{aligned} I_{\boldsymbol{h}}(X;\boldsymbol{Z}) &= 1 - \mathrm{E}\left[\log_2\left\{\frac{\sum_{\ell=0}^{1} p(\boldsymbol{z}|\ell)}{p(\boldsymbol{z}|0)}\right\}\Big| X = x_0\right] \\ &= 1 - \mathrm{E}\left[\log_2\left\{1 + L(\boldsymbol{Z})\right\}\,\Big|\, X = x_0\right] \end{aligned} \tag{3.3}$$

where

$$L(\boldsymbol{Z}) = \frac{p(\boldsymbol{z}|1)}{p(\boldsymbol{z}|0)} = \frac{p_{\boldsymbol{Z}|X}(\boldsymbol{Z}|X = x_1)}{p_{\boldsymbol{Z}|X}(\boldsymbol{Z}|X = x_0)} = \frac{\mathrm{Prob}(X = x_1 \,|\, \boldsymbol{Z})}{\mathrm{Prob}(X = x_0 \,|\, \boldsymbol{Z})}.$$

Conditioning on $X = x_k$, the elements of $\boldsymbol{Z}$ are conditionally independent and we can write

$$p_{\boldsymbol{Z}|X}(\boldsymbol{z}|X = x_k) = \prod_{i=1}^{N} p_{Z_i|X}(z_i|X = x_k).$$

Hence

$$L(\boldsymbol{z}) = \prod_{i=1}^{N}\frac{p_{Z_i|X}(z_i|X = x_1)}{p_{Z_i|X}(z_i|X = x_0)} = \prod_{i=1}^{N} L_i(z_i) \tag{3.4}$$

and the log-likelihood $\ell(\boldsymbol{z}) = \sum_{i=1}^{N}\ell_i(z_i)$.

In the proposed distributed reception system, since one or more of the outputs in the vector channel is unquantized, the expectation in (3.3) must be approximated numerically, either by numerical integration or by Monte-Carlo simulation.

3.4.1 Unquantized channel outputs

For an equiprobable binary input and an unquantized i^{th} output, we have $Z_i = Y_i = \sqrt{\rho_i}X + W_i$, hence

$$L_i(z_i) = \frac{p_{Z_i|X}(z_i|X = x_1)}{p_{Z_i|X}(z_i|X = x_0)} = \exp\left\{2z_i\sqrt{\rho_i}\right\}. \tag{3.5}$$

The log-likelihood ratio in this case is then $\ell_i(z_i) = 2z_i\sqrt{\rho_i}$.

3.4.2 Quantized channel outputs

Quantization of the soft demodulator outputs at receive node i induces a discrete memoryless channel from the distant transmitter to that receiver, as shown in Figure 3.5. In general, for a quantized i^{th} output, the quantizer partition at the i^{th} receive node specifies a mapping from continuous observations $Y_i = \sqrt{\rho_i}X + W_i$ to a codebook index $Z_i \in \{0, \ldots, K_i - 1\}$. The conditional distribution $p_{Z_i|X}(z_i|X = x_k)$ in this case is a probability mass function with probabilities

$$\text{Prob}(Z_i = z_i \,|\, X = x_k) = p^{(i)}_{z_i|k}$$

for $z_i = 0, \ldots, K_i - 1$. Hence, for equiprobable binary inputs and arbitrarily quantized outputs, we have

$$L_i(z_i) = \frac{p_{Z_i|X}(z_i|X = x_1)}{p_{Z_i|X}(z_i|X = x_0)} = \frac{p^{(i)}_{z_i|1}}{p^{(i)}_{z_i|0}}.$$

The quantity $p^{(i)}_{z_i|k}$ can be thought of as the probability of observing quantizer output $Z_i = z_i$ at node i given a channel input $X = x_k$, i.e., $p^{(i)}_{z_i|k}$ is the discrete memoryless channel transition probability from input k to output z_i.

For the specific case of one-bit quantized channels, since the symbols and noise are symmetric, we will assume the one-bit quantizer partition is based on the sign of the observation at receiver i. Hence, at receiver i we have

$$z_i = \begin{cases} 0 & y_i < 0 \\ 1 & y_i \geq 0. \end{cases}$$

Observe that one-bit quantization induces a binary symmetric channel (BSC) at the i^{th} receiver. The transition probability for the resulting BSC is the error probability

$$p = p^{(i)}_{0|1} = p^{(i)}_{1|0} = Q\left(\sqrt{\rho_i}\right). \tag{3.6}$$

The likelihood ratio is then

$$L_i(z_i) = \frac{p^{(i)}_{z_i|1}}{p^{(i)}_{z_i|0}} = \begin{cases} \frac{p}{1-p} & z_i = 0 \\ \frac{1-p}{p} & z_i = 1 \end{cases} \tag{3.7}$$

and the LLR is given as

$$\ell_i(z_i) = \begin{cases} \ln \frac{p}{1-p} & z_i = 0 \\ \ln \frac{1-p}{p} & z_i = 1. \end{cases} \tag{3.8}$$

3.4.3 Numerical example

Figure 3.6 shows an example of the mutual information for distributed reception with $N = 10$ receive nodes and fixed channels $\boldsymbol{h} = [1, \ldots, 1]^\top$. All receive nodes

are assumed to participate in the distributed reception protocol. The binary-input, all unquantized outputs result corresponds to the capacity of ideal receive beamforming. Since the forward link channels to each receive node are the same in this example, the performance when one output is unquantized and $N-1$ outputs are one-bit quantized is the same for all receive nodes (this is not the case for general $\boldsymbol{h}$, however). These results show that distributed reception can provide significant capacity gains with respect to single-receiver processing and that receiving just one bit of information from each of the other nodes in the receive cluster can result in performance within approximately 2 dB of ideal receive beamforming for fixed, equal-gain channels.

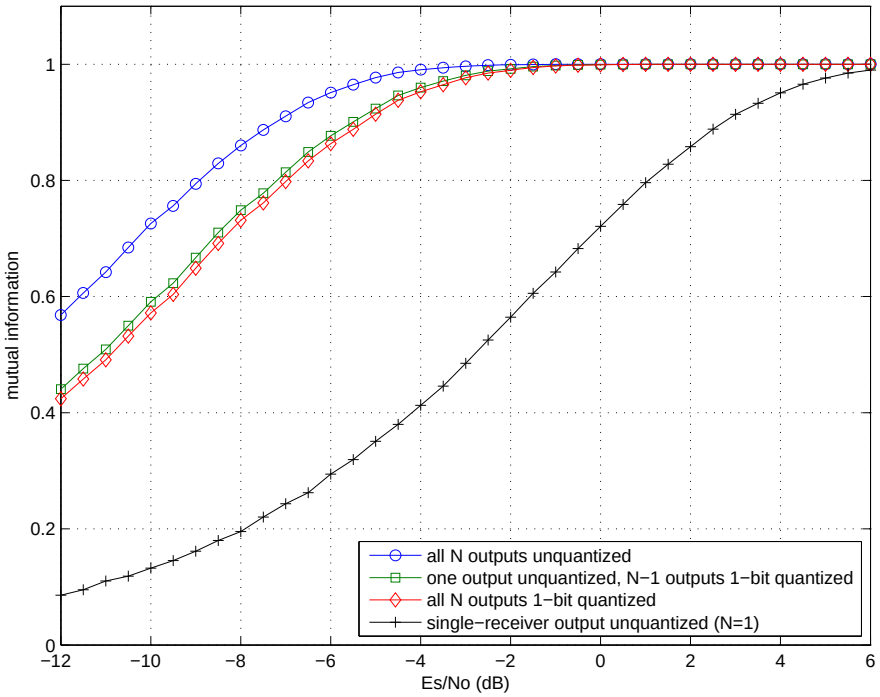

Figure 3.6: Mutual information for a binary-input distributed reception system with $N = 10$ receive nodes, full participation, and $\boldsymbol{h} = [1, \ldots, 1]^\top$.

3.5 Combining Quantized Observations

During the distributed reception protocol, each node receives quantized observations from all of the participating nodes in the receive cluster. These quantized observations are then scaled and combined with each other as well as with the local likelihoods to generate aggregate LLRs for input to the local block decoder.

To compute the aggregate likelihoods, it is sufficient for each node to use its knowledge of the participating nodes' SNRs (exchanged prior to the quantized observations as shown in Figure 3.2) and quantizer partitions. For example, for one-bit quantization, knowledge of the SNR allows for calculation of the BSC error probability in (3.6) and subsequent reconstruction of the marginal BSC output LLRs via (3.8). Denoting the set of participating nodes as $\mathcal{M}$, once the quantized observations received over the LAN have been converted to LLRs, they can be combined directly with the locally unquantized LLR at node j by computing $\ell(\boldsymbol{z}) = \ell_j(z_j) + \sum_{i \in \mathcal{M} \setminus j} \ell_i(z_i)$.

The log-likelihood ratio of the combined quantized observation at receive node j can be written as

$$\ell(\boldsymbol{z}) = \ln \left\{ \exp\{2 z_j \sqrt{\rho_j}\} \frac{\prod_{i=1, i \neq j}^{N} p_{z_i|1}^{(i)}}{\prod_{i=1, i \neq j}^{N} p_{z_i|0}^{(i)}} \right\}.$$

Note that, in general, the log-likelihood sum $\ell(\boldsymbol{z})$ will be different at each node in the receive cluster since the unquantized element in $\boldsymbol{z}$ is different at each receive node. Also, if node j does not participate ($j \notin \mathcal{M}$), it will have one more element in the log-likelihood sum than if it does participate ($j \in \mathcal{M}$). Hence, unlike ideal receive beamforming where the decision statistic is identical at all of

the receive nodes, the different decision statistics in a distributed reception system with quantized observation exchanges makes it possible that some nodes will be able to decode the received message while others will not. This motivates the broadcast of successfully decoded blocks as discussed in Section 3.3.

3.6 Numerical Results

This section provides numerical results demonstrating the efficacy of distributed reception with coarse quantization. All of the results in this section assume spatially and temporally i.i.d. block fading channels with $h_i \sim \mathcal{CN}(0,1)$.

Figure 3.7 shows the outage probability of distributed reception versus $\mathcal{E}_s/N_0$ for $N = 1, 2, 5, 10$ and full participation ($M = N$). These results are obtained from the information-theoretic analysis in Section 3.4 with 10000 channel realizations per receive node and 10000 noise realizations for each channel realization. An outage event occurs when $I_{\boldsymbol{h}}(X; \boldsymbol{Z}) < r_{out} = \frac{1}{2}$ at all of the receive nodes. The two-bit quantizer results used the partition[2]

$$z_i = \begin{cases} 0 & y_i < -q_i \\ 1 & -q_i \leq y_i < 0 \\ 2 & 0 \leq y_i < q_i \\ 3 & y_i \geq q_i \end{cases}$$

where q_i is the quantizer amplitude threshold selected to maximize the marginal mutual information $I(X; Z_i)$. These results show that significant improvements in

[2]Due to the symmetry of the input constellation and noise, this quantizer is intuitively reasonable but we make no claim as to its optimality.

outage probability can be obtained through combining locally unquantized LLRs with quantized observations from other nodes in the receive cluster and that the gap between exchanging ideal receive beamforming (unquantized LLRs) and exchanging just one bit per coded bit is less than 1.5 dB in the cases tested. Two bits per coded bit reduces this gap to better than 0.5 dB at the expense of approximately doubling the LAN throughput requirements.

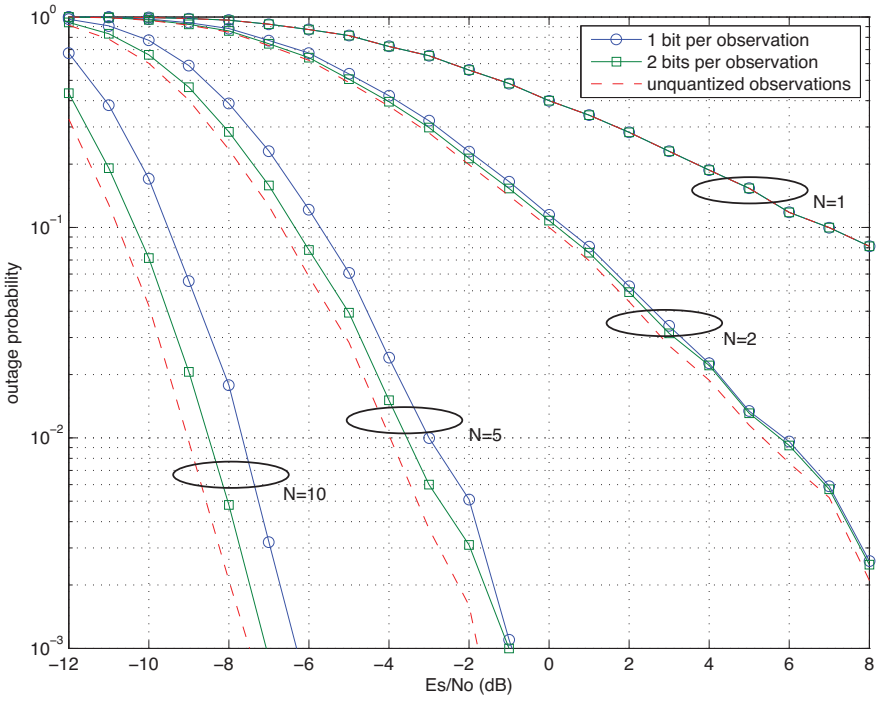

Figure 3.7: Outage probability versus $\mathcal{E}_s/N_0$ for distributed reception with quantized observations, outage rate $r_{out} = 1/2$, and full participation ($M = N$).

Figure 3.8 shows outage probability and normalized LAN throughput η_{LAN} from (3.2) versus the number of participating nodes M for $N = 10$ and $\mathcal{E}_s/N_0$ set to -8 dB. The set of participating nodes was selected by choosing the M receive nodes with the strongest channel magnitudes/SNRs. The simulation parameters in Figure 3.8 were otherwise identical to those in Figure 3.7. Even with $M = 0$,

distributed reception provides a diversity gain since the marginal mutual informations must all be less than r_{out} for an outage event to occur. This diversity gain can be seen by the fact that the outage probability when $M = 0$ and $N = 10$ (corresponding to no exchange of quantized observations over the LAN) is approximately 0.7 in Figure 3.8, whereas the outage probability at $\mathcal{E}_s/N_0 = -8$ dB and $N = 1$ in Figure 3.7 is close to one. The results in Figure 3.8 show the tradeoff between improved performance and increased LAN throughput for a fixed cluster size N, since the normalized LAN throughput scales linearly with M and b. In this example, the performance gain obtained by doubling the number of participating nodes tends to be better than the performance gain obtained by doubling the number of bits per observation when M is small. For larger values of M, e.g. $M = 5$, using two bits per observation gives a slightly better performance improvement than doubling M.

Figure 3.9 shows the outage probability and block error rate (BLER) performance of an LDPC code implementation of the distributed reception protocol with one-bit quantization. The rate $r = 1/2$ LDPC code was selected from proposed codes for DVB-S2 in [89, 90] with $n = 8100$ and $k = 4050$. These results demonstrate that the achievable performance with real block codes can be close to the information-theoretic predictions.

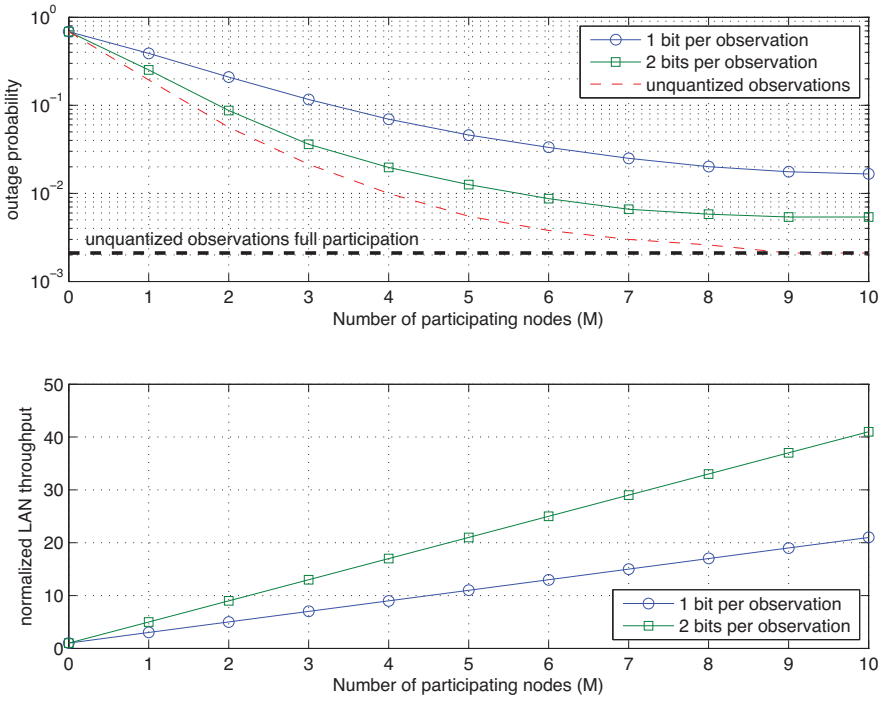

Figure 3.8: Outage probability and normalized LAN throughput (in LAN bits per forward link information bit) versus number of participating nodes M for distributed reception with quantized observations, outage rate $r_{out} = 1/2$, $\mathcal{E}_s/N_0 = -8$ dB, and $N = 10$.

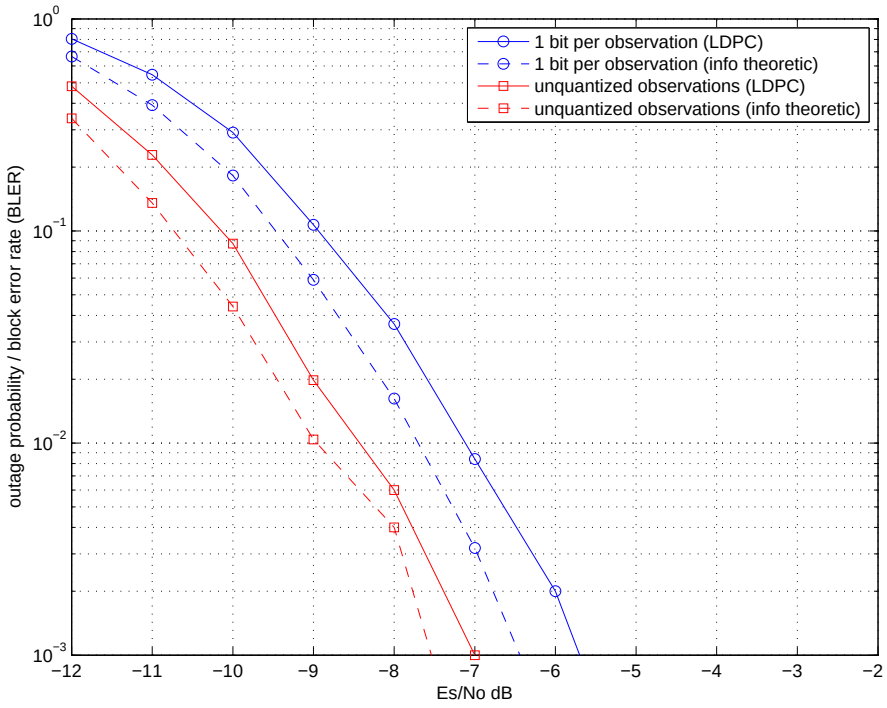

Figure 3.9: Outage probability and block error rate versus $\mathcal{E}_s/N_0$ for distributed reception with quantized observations, outage rate $r_{out} = 1/2$, and $M = N = 10$.

3.7 Bounds Approximations on Distributed Reception with BPSK Forward Link Modulation

So far, all results shown in the previous section are obtained through massive Monte-Carlo simulations. Typically, to show the outage probability performance on the order of 10^{-3} which corresponds to high SNR cases, the results need to be averaged over 10000 channel/noise realizations. To circumvent massive simulations, it is instructive to derive certain bounds or approximations for such system. However, current literature mainly focuses on bounds for "information combining" which is defined in a very strict sense [91–94] and the optimum way of doing such combining is often simply addition of the LLRs [95]. Therefore, it is of interest to derive bounds for the distributed reception technique proposed in this chapter.

In this section, a conjectured lower bound and an upper bound on the distributed reception technique with BPSK forward link modulation is presented which offers an efficient way of predicting the performance of distributed reception systems with coarsely-quantized observation exchange.

3.7.1 Single-receiver case

This section begins with the simplest scenario where only single receiver is assumed with one-bit channel inputs and outputs, and soft inputs and outputs. It shows that, in this case, a pretty fast way can be found to compute the outage probabilities given a rate r.

1-bit channel inputs and outputs

Starting with the single-receiver case, we know that given a binary channel input of $X = \pm 1$, the phase-corrected signal received at receive node is given as

$$Y = \sqrt{\rho}X + W$$

where $\rho = 2|h|^2\mathcal{E}_s/N_0$, $\mathcal{E}_s$ is the energy per coded forward link bit, $N_0/2$ is the additive white Gaussian noise power spectral density, $|h|$ is the channel magnitude, and $W \sim \mathcal{N}(0,1)$. The noise realizations are assumed to be temporally i.i.d.

Conditioning on the channel and given hard decisions at the output, the error probability of the BSC is

$$\begin{aligned} p &= \text{Prob}(\text{sign}(Y) \neq X) \\ &= Q(\sqrt{\rho}) = \int_{\sqrt{\rho}}^{+\infty} \frac{1}{\sqrt{2\pi}} e^{-t^2/2} dt \end{aligned}$$

and the mutual information with single receiver is

$$\begin{aligned} I_\rho^{(1)}(X;Y) &= g(p) \\ &= 1 + p\log_2(p) + (1-p)\log_2(1-p). \end{aligned}$$

The function $g : [0, 0.5] \mapsto [0, 1]$ is one-to-one. Hence $g^{-1} : [0, 1] \mapsto [0, 0.5]$ exists.

$$\begin{aligned} |h| &= \sqrt{\frac{\rho}{2\mathcal{E}_s/N_0}} \\ &= \frac{Q^{-1}(p)}{\sqrt{2\mathcal{E}_s/N_0}} \\ &= \frac{Q^{-1}(g^{-1}(r))}{\sqrt{2\mathcal{E}_s/N_0}} \\ &= f(r). \end{aligned}$$

The function $f : [0, 1] \mapsto [0, +\infty)$. The channel magnitude realization are assumed to be Rayleigh distributed with

$$p_{|h|}(u) = 2ue^{-u^2}. \tag{3.9}$$

Hence the outage probability can be written as

$$\begin{aligned} \text{Prob}(I_\rho^{(1)}(X;Y) < r) &= \text{Prob}(|h| < f(r)) \\ &= \int_0^{f(r)} 2ue^{-u^2} du \\ &= 1 - \exp(-f^2(r)). \end{aligned}$$

This provides a fast way to compute outage probabilities for this case without Monte-Carlo simulation.

Soft channel inputs and outputs

Conditioning on the channel, the mutual information with single receiver, soft inputs and outputs can be written as

$$I_\rho^{(1)}(X;Y) = \frac{1}{2}\log_2(1+\rho).$$

Given a rate $r \in [0, +\infty)$, the SNR can be computed as

$$\begin{aligned} \rho &= 2^{2r} - 1 \\ |h| &= \sqrt{\frac{2^{2r}-1}{2\mathcal{E}_s/N_0}}. \end{aligned}$$

Since the $|h|$ follows Rayleigh distribution, i.e., Rayleigh(σ) where $\sigma^2 = 0.5$,

the outage probability for a soft inputs and soft outputs channel can be written as

$$\begin{aligned}\text{Prob}(I_\rho^{(1)}(X;Y) < r) &= \text{Prob}(|h| < f(r)) \\ &= \int_0^{\sqrt{\frac{2^{2r}-1}{2\mathcal{E}_s/N_0}}} 2ue^{-u^2}du \\ &= 1 - \exp\left(-\frac{2^{2r}-1}{2\mathcal{E}_s/N_0}\right).\end{aligned}$$

which provides a fast way to compute outage probabilities without Monte-Carlo simulation.

In fact, this result can be easily extended to the N-receiver case where the outage probability equals to the CDF of a Gamma distribution, i.e., $\sum_{i=1}^{N} |h_i|^2 \sim \Gamma(N,1)$ with integration interval from 0 to $\frac{2^{2r}-1}{2\mathcal{E}_s/N_0}$:

$$\begin{aligned}\text{Prob}(I_\rho^{(N)}(X;Y) < r) &= \int_0^{\frac{2^{2r}-1}{2\mathcal{E}_s/N_0}} \frac{1}{\Gamma(N,1)} u^{N-1}e^{-u}du \\ &= 1 - \sum_{i=0}^{N-1} \frac{1}{i!}\left(\frac{2^{2r}-1}{\alpha^2}\right)^i \exp\left[-\left(\frac{2^{2r}-1}{\alpha^2}\right)\right] \qquad (3.10) \\ &= 1 - \sum_{i=0}^{N-1} \frac{1}{i!}\left(\frac{1}{\alpha}\right)^{2i} \exp\left[-\left(\frac{1}{\alpha}\right)^2\right] \qquad (3.11)\end{aligned}$$

where $\alpha = \sqrt{2\mathcal{E}_s/N_0}$

3.7.2 Two-receiver case

Following the analysis for the single-receiver system, we provide a similar analysis for the two-receiver case where conjectures can be illustrated in a two-dimensional space which helps extending to more complicated situations.

1-bit channel inputs and outputs

Since two receivers are assumed, the system model is defined as the follows

$$Y_k = \sqrt{\rho_k} X + W_k$$

where $\rho_k = 2|h_k|^2 \mathcal{E}_s/N_0$, $\mathcal{E}_s/N_0$ is the energy per coded forward link bit, $N_0/2$ is the additive white Gaussian noise power spectral density, $|h_k|$ is the channel magnitude and $W_k \overset{\text{i.i.d.}}{\sim} \mathcal{N}(0,1)$. The noise realizations are assumed to be spatially and temporarily i.i.d.

Conditioning on the channel and given hard decisions at the output, the error probability of each BSC is

$$\begin{aligned} p_k &= \text{Prob}(\text{sign}(Y_k) \neq X) \\ &= Q(\sqrt{\rho_k}) \\ &= \int_{\sqrt{\rho_k}}^{+\infty} \frac{1}{\sqrt{2\pi}} e^{-t^2/2} dt. \end{aligned}$$

Since two receive nodes are assumed, the model corresponds to a two-input four-output system. The mutual information of this system can be written as

$$\begin{aligned} I_\rho^{(2)}(X;Y) &= g(p_1,p_2) \\ &= 1 - (1-p_1)(1-p_2)\log_2\left(1 + \frac{p_1 p_2}{(1-p_1)(1-p_2)}\right) - \\ &\quad p_1(1-p_2)\log_2\left(1 + \frac{p_2(1-p_1)}{p_1(1-p_2)}\right) - p_2(1-p_1)\log_2\left(1 + \frac{p_1(1-p_2)}{p_2(1-p_1)}\right) \\ &\quad - p_1 p_2 \log_2\left(1 + \frac{(1-p_1)(1-p_2)}{p_1 p_2}\right). \end{aligned}$$

Let $\Lambda = [0, 0.5]^2$ denote the two-dimensional transition probability space. Given a value of rate $r \in [0,1]$, there is an associated inverse image Λ_r in the transition probability space Λ such that $I_\rho^{(2)}(X;Y) \leq r$.

Several remarks about function g and its inverse function: first of all, if $(p_1, p_2) \in \Lambda_r$, $(p_2, p_1) \in \Lambda_r$; g is a monotonic function of p_k. For example, given $g(p_1, p_2) = r$, $g(q_1, q_2) < r$ when $p_1 < q_1 \leq 0.5$ and $p_2 \leq q_2 \leq 0.5$, or $p_1 \leq q_1 \leq 0.5$ and $p_2 < q_2 \leq 0.5$.

In order to show the outage/no outage region on a two-dimensional plain Λ, assume that the rate is fixed at 0.5, i.e., $r = I_\rho^{(2)}(X;Y) = 0.5$. It means that all (p_1, p_2) on the curve $\mathcal{C}$ satisfy $I_\rho^{(2)}(X;Y) = 0.5$. Figure 3.10 shows the boundary of the outage/no outage region when $r = 0.5$.

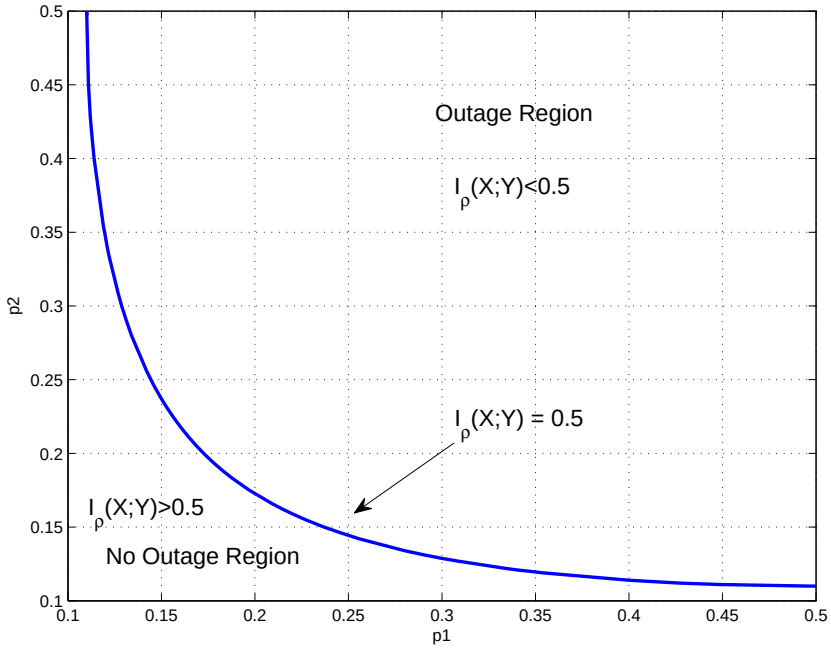

Figure 3.10: Outage/no outage region when $r = 0.5$ in Λ domain.

Lower bound Approximation R_1

In order to map the boundary $\mathcal{C}$ from the transition probability domain Λ to the magnitude domain Γ, define

$$\tilde{h}_1 = Q^{-1}(p_1) = \sqrt{\frac{2\mathcal{E}_s}{N_0}}|h_1|$$
$$\tilde{h}_2 = Q^{-1}(p_2) = \sqrt{\frac{2\mathcal{E}_s}{N_0}}|h_2|$$

where $(\tilde{h}_1, \tilde{h}_2) \in \Gamma$.

Thus the corresponding boundary in Γ domain is shown in Figure 3.11 where the blue solid curve is the direct mapping of the boundary.

The dashed green curve shown in the same figure is a circle approximation of the boundary with radius R_1 equals to the solution of $I_\rho^{(2)}(X;Y) = 0.5$ in Γ domain when setting one transition probability to be 0.5, i.e.,

$$R_1 = \sqrt{\tilde{h}_1^2 + \tilde{h}_2^2} = \tilde{h}_1 \tag{3.12}$$

since $p_2 = 0.5$, i.e., $\tilde{h}_2 = Q^{-1}(p_2) = 0$, $R_1 = \tilde{h}_1 = Q^{-1}(p_1)$ and p_1 satisfies the following equation

$$\begin{aligned} I_\rho^{(2)}(X;Y) &= 1 - p_1 \log_2(1 + \frac{1-p_1}{p_1}) - (1-p_1)\log_2(1 + \frac{p_1}{1-p_1}) \\ &= 0.5. \end{aligned} \tag{3.13}$$

Observation from Figure 3.11 shows that the dashed curve is inside the boundary which implies that integration in that area may provide us a lower bound approximation of the outage probability. To prove this idea, the outage probability inferred by the circle approximation needs to be calculated.

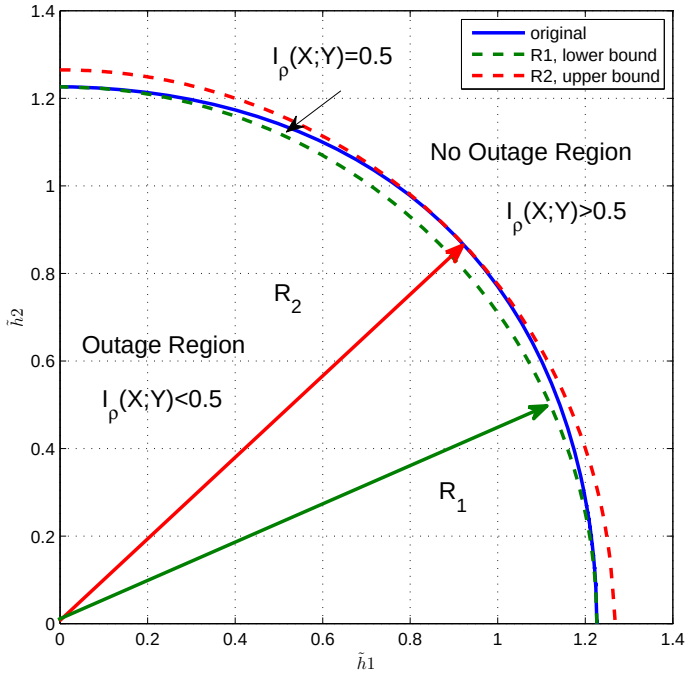

Figure 3.11: Outage/no outage region when $I_\rho^{(2)}(X;Y) = 0.5$ in Γ domain.

Recall equation (3.9), the PDF of $\tilde{h}_1$ and $\tilde{h}_2$ can be written as

$$\begin{aligned} p_{\tilde{h}_1} = p_{\tilde{h}_2} &= p_{|h_1|}\left(\frac{u}{\alpha}\right)\frac{1}{\alpha} \\ &= 2\left(\frac{u}{\alpha}\right)\exp\left[-\left(\frac{u}{\alpha}\right)^2\right]\frac{1}{\alpha}. \end{aligned}$$

The outage probability can thus be written as

$$\begin{aligned} \text{Prob}(I_\rho^{(2)}(X;Y) \le 0.5) &= \int_0^R \left(\int_0^{\sqrt{R^2-u_1^2}} p_{\tilde{h}_2}(u_2)du_2\right) p_{\tilde{h}_1}(u_1)du_1 \\ &= \int_0^R \left(\int_0^{\sqrt{R^2-u_1^2}} 2\left(\frac{u_2}{\alpha}\right)\exp\left[-\left(\frac{u_2}{\alpha}\right)^2\right]\frac{1}{\alpha}du_2\right) \\ &\quad 2\left(\frac{u_1}{\alpha}\right)\exp\left[-\left(\frac{u_1}{\alpha}\right)^2\right]\frac{1}{\alpha}du_1 \\ &= 1 - \left(1+\left(\frac{R}{\alpha}\right)^2\right)\exp\left[-\left(\frac{R}{\alpha}\right)^2\right]. \end{aligned} \tag{3.14}$$

From equation (3.13), we have $p_1 = 0.11$ and thus $R_1 = Q^{-1}(p_1) = 1.226$. Therefore, for the circle approximation with radius R_1 shown in Figure 3.11, the lower bound approximation for the outage probability can be written as

$$\text{Prob}(I_\rho(X;Y) \leq 0.5) > 1 - \left(1 + \left(\frac{R_1}{\alpha}\right)^2\right) \exp\left[-\left(\frac{R_1}{\alpha}\right)^2\right]$$

which provides a fast way to compute the conjectured lower bound for the outage probability for a given $\mathcal{E}_s/N_0$ value.

Upper bound Approximation R_2

The upper bound approximation can be obtained by the circle approximation as well only with different radius. The radius R_2 is equal to $\sqrt{2}$ times $\tilde{h} = Q^{-1}(p)$ where p is the solution when $I_\rho^{(2)}(X;Y) = r$ and $p = p_1 = p_2$.

By using equation (3.14), the upper bound approximation for the outage probability with 2-receiver is

$$\text{Prob}(I_\rho^{(2)}(X;Y) \leq 0.5) < 1 - \left(1 + \left(\frac{R_2}{\alpha}\right)^2\right) \exp\left[-\left(\frac{R_2}{\alpha}\right)^2\right].$$

3.7.3 N-receiver case

For N-receiver systems, to get the outage probability, we need to integrate inside the boundary as follows

$$\text{Prob}(I_\rho^{(N)}(X;Y) \leq 0.5) = \int\int\cdots\int_{\Gamma^N} p_{\tilde{h}_1}(u_1)p_{\tilde{h}_2}(u_2)\cdots p_{\tilde{h}_K}(u_K)du_1du_2\cdots du_K.$$

Using the multi-dimensional sphere to approximate the boundary, i.e.,

$$\sum_{i=1}^{N} u_i^2 = R^2,$$

the general circle approximation for the N-receiver outage probability is

$$\text{Prob}(I_\rho^{(N)}(X;Y) \leq 0.5) = 1 - \sum_{i=0}^{N-1} \frac{1}{i!} \left(\frac{R}{\alpha}\right)^{2i} \exp\left[-\left(\frac{R}{\alpha}\right)^2\right] \tag{3.15}$$

which is the CDF of Gamma distribution, i.e., $\Gamma(N,1)$ with integration interval from 0 to $\frac{\left(2^{2r}-1\right)h_0^2}{2\mathcal{E}_s/N_0} = \frac{h_0^2\left(2^{2r}-1\right)}{\alpha^2}$.

Hence the corresponding lower and upper bound conjecture based on this approximation can be obtained by substituting R_1 and R_2 where R_1 is the Q inverse of the solution of $I^{(N)}(X;Y) = r$ when setting $N-1$ transition probabilities to 0.5; R_2 is equal to $\sqrt{N}$ times the Q inverse of the solution of $I^{(N)}(X;Y) = r$ when setting $p = p_1 = p_2 = \cdots = p_N$.

Recall the outage probability for the N-receiver soft inputs and soft output system:

$$\text{Prob}(I_\rho(X;Y) \leq 0.5) = 1 - \sum_{i=0}^{N-1} \frac{1}{i!} \left(\frac{1}{\alpha}\right)^{2i} \exp\left[-\left(\frac{1}{\alpha}\right)^2\right] \tag{3.16}$$

which is $\Gamma(N,1)$ with integration interval from 0 to $\frac{2^{2r}-1}{2\mathcal{E}_s/N_0} = \frac{2^{2r}-1}{\alpha^2}$. The only difference between (3.15) and (3.16) is the integration interval. To be specific, the "radius" of the multi-dimensional sphere for the soft inputs and soft outputs system in Γ domain is $\frac{1}{\alpha}$ rather than $\frac{R}{\alpha}$.

3.7.4 Numerical results

Figure 3.12 shows the outage probability performance for distributed reception with unquantized/1-bit quantized observations, full participation and $r = 0.5$ by

Monte-Carlo simulations and analytical predictions. It is shown in this figure that the analytical predictions for soft inputs and soft output are very close to the Monte-Carlo simulation results. The analytical lower/upper bounds approximations for the 1-bit quantized observation get better and better when the number of receivers increases. As expected, the outage probability with 1-bit quantized observations obtained by Monte-Carlo simulations lie between the conjectured lower/upper bounds. Only when the outage probability becomes very small (close to 10^{-3}) may the Monte-Carlo simulation results tend to perform worse the conjectured upper bound due to lack of number of channel/noise realizations. It is reasonable to believe that the Monte-Carlo simulations will be strictly bounded by the conjectured lower/upper bound when the number of channel/noise realizations goes to infinity ($> 10^6$).

In [96], it is shown that R_2 does not grow unbounded but goes to some constant and thus the gap between the ideal beamforming and 1-bit belief combining is at most $20\log(R_2) = 2.1483$ dB for any number of receive nodes N.

3.8 Conclusion

We have shown in this chapter that, in the low SNR regimes enabled by receiver cooperation, coarse quantization of observations followed by LLR reconstruction and combining across receivers results in little loss of performance relative to ideal beamforming, which is equivalent to summing unquantized LLRs for BPSK. Thus, good performance can be achieved with significant reduction in LAN throughput requirements relative to sharing conventionally quantized LLRs. Our information-

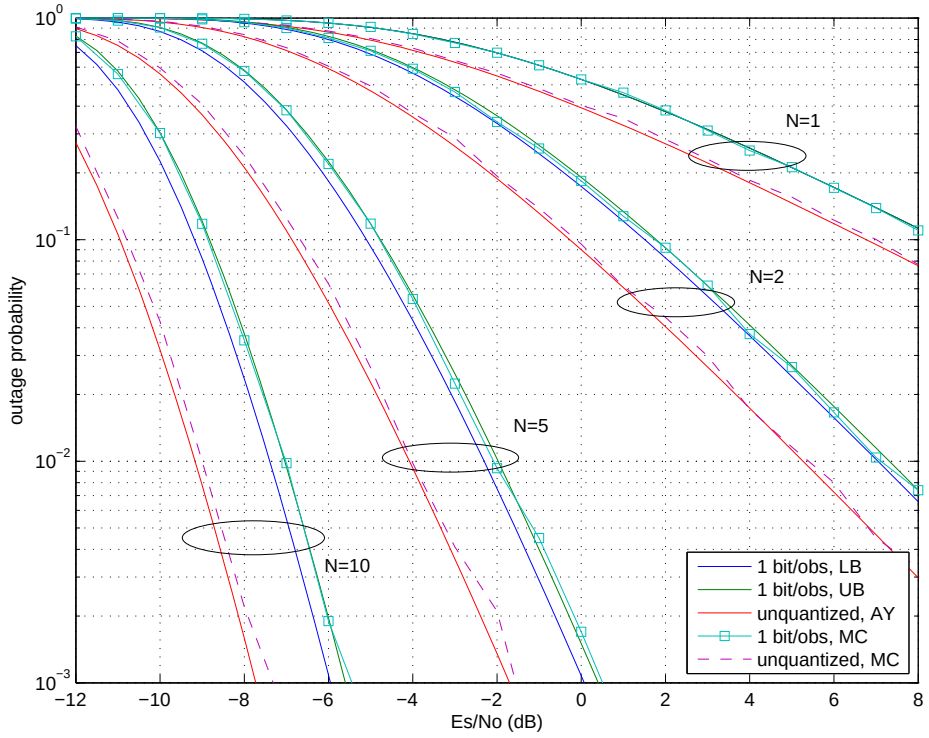

Figure 3.12: Outage probability versus $\mathcal{E}_s/N_0$ for distributed reception with unquantized/1-bit quantized observations, outage rate $r = 1/2$ and full participation ($N = 1, 2, 5, 10$) by Monte-Carlo simulations and analytical predictions.

theoretic framework provides quick performance estimates that agree with that of LDPC-coded systems.

While the results in this chapter extend immediately to Gray-coded QPSK, we are currently investigating extension of this approach to systems with forward links with higher-order, more spectrally efficient, constellations.

Chapter 4

Distributed Reception with Higher-order Forward Link Modulation

In order to improve the spectrum efficiency, we extend the approach in the previous chapter to system with forward link with higher-order modulations such as QPSK, 8PSK, 4PAM and 16QAM.

Under the same distributed reception scenario, the extension from BPSK to QPSK is simple, it uses both I and Q channels so that the attainable rate for a given bandwidth is doubled. For 8PSK however, it is easy to show that summing the unquantized LLRs is no longer equivalent to ideal beamforming which means exchanging the quantized LLRs does not provide similar SNR gain as BPSK and QPSK. Hence new combining strategy is needed in order to maintain the nice properties obtained by cooperative distributed reception. We will first introduce a suboptimal combining technique for 8PSK and then discuss the optimal combining approach which establishes a general framework for any forward link modulation. Numerical results of the info-theoretic analysis and LDPC code suggest that in the low SNR regimes enabled by receiver cooperation, coarse quantization of observations followed by likelihood reconstruction and combining across receivers results in little loss of performance relative to ideal receive beamforming.

4.1 Distributed Reception with MPSK Forward Link Modulation

In this section, info-theoretic analysis is provided for systems with MPSK (BPSK, QPSK and 8PSK) forward link modulation and the optimal belief combining strategy is discussed together with a suboptimal combining approach.

4.1.1 Information theoretic analysis

Based on the same information-theoretic model in section 3.4, we compute the mutual information with discrete-input, continuous/discrete-output for a fixed realization of the channels $\boldsymbol{h} = [h_1, \cdots, h_N]^\top$ and equiprobable inputs. Fading channel performance metrics such as ergodic capacity or outage capacity can be obtained by computing $I_{\boldsymbol{h}}(X; \boldsymbol{Z})$ over multiple draws of $\boldsymbol{h}$. This later can be used as upper/lower bound for the belief combining.

Capacity of the AWGN channel

The mutual information, i.e. capacity, of an AWGN channel with Gaussian distributed input [97] is given as

$$C^{1-\dim} = \frac{1}{2}\log_2(\pi e \sigma^2_{\mathcal{Y}'}) - \frac{1}{2}\log_2(\pi e \sigma^2_{\mathcal{N}'}) = \frac{1}{2}\log_2\left(1 + 2\frac{\mathcal{E}_s}{N_0}\right) \tag{4.1}$$

$$\begin{aligned} C^{2-\dim} &= \log_2(\pi e \sigma^2_{\mathcal{Y}}) - \log_2(\pi e \sigma^2_{\mathcal{N}}) \\ &= \log_2\left(\frac{\sigma^2_{\mathcal{X}} + \sigma^2_{\mathcal{N}}}{\sigma^2_{\mathcal{N}}}\right) = \log_2\left(1 + \frac{\mathcal{E}_s}{N_0}\right) \end{aligned} \tag{4.2}$$

where $\sigma^2_{\mathcal{X}'} = \sigma^2_{\mathcal{X}} = 2B\mathcal{E}_s$ and $\sigma^2_{\mathcal{N}'} = \frac{1}{2}\sigma^2_{\mathcal{N}} = BN_0$. Since $\mathcal{E}_s = r\mathcal{E}_b = \frac{k}{n}\mathcal{E}_b$, we have

$$C^{1-\text{dim}} = \frac{1}{2}\log_2\left(1 + 2r\frac{\mathcal{E}_b}{N_0}\right) \tag{4.3}$$

$$C^{2-\text{dim}} = \log_2\left(1 + r\frac{E_b}{N_0}\right). \tag{4.4}$$

The highest spectral efficiency in maintaining an error-free transmission is obtained for $C = r$, hence

$$\begin{aligned} \frac{E_b}{N_0} &= \frac{2^{2C} - 1}{2C} \\ \lim_{C\to 0}\frac{E_b}{N_0} &= \lim_{C\to 0}\frac{2^{2C+1}\log 2}{2} = -1.59 \text{ dB}. \end{aligned} \tag{4.5}$$

This means that no reliable communication can be achieved below -1.59 dB.

When the output is discrete, the capacity of an AWGN channel is

$$\begin{aligned} C &= I_{\boldsymbol{h}}(X;\boldsymbol{Z}) \\ &= H(X) - H_{\boldsymbol{h}}(X|\boldsymbol{Z}) \\ &= \log_2(|\mathcal{X}|) - \frac{1}{|\mathcal{X}|}\int_{\mathcal{Y}}\sum_{\mu} p_{Y|X_\mu}(y)\log_2\frac{\sum_l p_{Y|X_l}(y)}{p_{Y|X_\mu}(y)}dy \\ &= \log_2(K) - \frac{1}{K}\sum_{k=0}^{K-1}\int_{-\infty}^{+\infty} p_{\boldsymbol{Z}|X}(z|X=x_k)\log_2\left(\frac{\sum_{\ell=0}^{K-1} p_{\boldsymbol{Z}|X}(z|X=x_\ell)}{p_{\boldsymbol{Z}|X}(z|X=x_k)}\right)dz \\ &= \log_2(K) - \frac{1}{K}\sum_{k=0}^{K-1}\mathrm{E}\left[\log_2\left(\frac{\sum_{\ell=0}^{K-1} p_{\boldsymbol{Z}|X}(z|X=x_\ell)}{p_{\boldsymbol{Z}|X}(z|X=x_k)}\right)\middle| X=x_k\right] \end{aligned} \tag{4.6}$$

If all of the outputs are quantized, $\boldsymbol{Z}$ is drawn from a finite set and the mutual information can be exactly calculated by computing and cycling through the conditional probabilities for all possible $\boldsymbol{Z}$. If one or more of the outputs is unquantized,

then $\boldsymbol{Z}$ is drawn from an infinite set and this expectation must be approximated numerically, either by numerical integration or by Monte-Carlo simulation.

Figure 4.1 shows the capacity versus $\mathcal{E}_s/N_0$ with fixed $\boldsymbol{h}$ for various modulation schemes. As can be seen, while the BPSK curves are bounded by the real Gaussian input and continuous output curve, other complex-valued modulation schemes are bounded by the complex Gaussian input and continuous output curve. The discrete input, discrete output exact results match the corresponding Monte-Carlo results except for 8PSK since a high SNR approximated error probability is used for 8PSK.

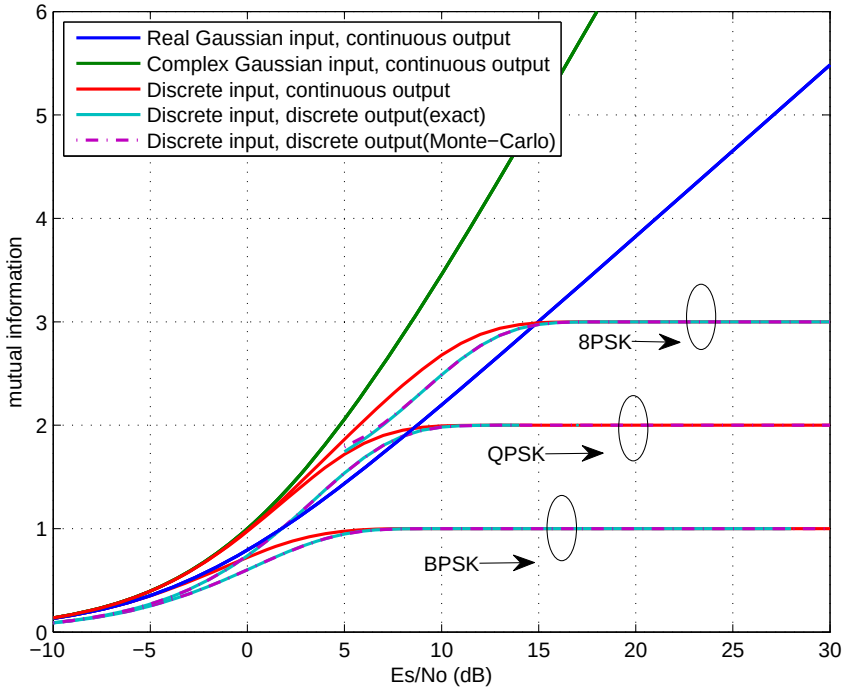

Figure 4.1: Channel capacity versus $\mathcal{E}_s/N_0$ with fixed $\boldsymbol{h}$ for various modulation schemes.

Similar to Figure 4.1, figure 4.2 shows the capacity versus E_b/N_0 with fixed $\boldsymbol{h}$. As expected, all of the discrete input schemes are bounded either by the real

Gaussian input or the complex Gaussian input curves. It also agrees with the Shannon limit in (4.5) that no reliable communication can be achieved below -1.59 dB.

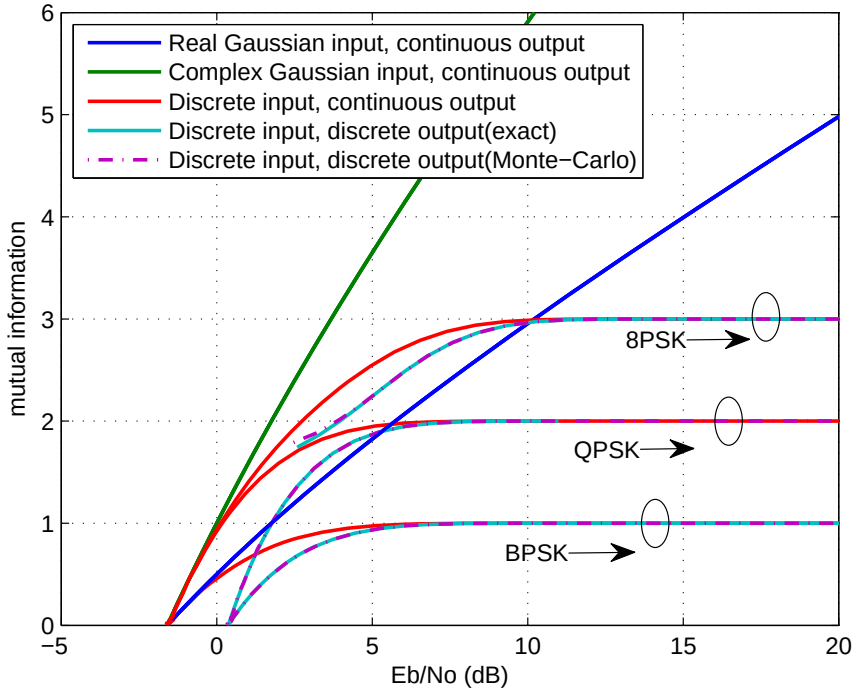

Figure 4.2: Channel capacity versus E_b/N_0 with fixed $\boldsymbol{h}$ for various modulation schemes.

Since BPSK has already been discussed in the previous chapter, we will start with QPSK here. If we assume QPSK channel input and no quantization, the optimum receiver computes $Z_{bf} = \boldsymbol{h}^H \boldsymbol{Y}$. The channel from X to Z_{bf} is effectively a SISO QPSK-input continuous-output channel. The capacity of this channel can only be computed numerically via

$$C = 2 - \frac{1}{4} \sum_{k=0,1,2,3} \mathrm{E}\left[\log_2 \left(\frac{\sum_{\ell=0}^{3} p_{\boldsymbol{Z}|X}(\boldsymbol{Z}|X = x_\ell)}{p_{\boldsymbol{Z}|X}(\boldsymbol{Z}|X = x_k)} \right) \,\middle|\, X = x_k \right] \tag{4.7}$$

where $\mathcal{X} = \Big\{x_0 = +\|\boldsymbol{h}\|\sqrt{2\mathcal{E}_s/N_o}, x_1 = +j\|\boldsymbol{h}\|\sqrt{2\mathcal{E}_s/N_o},\ x_2 = -\|\boldsymbol{h}\|\sqrt{2\mathcal{E}_s/N_o}, x_3 = -j\|\boldsymbol{h}\|\sqrt{2\mathcal{E}_s/N_o}\Big\}$.

Unlike BPSK/QPSK, the bit error rate of 8PSK is an approximated value which might result in loose or even misleading lower bound for the one-bit belief combining. More accurate probability transition matrix can be obtained by using

$$P_e = Q(d/\sigma) = Q(|h_i|\sqrt{2\mathcal{E}_s/N_0}\sin\frac{\pi}{8}). \tag{4.8}$$

under high SNR assumption which means that the symbol can only be wrongly detected as its nearest neighbours. In other words, given one of the 8 inputs, only 3 possible outputs can be observed: either the correct input or its two nearest neighbours. We can also run Monte-Carlo simulations to get the probability transition matrix.

Figure 4.3 shows the mutual information versus $\mathcal{E}_s/N_0$ with fixed and the average mutual information with fading channels. As can be seen in the figure, the average mutual information of the discrete channel outputs by using approximated channel transition matrix is greater than the continuous outputs case until it reaches 4 dB for the fixed channel case and 8 dB for the fading channels case. The average mutual information of the discrete channel outputs with channel transition matrix obtained by Monte-Carlo simulations is always less than the continuous channel outputs case at low SNR and then gradually converges to 3 bits/channel use when SNR approaches infinity.

Figure 4.4 shows the outage probability versus $\mathcal{E}_s/N_0$ with $C_o = 1.5$ and $N = 1$. While the outage probabilities of the discrete outputs with MC is worse than the continuous outputs which makes sense, the outage probability of the discrete

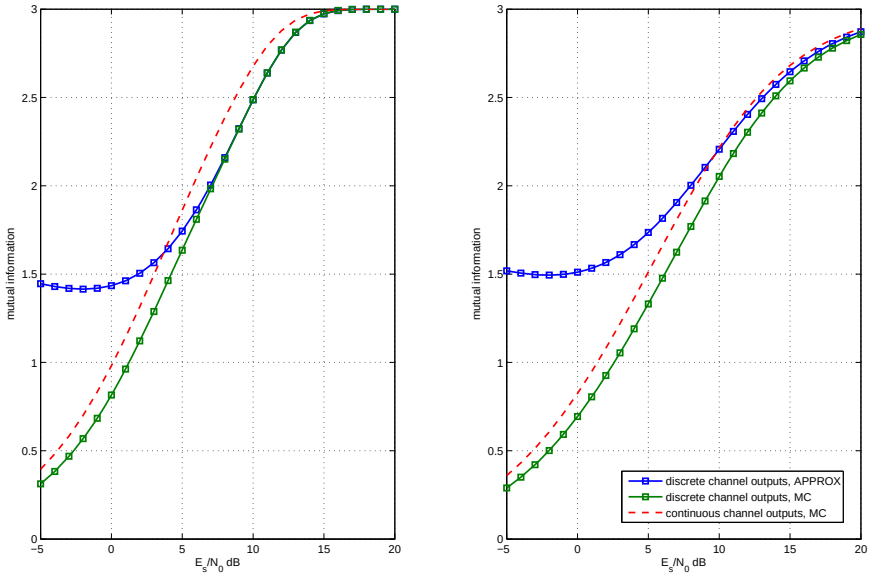

Figure 4.3: Mutual information versus $\mathcal{E}_s/N_0$. LHS is with fixed channels and RHS is with fading channels.

outputs with approximated channel transition probability behaves unexpectedly. It is obvious that the approximated channel transition probability does not hold at low SNR which explains the bump at -2 dB but it still does not explain why it outperforms the continuous output case at high SNR since in figure 4.3, the average mutual information of the discrete output MC is lower than that of the continuous outputs.

The only possible explanation for this is that the average mutual information of the discrete outputs with APPROX is greater than that of the continuous outputs, but the distribution is skewed somehow such that the probability of the mutual information being less than 1.5 is less for the discrete outputs with APPROX.

To confirm this, figure 4.5 shows a histogram of the average mutual informa-

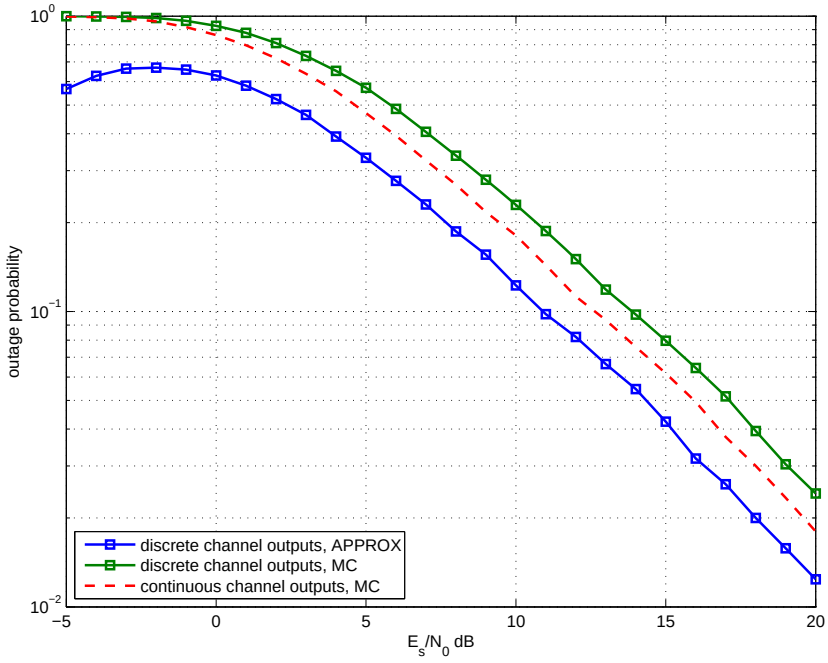

Figure 4.4: Outage probability (BLER) versus $\mathcal{E}_s/N_0$ for 8PSK with $C_o = 1.5$ and $N = 1$.

tion obtained by the continuous channel outputs, discrete channel outputs with APPROX and with Monte-Carlo simulations. 5000 channel realizations are performed and each is averaged over 2000 noise realizations. From this figure we can see that while the average mutual information of the continuous outputs is spread over 0 to 3, the distribution of the discrete output with APPROX is skewed. Most of the average mutual information is around or above 1.5 which agrees with our hypothesis. Hence, the approximation alone cannot be used as the lower bound for the one-bit belief combining.

In order to move forward on this and achieve our main goal of understanding how close the 3-bit belief combining for 8PSK is to the information-theoretic receive beamforming, we used a hybrid approach to compute the channel transition matrices (LUT+APPROX) which is described as follows:

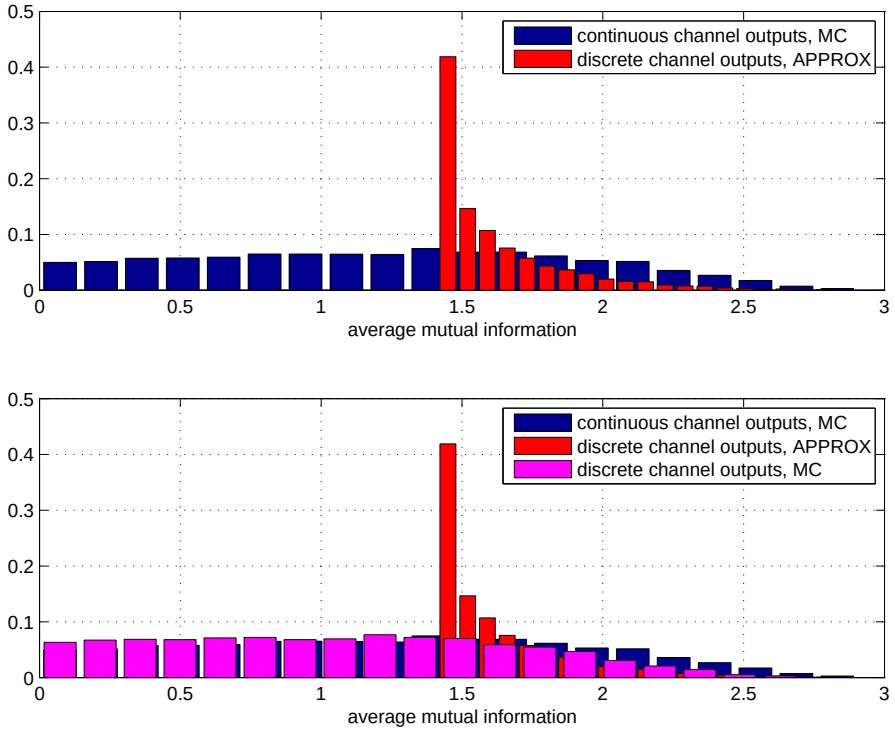

Figure 4.5: Histogram of the average mutual information for 8PSK by using approximated channel transition matrix and Monte-Carlo simulations.

1. Set up a separate simulation to generate channel transition matrices via the Monte-Carlo method for a set of $|h|^2\mathcal{E}_s/N_0 \in [0 : 0.01 : 10]$. Store the result in an $8 \times 8 \times 1001$ array table.

2. In the main simulation, depending on $\mathcal{E}_s/N_0$ and the channel realization compare $|h|^2\mathcal{E}_s/N_0$ with 10:

   (a) if $|h|^2\mathcal{E}_s/N_0 < 10$, look up one of these channel transition matrices from the table we generated in step 1 and use it.

   (b) if $|h|^2\mathcal{E}_s/N_0 > 10$, use the approximated channel transition matrices.

3. Compute the average mutual information and the outage probability.

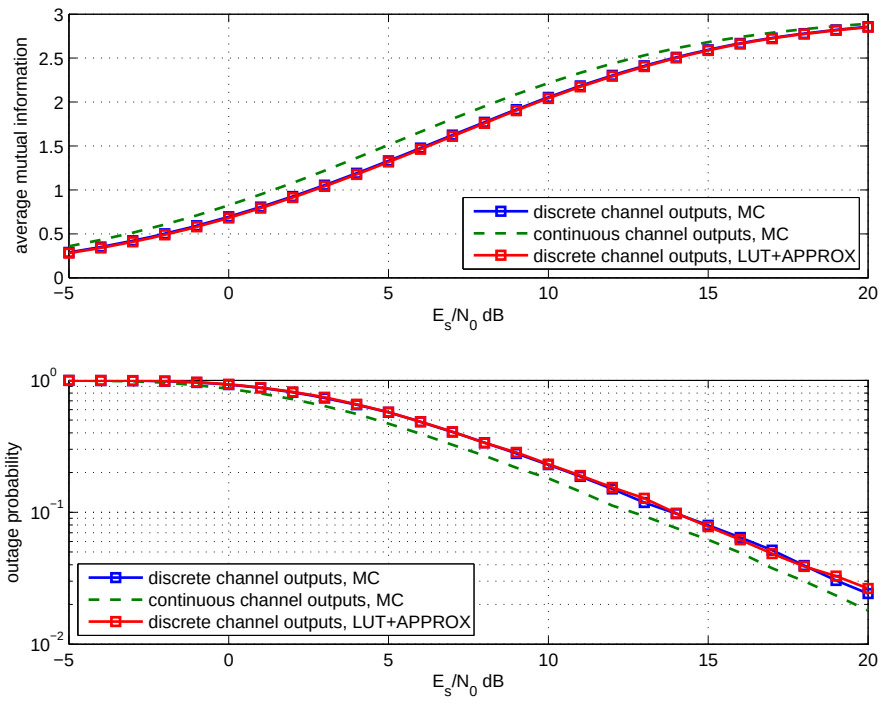

Figure 4.6: Mutual information and the outage probability for 8PSK with hybrid approach (LUT+APPROX).

Figure 4.6 shows the mutual information computed by the hybrid algorithm. It matches the discrete channel outputs with transition matrix obtained by Monte-Carlo simulations and it is always less than the continuous output case. The outage probability indicates that this hybrid approach can yield a reliable and efficient lower bound for the 3-bit belief combining with 8PSK forward link modulation.

4.1.2 Pseudobeamforming for 8PSK forward link modulation

In Appendix C, it is shown that summing LLRs of unquantized observations is equivalent to ideal receive beamforming for BPSK and QPSK and thus combining the quantized LLRs results in little loss of performance and significantly reduces the LAN throughputs. However, for 8PSK $\ell_{\text{bf}}(x_{ki}|z) = \sum_{i=1}^{N} \ell_{\text{unquantized}}(x_{ki}|z_i)$ no long holds true. Detailed explanations are provided in Appendix D.

The main idea of pseudobeamforming is to map the quantized LLRs to the 8PSK constellation and combine the mapped outputs from neighbouring nodes with the local unquantized observation as beamforming. Figure 4.7 illustrates the pseudobeamforming process.

The protocol is almost the same as that in 3.3 for the BPSK, except that instead of forwarding their quantized LLRs over the LAN, the receive nodes participate by forwarding their pseudo symbols which is a scaled version of the mapped constellation points.

In real implementation, the combined pseudo symbols are fed into the demod-

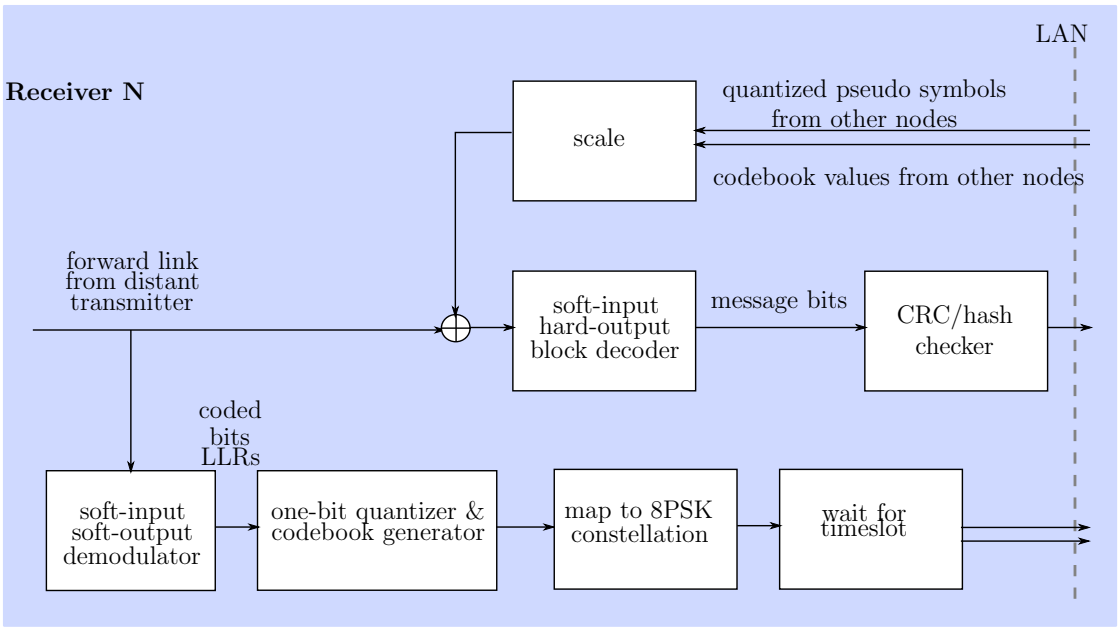

Figure 4.7: Pseudobeamforming receive node functional block diagram.

ulator and turn into LLRs. If correct LLRs are fed into the LDPC decoder, few block errors will occur. Hence, it is crucial to feed the demodulator the correct statistics of the quantization noise. Conventional demodulator considers that the noise has zero-mean, independent and identically distributed real/imaginary parts and is independent of transmitted signal. However, none of these assumptions are true for the aggregate quantization noise at the output of the pseudobeamformer.

To study the statistics of the quantization noise, we assume that for large enough receive clusters, the aggregate quantization error (after combining by the pseudobeamfomer) will be Gaussian. For example, suppose N receive nodes participate the pseudobeamforming and all observations are quantized (no locally unquantized observations). The analytical mean and covariance conditioned on a

transmitted symbol s and channel state $\boldsymbol{h}$ are

$$\begin{aligned}
\mu(s,\boldsymbol{h}) &= \mathrm{E}\left[s_i|s,\boldsymbol{h}\right] \\
&= \mathrm{E}\left[\frac{1}{\|\boldsymbol{h}\|^2}\sum_{n=1}^{N}|h_n|^2 s_i \mathrm{Pr}(s_i|s,h_n)\right] \\
&= \frac{1}{\|\boldsymbol{h}\|^2}\sum_{i=0}^{7}\sum_{n=1}^{N}|h_n|^2 s_i \mathrm{Pr}(s_i|s,h_n) \qquad (4.9)\\
\sigma_x^2(s,\boldsymbol{h}) &= \mathrm{E}\left[\left(|h_n|^2\mathrm{Re}(s_i)-\mu_x(s,h_n)\right)^2|s,\boldsymbol{h}\right] \\
&= \frac{1}{\|\boldsymbol{h}\|^2}\sum_{n=1}^{N}\sum_{i=0}^{7}\mathrm{Pr}(s_i|s,h_n)\left(|h_n|^2\mathrm{Re}(s_i)-\mu_x(s,h_n)\right)^2 \qquad (4.10)\\
\sigma_y^2(s,\boldsymbol{h}) &= \mathrm{E}\left[\left(|h_n|^2\mathrm{Im}(s_i)-\mu_x(s,h_n)\right)^2|s,\boldsymbol{h}\right] \\
&= \frac{1}{\|\boldsymbol{h}\|^2}\sum_{n=1}^{N}\sum_{i=0}^{7}\mathrm{Pr}(s_i|s,h_n)\left(|h_n|^2\mathrm{Im}(s_i)-\mu_y(s,h_n)\right)^2 \qquad (4.11)\\
\rho(s,\boldsymbol{h}) &= \mathrm{E}\left[\left(|h_n|^2\mathrm{Re}(s_i)-\mu_x(s,h_n)\right)\left(|h_n|^2\mathrm{Im}(s_i)-\mu_x(s,h_n)\right)|s,\boldsymbol{h}\right] \\
&= \frac{1}{\|\boldsymbol{h}\|^2}\sum_{n=1}^{N}\sum_{i=0}^{7}\mathrm{Pr}(s_i|s,h_n)\left(|h_n|^2\mathrm{Re}(s_i)-\mu_x(s,h_n)\right)\left(|h_n|^2\mathrm{Im}(s_i)-\mu_y(s,h_n)\right) \\
& \qquad (4.12)
\end{aligned}$$

where $\Sigma(s,\boldsymbol{h}) = \begin{bmatrix}\sigma_x^2(s,\boldsymbol{h}) & \rho(s,\boldsymbol{h})\\ \rho(s,\boldsymbol{h}) & \sigma_y^2(s,\boldsymbol{h})\end{bmatrix}$ and $\mathrm{Pr}(s_i|s,h_n)$ is channel transition matrix conditioned on s and $|h_n|^2\mathcal{E}_s/N_0$ according to the lookup table.

Figure 4.8 shows the combined 8PSK pseudo symbols conditioned on s_0 and a particular channel $\boldsymbol{h}$ after 10,000 noise realizations with $N = 100$ receive nodes at 0 dB. The analytical mean and variances of the real/imaginary parts of the combined pseudo symbols are also plotted on top of the simulated results.

The relationship between the pseudobeamforming with $\boldsymbol{h} = \mathbf{1}$/fixed $\boldsymbol{h}$ channels can be demonstrated more clearly in Figure 4.9. For this particular channel

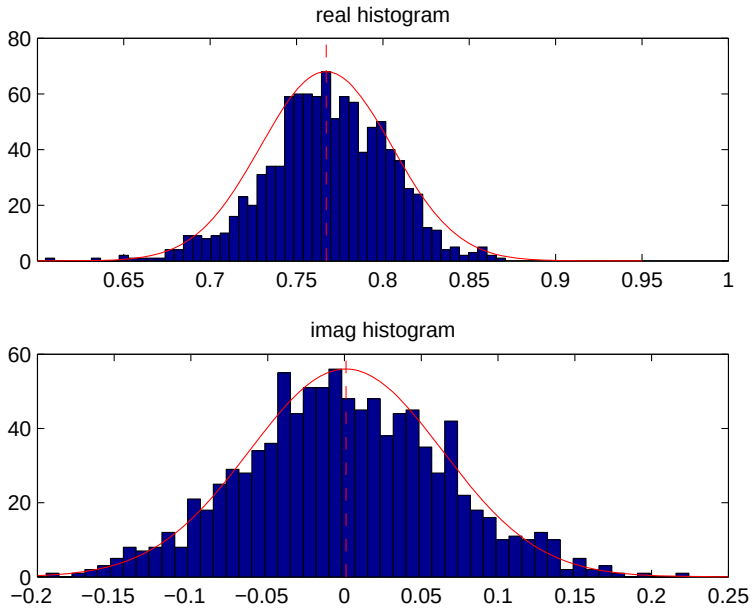

Figure 4.8: Combined quantized symbols conditioned on s_0 and a particular $\boldsymbol{h}$ with $N = 100$ and fading channels at 0 dB.

realization $\boldsymbol{h}$, we can see that the pseudobeamforming with fading channels are located further away from the origin than with $\boldsymbol{h} = \mathbf{1}$.

Therefore instead of using the conventional demodulator, the demodulator function for pseudobeamforming with different channels to each receiver is designed as

$$\texttt{llr}_{\texttt{IQ}} = \texttt{IQ8PSK\_demod}(\texttt{r}, \texttt{EsNo}, \texttt{h})$$

which first computes the analytical mean and covariance according to equation (4.9), (4.10), (4.11) and (4.12), then feeds them to the demodulator as follows

$$\begin{aligned}\texttt{llr}_{\texttt{IQ}}(b|r, \boldsymbol{h}) &= \ln\left\{\frac{\Pr(b=+1|r,\boldsymbol{h})}{\Pr(b=-1|r,\boldsymbol{h})}\right\} \\ &= \ln\left\{\frac{\sum_{s\in S_0}\frac{1}{|\boldsymbol{\Sigma}(s,\boldsymbol{h})|^{1/2}}e^{-\frac{1}{2}(\boldsymbol{r}-\boldsymbol{\mu}(s,\boldsymbol{h}))^\top\boldsymbol{\Sigma}^{-1}(s,\boldsymbol{h})(\boldsymbol{r}-\boldsymbol{\mu}(s,\boldsymbol{h}))}}{\sum_{s\in S_1}\frac{1}{|\boldsymbol{\Sigma}(s,\boldsymbol{h})|^{1/2}}e^{-\frac{1}{2}(\boldsymbol{r}-\boldsymbol{\mu}(s,\boldsymbol{h}))^\top\boldsymbol{\Sigma}^{-1}(s,\boldsymbol{h})(\boldsymbol{r}-\boldsymbol{\mu}(s,\boldsymbol{h}))}}\right\}. \end{aligned} \tag{4.13}$$

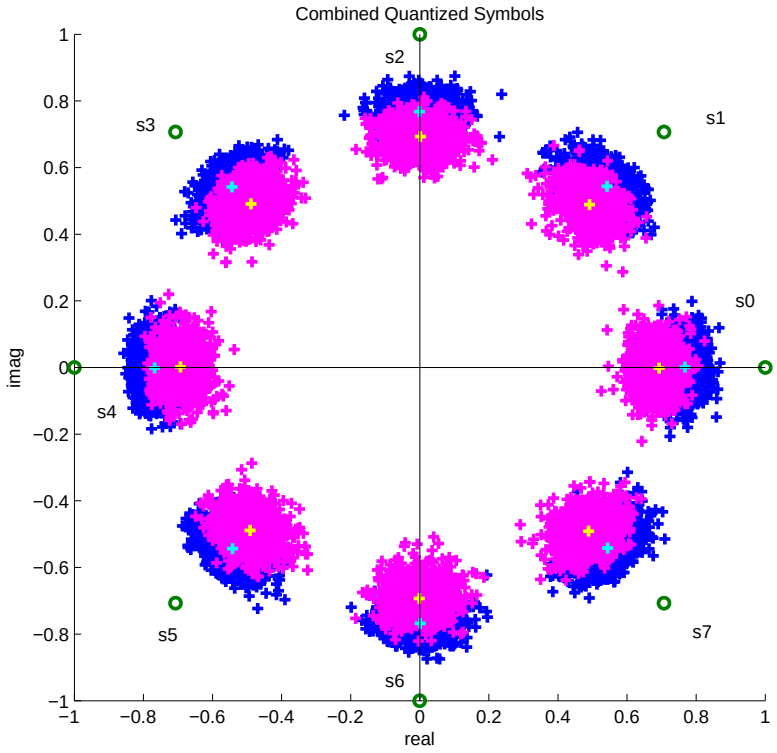

Figure 4.9: Combined quantized symbols conditioned on a particular $\boldsymbol{h}$ with $N = 100$ at 0 dB. The blue clusters indicate the pseudobeamforming with independent fading channels and the cyan "+" is the corresponding analytical mean prediction; the magenta clusters indicate the pseudobeamforming with fixed channels and the yellow "+" is the corresponding analytical mean prediction.

4.1.3 Three-bit belief combining for 8PSK forward link modulation

This section presents an optimal distributed reception scheme for 8PSK forward link modulation where each node in the receive cluster combines their local unquantized observations with quantized observations from other nodes in the receive cluster.

Recall equation (4.6), the symmetry of the input constellation and the noise can be exploited to simplify this equation. Since the conditional expectation in (4.6) is identical for all $X = x_k$, we can write

$$\begin{aligned} I_{\boldsymbol{h}}(X;\boldsymbol{Z}) &= \log_2(K) - \mathrm{E}\left[\log_2\left\{\frac{\sum_{\ell=0}^{K-1} p(\boldsymbol{z}|\ell)}{p(\boldsymbol{z}|0)}\right\}\Big| X = x_0\right] \\ &= \log_2(K) - \mathrm{E}\left[\log_2\left\{1 + L(\boldsymbol{Z})\right\}\,\Big|\, X = x_0\right] \end{aligned} \tag{4.14}$$

where

$$\begin{aligned} L(\boldsymbol{z}) &= \frac{\sum_{\ell=1}^{K-1} p(\boldsymbol{z}|\ell)}{p(\boldsymbol{z}|0)} = \frac{\sum_{\ell=1}^{K-1} p_{\boldsymbol{Z}|X}(\boldsymbol{z}|X = x_\ell)}{p_{\boldsymbol{Z}|X}(\boldsymbol{z}|X = x_0)} \\ &= \frac{\sum_{\ell=1}^{K-1} \mathrm{Prob}(X = x_\ell \,|\, \boldsymbol{Z} = \boldsymbol{z})}{\mathrm{Prob}(X = x_0 \,|\, \boldsymbol{Z} = \boldsymbol{z})}. \end{aligned} \tag{4.15}$$

Note that the numerator of $L(\boldsymbol{Z})$ is a sum of all of the conditional probabilities except $p(\boldsymbol{z}|0)$. Since the elements of $\boldsymbol{Z}$ are conditionally independent, we can write

$$p_{\boldsymbol{Z}|X}(\boldsymbol{z}|X = x_k) = \prod_{i=1}^{N} p_{Z_i|X}(z_i|X = x_k) \tag{4.16}$$

hence

$$L(\boldsymbol{z}) = \frac{\sum_{\ell=1}^{K-1} \prod_{i=1}^{N} p_{Z_i|X}(z_i|X = x_\ell)}{\prod_{i=1}^{N} p_{Z_i|X}(z_i|X = x_0)}. \tag{4.17}$$

Unquantized channel outputs

For QPSK and 8PSK, the likelihood ratio for the unquantized outputs can be computed by equation (4.17) where

$$p_{Z_i|X}(z_i|X = x_\ell) = \frac{1}{2\pi} \exp\left\{-\frac{|z_i - \sqrt{\rho_i}x_\ell|^2}{2}\right\}. \tag{4.18}$$

Quantized channel outputs

Quantization of the soft demodulator outputs at receive node i induces a discrete memoryless channel from the distant transmitter to that receiver, as shown in Figure 3.5. In general, for a quantized i^{th} output, the quantizer partition at the i^{th} receive node specifies a mapping from continuous observations $Y_i = \sqrt{\rho_i}X + W_i$ to a codebook index $Z_i \in \{0, \ldots, K_i - 1\}$. The conditional distribution $p_{Z_i|X}(z_i|X = x_k)$ in this case is a probability mass function with probabilities

$$\text{Prob}(Z_i = z_i \,|\, X = x_k) = p^{(i)}_{z_i|k}$$

for $z_i = 0, \ldots, K_i - 1$. The quantity $p^{(i)}_{z_i|k}$ can be thought of as the probability of observing quantizer output $Z_i = z_i$ at node i given a channel input $X = x_k$, i.e., $p^{(i)}_{z_i|k}$ is the discrete memoryless channel transition probability from input k to output z_i.

For the specific case of one-bit quantized channels for BPSK modulation, the likelihood ratio can be calculated by equation (3.4) by plugging the individual likelihood ratio at each receive node i.e., (3.7).

Similarly, for QPSK and 8PSK, two-bit and three-bit quantizer partitions can be specified respectively based on demodulator hard decisions or, equivalently, the

sign of the demodulator soft LLR outputs. Assume that $u_{i,j}$ is the j^{th} soft LLR based on the observation y_i at receive node i where $j = \{0, \cdots, \log_2(K) - 1\}$. Then, like BPSK, we have

$$z_{i,j} = \begin{cases} 0 & u_{i,j} < 0 \\ 1 & u_{i,j} \geq 0. \end{cases}$$

Observe that two-bit and three-bit quantization induces a 4×4 and 8×8 symmetric channel for QPSK and 8PSK, respectively, at the i^{th} receiver. The transition probabilities for the resulting symmetric channels are the usual channel transition probabilities for channels with discrete inputs and outputs. These transition probabilities can be computed in terms of Q-functions for QPSK but must be evaluated numerically for 8PSK and higher order PSK constellations. By plugging the appropriate transition probabilities to equation (4.17), we can get the likelihood ratios and then compute the mutual information by equation (4.14).

4.2 Distributed Reception with 4PAM/16QAM Forward Link Modulation

Since the PAM and QAM do not have symmetric constellations as the MPSK, minor changes need to be made when compute the mutual information.

4.2.1 4PAM

Consider the 4PAM constellation: $x_0 = -3A$, $x_1 = -A$, $x_2 = +A$ and $x_3 = +3A$. The middle points x_1 and x_2, the edge points x_0 and x_3 are symmetric with respect

to $x = 0$ respectively, hence the conditional expectation is identical for $X = x_0$ and $X = x_3$, and is also identical for $X = x_1$ and $X = x_2$. The mutual information can be written as

$$\begin{aligned} I_{\boldsymbol{h}}(X;\boldsymbol{Z}) &= 2 - \tfrac{1}{2}\mathrm{E}\left[\log_2\left\{\tfrac{\sum_{\ell=0}^{3} p(\boldsymbol{z}|\ell)}{p(\boldsymbol{z}|0)}\right\}\Big| X = x_0\right] - \tfrac{1}{2}\mathrm{E}\left[\log_2\left\{\tfrac{\sum_{\ell=0}^{3} p(\boldsymbol{z}|\ell)}{p(\boldsymbol{z}|1)}\right\}\Big| X = x_1\right] \\ &= 2 - \tfrac{1}{2}\mathrm{E}\left[\log_2\left\{1 + L_0(\boldsymbol{Z})\right\}\Big| X = x_0\right] - \tfrac{1}{2}\mathrm{E}\left[\log_2\left\{1 + L_1(\boldsymbol{Z})\right\}\Big| X = x_1\right] \end{aligned} \tag{4.19}$$

where

$$L_0(\boldsymbol{Z}) = \frac{\sum_{\ell=1}^{3} p(\boldsymbol{z}|\ell)}{p(\boldsymbol{z}|0)} = \frac{\sum_{\ell=1}^{3} p_{\boldsymbol{Z}|X}(\boldsymbol{Z}|X = x_\ell)}{p_{\boldsymbol{Z}|X}(\boldsymbol{Z}|X = x_0)} = \frac{\sum_{\ell=1}^{3} \mathrm{Prob}(X = x_\ell \,|\, \boldsymbol{Z})}{\mathrm{Prob}(X = x_0 \,|\, \boldsymbol{Z})} \tag{4.20}$$

$$L_1(\boldsymbol{Z}) = \frac{\sum_{\ell=0,\ell\neq 1}^{3} p(\boldsymbol{z}|\ell)}{p(\boldsymbol{z}|1)} = \frac{\sum_{\ell=0,\ell\neq 1}^{3} p_{\boldsymbol{Z}|X}(\boldsymbol{Z}|X = x_\ell)}{p_{\boldsymbol{Z}|X}(\boldsymbol{Z}|X = x_1)} = \frac{\sum_{\ell=0,\ell\neq 1}^{3} \mathrm{Prob}(X = x_\ell \,|\, \boldsymbol{Z})}{\mathrm{Prob}(X = x_1 \,|\, \boldsymbol{Z})}. \tag{4.21}$$

By using the fact that the $p_{\boldsymbol{Z}_i|X}(z_i|X = x_k)$'s are conditionally independent, we can substitute these results into (4.16) and then compute (4.20) and (4.21) and the mutual information in (4.19).

The likelihood ratio for the unquantized outputs can be computed in the same manner as (4.17). This results in

$$p_{Z_i|X}(z_i|X = x_\ell) = \frac{1}{\sqrt{2\pi}} \exp\left\{-\frac{(\mathrm{Re}(z_i) - \sqrt{\frac{\rho_i}{5}}\mathrm{Re}(x_\ell))^2}{2}\right\}. \tag{4.22}$$

As for the quantized channel outputs, the two-bit quantizer partition is based on the sign of the soft LLRs. In this case, the quantization induces a 4×4 channel at the i^{th} receiver with the transition probabilities shown in Table 4.1. Once the channel transition probabilities are obtained, the likelihood ratio and the mutual information can be computed.

x_ℓ	$p_{x_\ell\|0}$	$p_{x_\ell\|1}$	$p_{x_\ell\|3}$	$p_{x_\ell\|2}$
0	$1-Q(\sigma)$	$Q(\sigma)$	$Q(3\sigma)$	$Q(5\sigma)$
1	$Q(\sigma)-Q(3\sigma)$	$1-2Q(\sigma)$	$Q(\sigma)-Q(3\sigma)$	$Q(3\sigma)-Q(5\sigma)$
2	$Q(3\sigma)-Q(5\sigma)$	$Q(\sigma)-Q(3\sigma)$	$1-2Q(\sigma)$	$Q(\sigma)-Q(3\sigma)$
3	$Q(5\sigma)$	$Q(3\sigma)$	$Q(\sigma)$	$1-Q(\sigma)$

Table 4.1: Channel transition probabilities for 4PAM where $\sigma = \sqrt{\frac{\rho_i}{5}}$.

4.2.2 16QAM

Since the 16QAM has corner, edge and inner points, the conditional expectation is different for each of the situations. The mutual information can be written as

$$I_{\boldsymbol{h}}(X;\boldsymbol{Z}) = 4 - \frac{1}{2}\mathrm{E}\left[\log_2\left\{\frac{\sum_{\ell\in\mathcal{S}} p(\boldsymbol{z}|\ell)}{p(\boldsymbol{z}|1)}\right\}\Big|X=x_1\right] - \frac{1}{4}\mathrm{E}\left[\log_2\left\{\frac{\sum_{\ell\in\mathcal{S}} p(\boldsymbol{z}|\ell)}{p(\boldsymbol{z}|0)}\right\}\Big|X=x_0\right] - \frac{1}{4}\mathrm{E}\left[\log_2\left\{\frac{\sum_{\ell\in\mathcal{S}} p(\boldsymbol{z}|\ell)}{p(\boldsymbol{z}|5)}\right\}\Big|X=x_5\right] \tag{4.23}$$

where $\mathcal{S}$ denotes the set of the 16QAM constellation points and $\ell = 0$ interprets one of the 4 corner points, $\ell = 1$ interprets one of the 8 edge points and $\ell = 5$ interprets one of 4 inner points. As before, the elements of $\boldsymbol{Z}$ are conditionally independent so $p(\boldsymbol{z}|\ell)$ can be computed as the product of the marginal distributions and thus $I_h(X|\boldsymbol{Z})$ can be subsequently obtained.

For 16QAM, the conditional distribution of the unquantized channel outputs is

$$p_{Z_i|X}(z_i|X=x_\ell) = \frac{1}{2\pi}\exp\left\{-\frac{|z_i - \sqrt{\frac{\rho_i}{10}}x_\ell|^2}{2}\right\}. \tag{4.24}$$

The channel transition probabilities of the 16QAM can be computed by using Table 4.1 since the real and imaginary parts of the observation are independent.

Figure 4.10 shows the capacity versus $\mathcal{E}_s/N_0$ for $N = 1$ with $h = 1$ which summarizes the mutual information for the forward link modulation schemes discussed so far. As can be seen, while the BPSK curves are bounded by the real Gaussian input and continuous output curve, other complex-valued modulation schemes are bounded by the complex Gaussian input and continuous output curve. These curves also agree with those in standard information theory and communications textbooks.

Similar to Figure 4.10, Figure 4.11 shows the capacity versus $\mathcal{E}_b/N_0$ for $N = 1$ with $h = 1$. The notation $\mathcal{E}_b$ denotes the energy per information bit. As expected, all of the discrete input schemes are bounded either by the real Gaussian input or the complex Gaussian input curves. It also agrees with the Shannon limit that no reliable communication can be achieved below -1.59 dB.

4.2.3 Better quantizer design for 4PAM and 16QAM

In Section 3.6, we have seen that by using 2-bit per observation for BPSK and choosing the proper quantizer amplitude threshold can greatly improve the mutual information and thus yield closer outage probability performance to the beamforming case. Although many quantization techniques such as Lloyd-Max [98, 99], scaler quantization [100], vector quantization [101] are available to minimize the distortion of a signal when the number of output bits is fixed, we consider optimizing the quantizer amplitude threshold by numerical maximization of the mutual information between the channel input and the quantized channel. This idea has been published in [102,103]. In this section, we borrow the same idea and consider

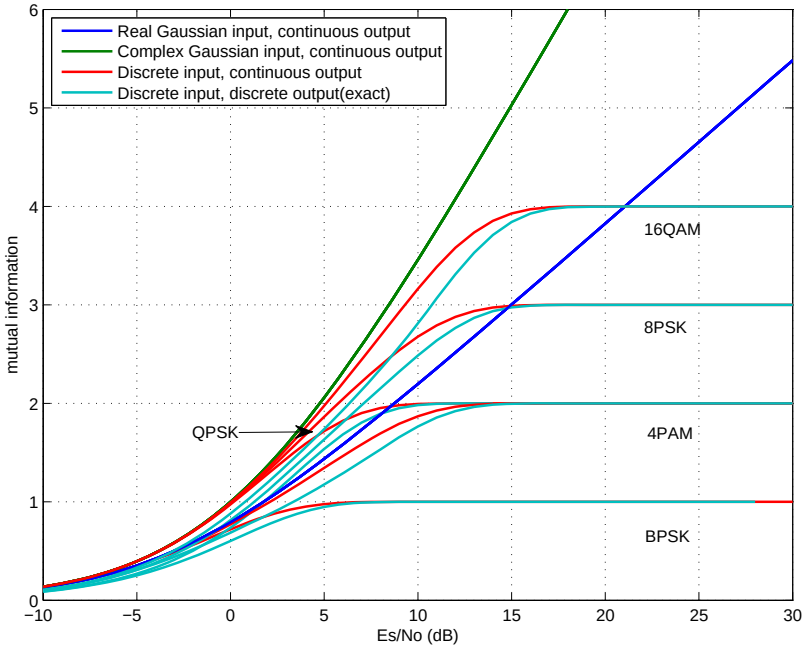

Figure 4.10: Channel capacity versus $\mathcal{E}_s/N_0$ for $N = 1$ with $h = 1$ for various modulation schemes.

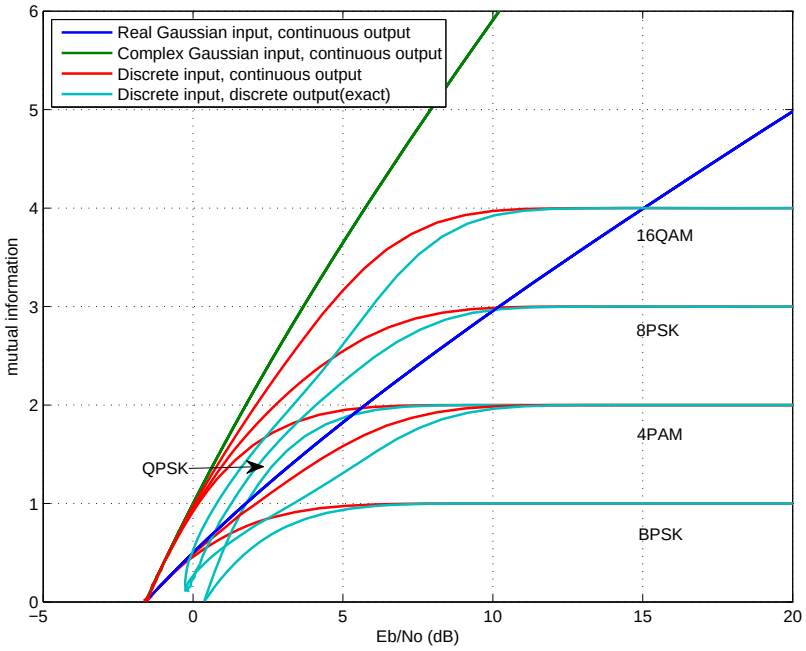

Figure 4.11: Channel capacity versus $\mathcal{E}_b/N_0$ for $N = 1$ with $h = 1$ for various modulation schemes.

the design of uniform quantization schemes for PAM and QAM.

A PAM constellation with $M = 2^k$ constellation symbols is defined as

$$\mathcal{S}_{PAM2^k} = \{-(2n-1), \cdots, -(2i-1), \cdots, -1, 1, \cdots, 2i-1, \cdots, 2n-1\}$$

where $i = 1, 2, \cdots, n$ and $n = 2^{k-1}$. The constellation symbols are selected with equal probability and $\mathcal{E}_s$ is given by $\mathcal{E}_s = \frac{4^k-1}{3}$. One can normalize these constellation such that every symbol has unit energy.

Define a uniform interval quantizer with 2^m levels (i.e., m-bit quantized) and spacing q. The set of quantization levels is given by

$$\{\mathcal{I}_i : i = 1, \cdots, 2^m\} = \{(-\infty, -nq], \cdots, (-iq, -(i-1)q], \cdots, (-q, 0],$$
$$(0, q], \cdots, ((i-1)q, iq], \ldots, (nq, +\infty)\}$$

where $i = 1, 2, \cdots, n$ and $n = 2^{m-1} - 1$.

To look at the effect of the quantizer amplitude threshold on the mutual information of the m-bit quantized single-receiver channel, we can compute the exact m-bit capacity for various values of the amplitude threshold and see where the maximum occurs. We define the normalized quantizer amplitude threshold as

$$q_{norm} = \frac{q}{|h|\sqrt{2\mathcal{E}_s/N_0}}$$

and vary q_{norm} over $(0, 5)$ for different values of $\mathcal{E}_s/N_0$ to see where the maximum mutual information occurs. The results are shown in Figure 4.12. These results show that the optimal amplitude threshold decreases as the SNR increases. Figure 4.13 shows the result obtained by using 6^{th} order polynomial fit over the range of $\mathcal{E}_s/N_0$ considered.

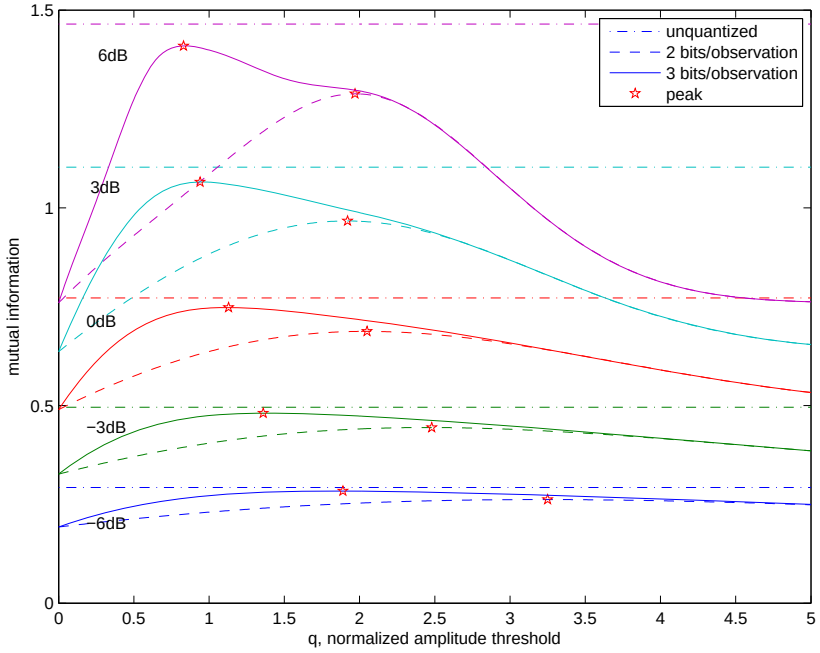

Figure 4.12: Effects of amplitude threshold on mutual information of two-bit and three-bit quantized single-receiver channel.

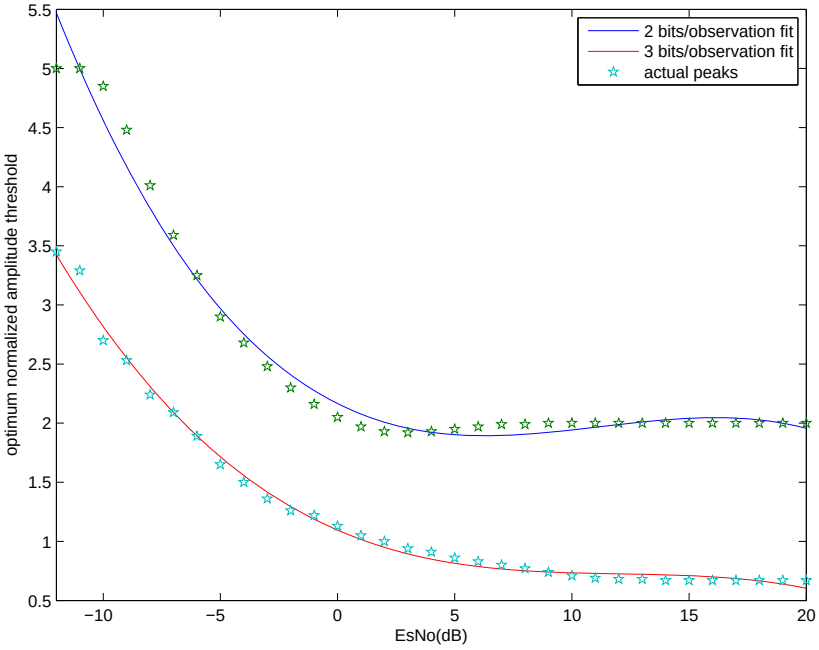

Figure 4.13: Optimum two-bit and three-bit quantizer normalized amplitude threshold to maximize mutual information at different values of $\mathcal{E}_s/N_0$ for the two-bit and three-bit quantized single-receiver channel.

The capacity of the binary-input single-receiver two-bit and three-bit quantized channel with optimum quantizer amplitude thresholds is shown in Figure 4.14. We see that the biggest capacity gains occur for $\mathcal{E}_s/N_0$ between 15 and 20dB. At low SNR values, the gain is less significant. These results are consistent with the gaps we see in Figure 4.12.

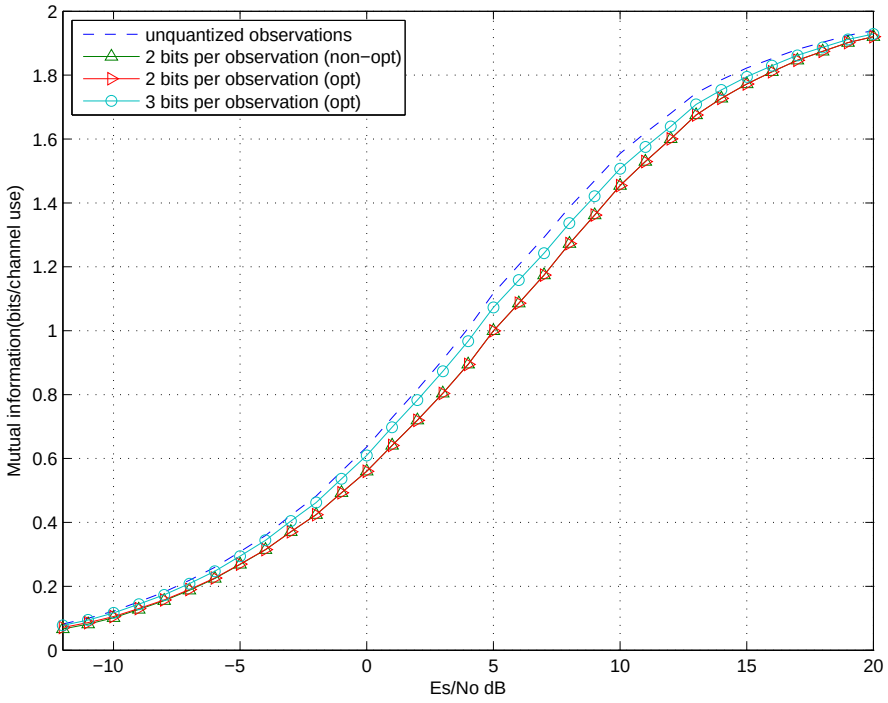

Figure 4.14: Capacities of various channels with one receiver and $h = 1$, including a receiver with two-bit/three-bit quantized channels and optimum two-bit/three-bit quantizer normalized amplitude threshold q_{norm}. The Monte-Carlo results for the binary-input unquantized-output channel were averaged over 10^6 realizations.

Similar results can be obtained for 16QAM. Figure 4.15 shows the capacity of the binary-input single-receiver four-bit and six-bit quantized channel with optimum quantizer amplitude thresholds.

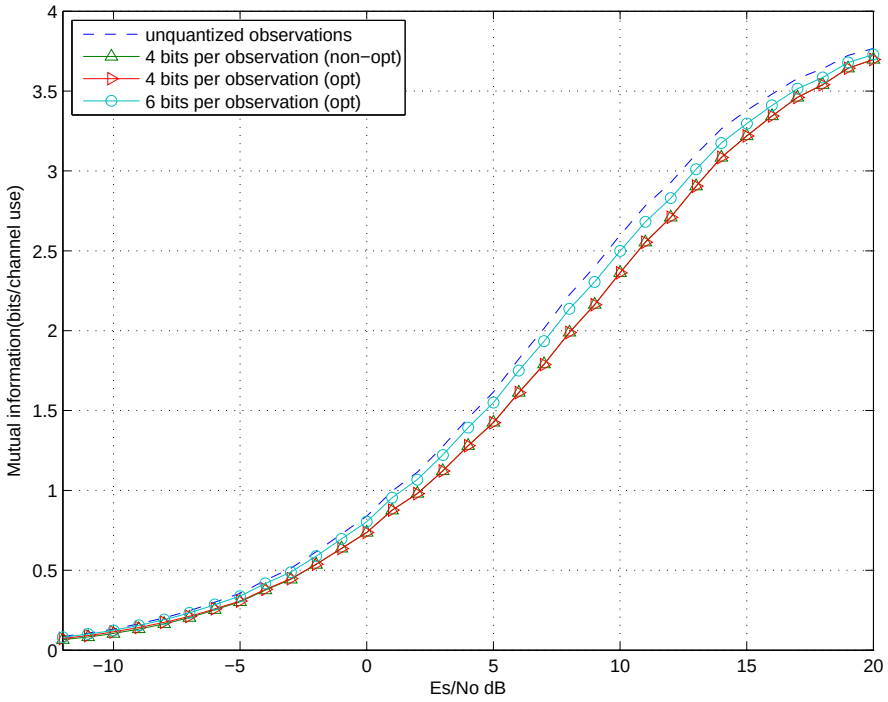

Figure 4.15: Capacities of various channels with one receiver and $h = 1$, including a receiver with four-bit/six-bit quantized channels and optimum four-bit/six-bit quantizer normalized amplitude threshold q_{norm}. The Monte-Carlo results for the binary-input unquantized-output channel were averaged over 10^6 realizations.

4.3 Numerical Results

This section provides numerical results demonstrating the efficacy of distributed reception with coarse quantization and higher-order forward link modulation. Two sets of simulations are performed: the information-theoretic and the LDPC code implementation of the distributed reception protocol with K-bit quantization where $K = \log_2 M$.

4.3.1 Information Theoretic Simulation

All of the results in this section assume spatially and temporally i.i.d. block fading channels with $h_i \sim \mathcal{CN}(0, 1)$. The first example in Figure 4.16 shows the outage probabilities for different modulation schemes by using information-theoretic simulation when the number of receive nodes $N = 1$ which means that there is no information exchanging between neighbouring nodes and each node uses its locally unquantized observations. 10,000 channel/noise realizations are performed and an outage event occurs when $I_{\boldsymbol{h}}(X; \boldsymbol{Z}) < r_{out} = \frac{\log_2(K)}{2}$ at all of the receive nodes.

It is known that 16QAM is 4 times better than the BPSK in the sense of spectrum efficiency. From Figure 4.16, it can be seen that this advantage is achieved at the penalty of 8 dB SNR decrease. Similarly, QPSK and 8PSK are 3 dB and 6 dB worse than BPSK in the outage probability sense but they are twice and three times more spetrally efficient than BPSK, respectively.

As the number of receive nodes N increases, it should be expected that the outage probability performance will be largely improved. Figure 4.17 to 4.19

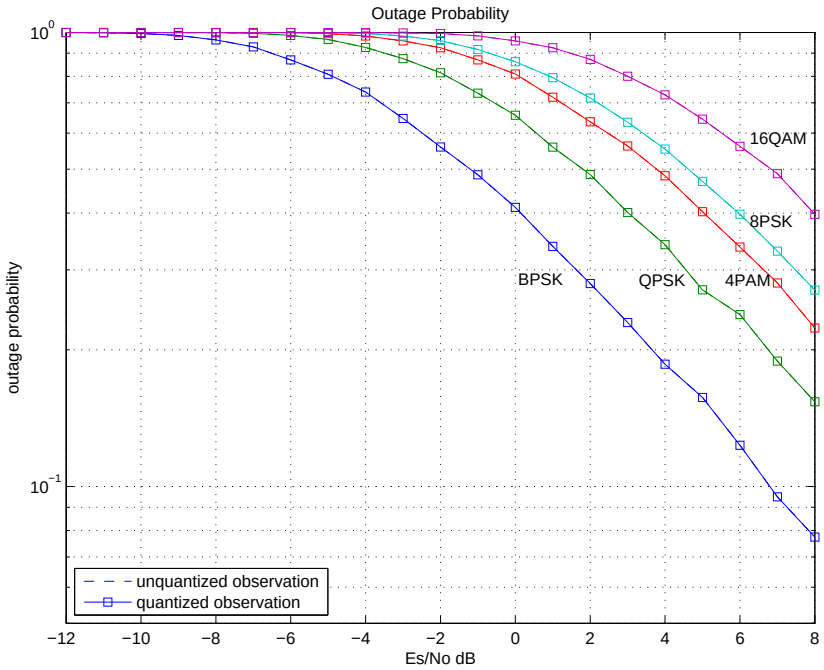

Figure 4.16: $N = 1$ node information-theoretic model example by using BPSK, QPSK, 4PAM, 8PSK and 16QAM.

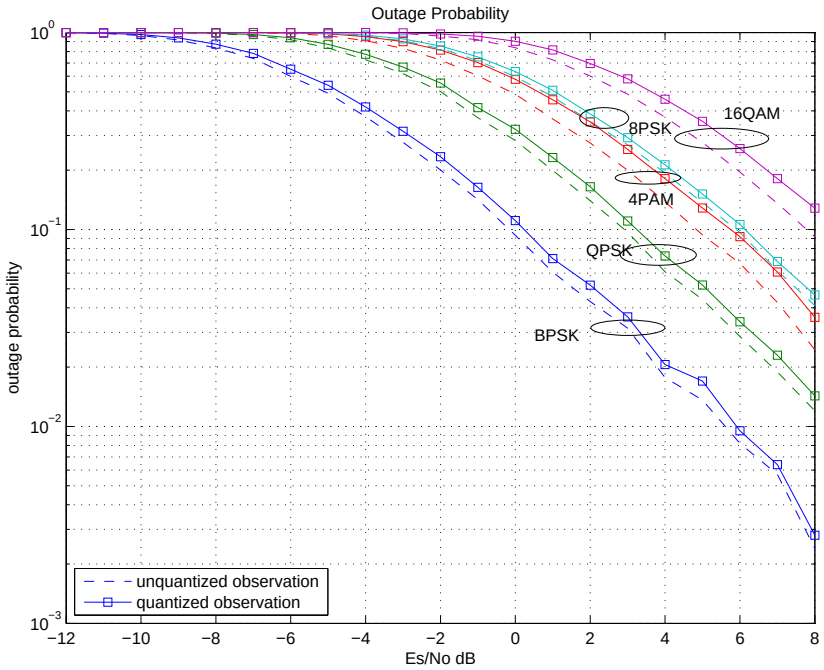

Figure 4.17: $N = 2$ node information-theoretic model example by using BPSK, QPSK, 4PAM, 8PSK and 16QAM.

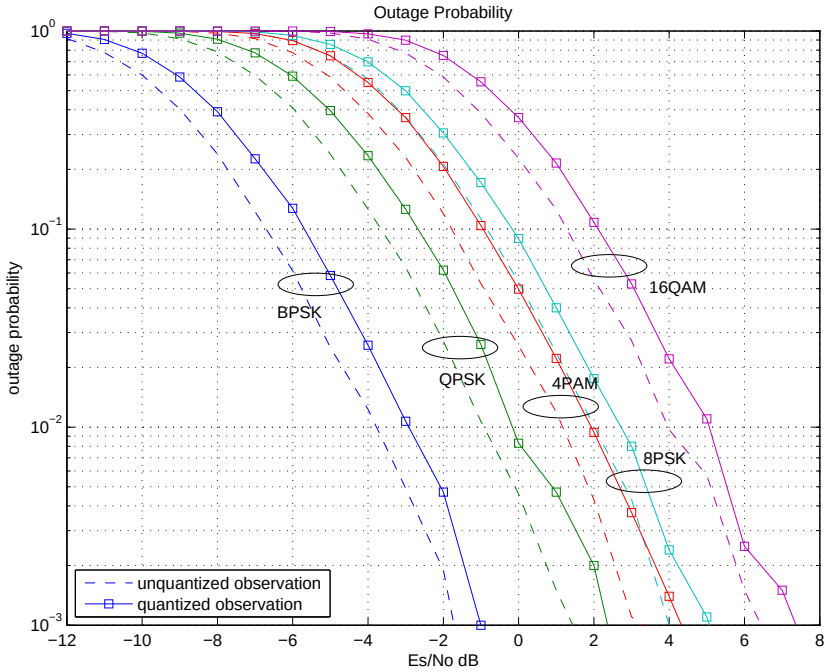

Figure 4.18: $N = 5$ node information-theoretic model example by using BPSK, QPSK, 4PAM, 8PSK and 16QAM.

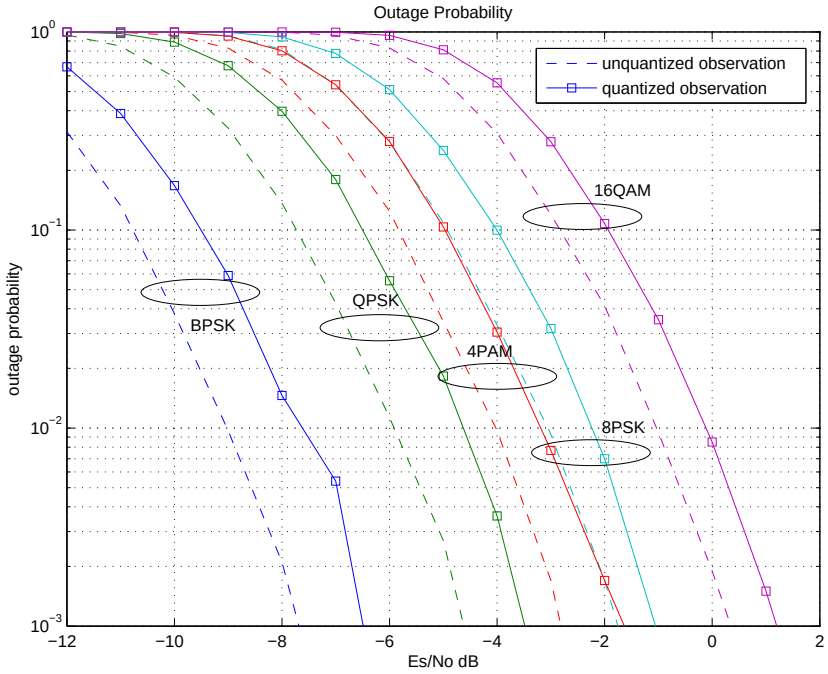

Figure 4.19: $N = 10$ node information-theoretic model example by using BPSK, QPSK, 4PAM, 8PSK and 16QAM.

demonstrate the improvement by using greater number of receive nodes. From these figures we can see that the gap between the outage probabilities of the ideal beamforming, i.e. unquantized observation and the quantized observation increases as the number of receive nodes increases. These results also show that significant improvements in outage probability can be obtained through combining locally unquantized observations with quantized observations from other nodes in the receive cluster and that the gap between exchanging ideal receive beamforming and exchanging just $\log_2(K)$ bits per coded bit is less than 1.5 dB in the cases tested.

As discussed in Section 4.2.3, the outage probability performance with the 4PAM and 16QAM forward link modulations can be further improved by using better quantizer design and finer quantization levels. Figure 4.20 and 4.21 show the results. In Figure 4.20, no significant improvement can be observed by using optimum two-bit quantizer normalized amplitude threshold q_{norm}. Only when $N = 10$ can it perform slightly better than the non-optimum case. However, when the optimum 3-bit quantizer is applied the outage probabilities almost achieve the same performance as the beamforming. The gap is no more than 0.2 dB.

Similar results are shown in Figure 4.21 for the 16QAM case. The optimum 6-bit quantizer achieves closest outage probability performance to the ideal beamforming with the gap less than 0.5 dB.

4.3.2 LDPC Simulation

In this section the numerical results of the LDPC implementation of the belief combining system are discussed. The code uses a 32-bit CRC check for block error

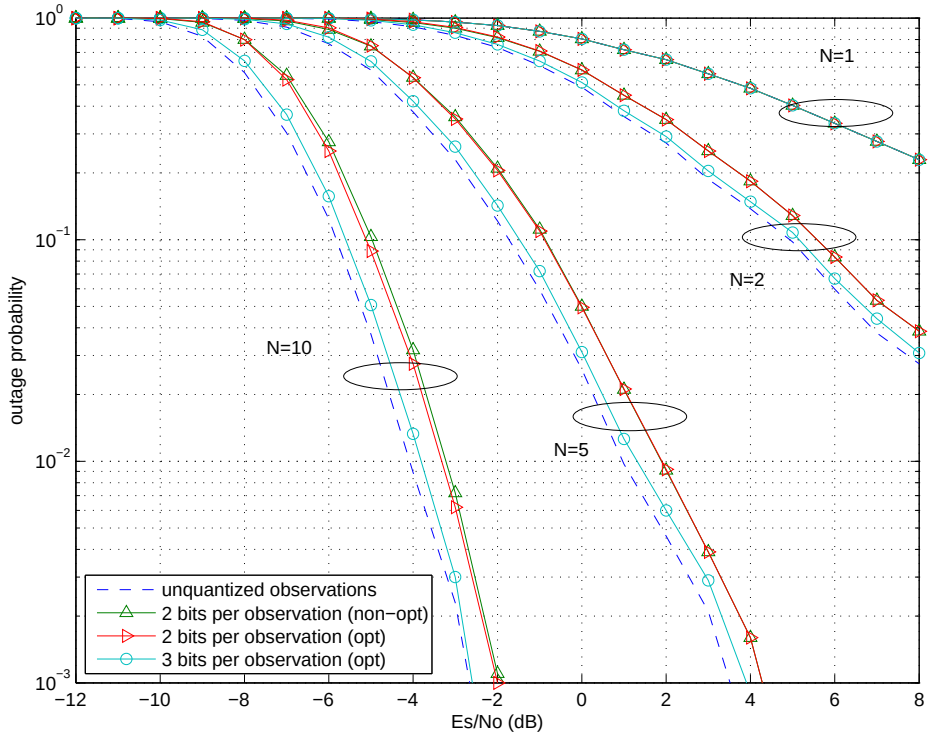

Figure 4.20: Outage probabilities of $N = 1, 2, 5, 10$ node information-theoretic model example by using 4PAM at various $\mathcal{E}_s/N_0$ values, including a receiver with two-bit quantized channels and optimum two-bit/three-bit quantizer normalized amplitude threshold q_{norm}.

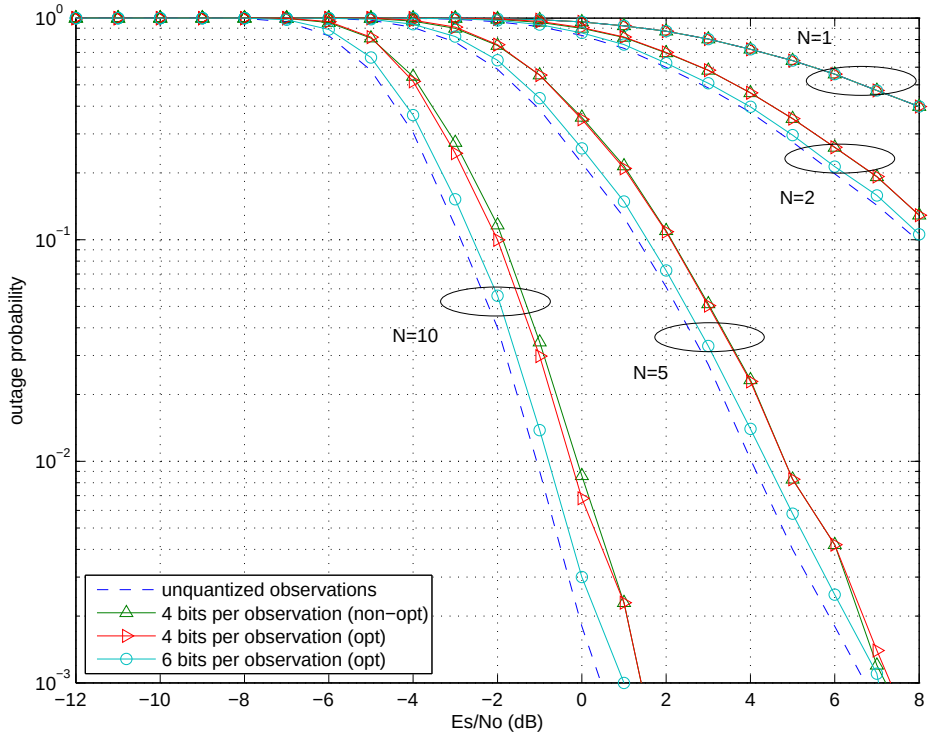

Figure 4.21: Outage probabilities of $N = 1, 2, 5, 10$ node information-theoretic model example by using 16QAM at various $\mathcal{E}_s/N_0$ values, including a receiver with four-bit quantized channels and optimum four-bit/six-bit quantizer normalized amplitude threshold q_{norm}.

detection and a rate $r = 1/2$ LDPC code with $n = 8100$ and $k = 4050$. It performs Monte-Carlo simulations at various $\mathcal{E}_s/N_0$ values by generating $M = 5000$ messages with different channel and noise realizations for each message. The block error rate at each $\mathcal{E}_s/N_0$ value is estimated by dividing the total number of block errors by M.

The first example shows the block error rate performance of the LDPC implementation of the 3-bit belief combining, i.e. 8PSK forward link modulation and the following observations are made from Figure 4.22:

1. There is a gap between all LDPC implementations and their corresponding information-theoretic predictions. The greater the number of receive nodes the larger the gap. When $N = 10$, the gap between the LDPC result and the information-theoretic predictions is approximately 1 dB.

2. Inspection of the three distributed reception approaches simulated, i.e. the receive beamforming, the belief combining and the pseudobeamforming shows that when $N > 1$, the receive beamforming always has the best performance amongst the three while it has the highest throughputs at the same time. The belief combining achieves satisfying block error rate performance while has much lower throughput requirement on LAN. The pseudobeamforming turns out to be a suboptimal approach in the sense of block error rate since it is approximately 1 dB worse than the belief combining.

3. As the number of receive nodes increases, the gap between the receive beamforming and the belief combining becomes larger. When the $N = 10$, the gap is approximately 1 dB.

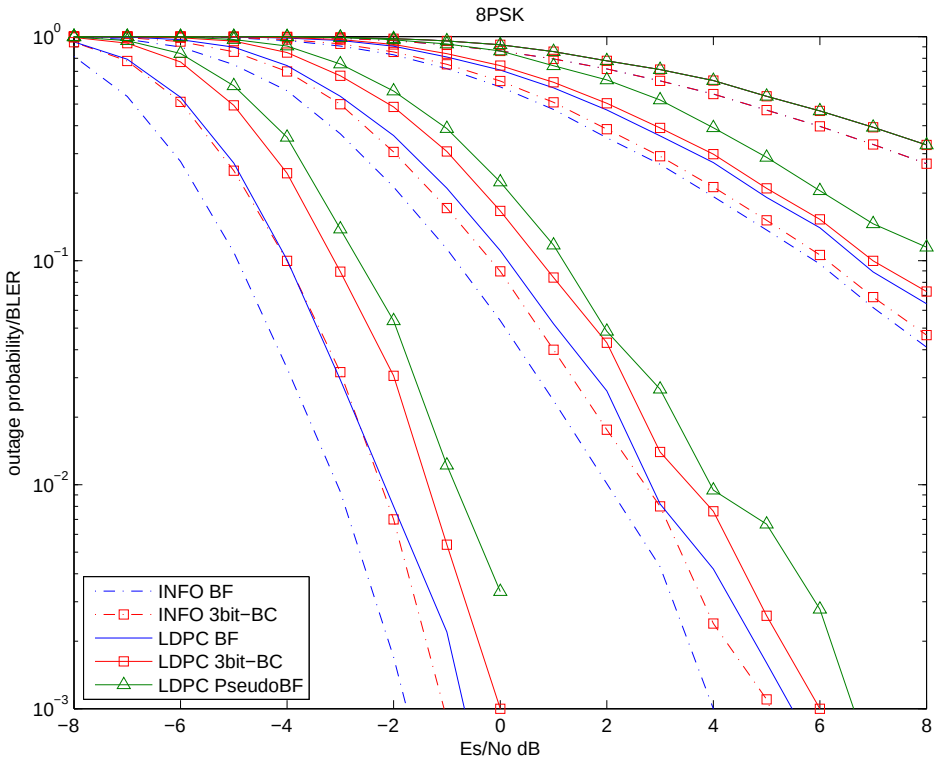

Figure 4.22: The LDPC implementation of the belief combining with 8PSK forward link modulation where $N = 1, 2, 5, 10$.

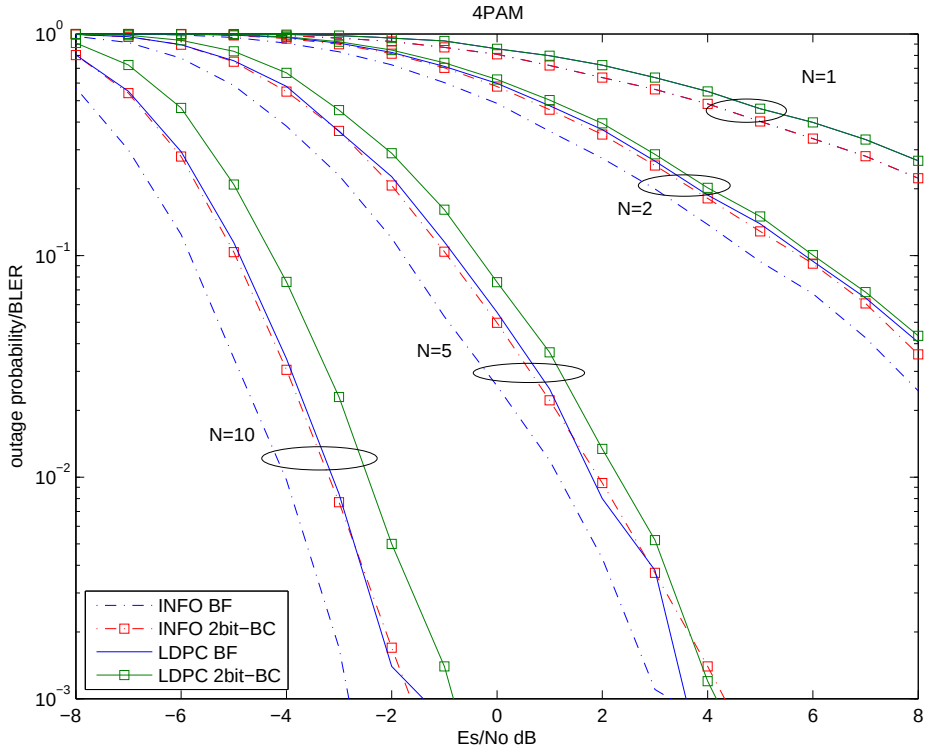

Figure 4.23: The LDPC implementation of the belief combining with 4PAM forward link modulation where $N = 1, 2, 5, 10$.

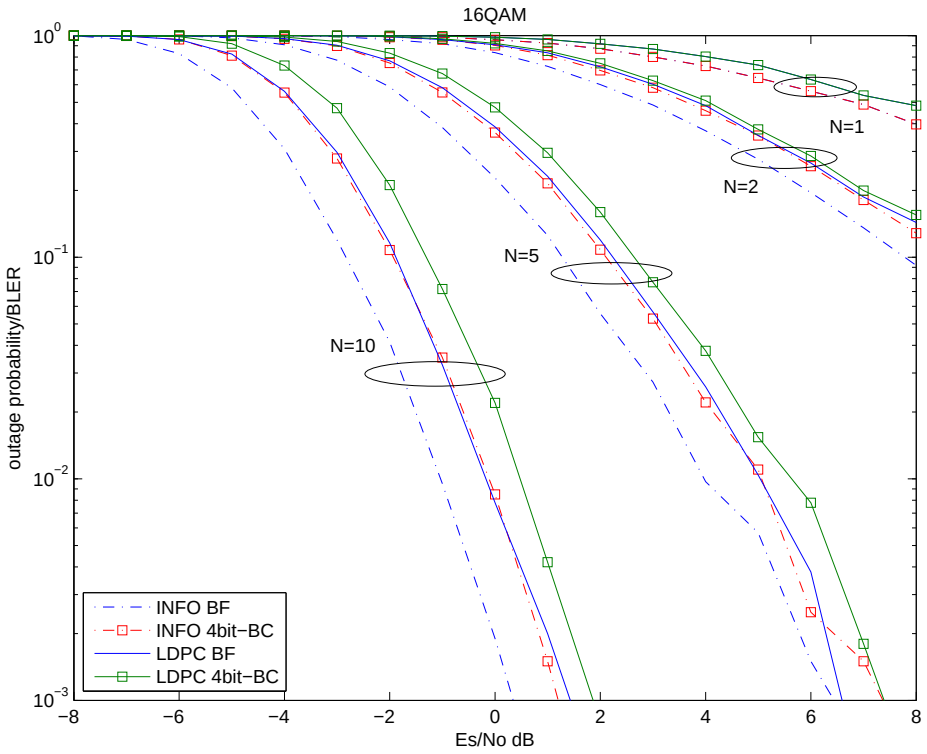

Figure 4.24: The LDPC implementation of the belief combining with 16QAM forward link modulation where $N = 1, 2, 5, 10$.

Figure 4.23 and 4.24 show the block error rates by using LDPC codes with 4PAM and 16QAM forward link modulations respectively. Similar observations can be made as the 8PSK case.

4.4 Conclusion

As an extension to Chapter 3, a more general framework with higher forward link modulation schemes is proposed in this chapter.

We first provided a suboptimal approximate distributed receive beamforming algorithm, i.e., pseudobeamforming for 8PSK based on the exchange of the hard decisions of the observations and fed it to a customized demodulator based on the statistics of the aggregate quantization error after combining. However, it turns out to be suboptimal in the outage probability sense. In fact, the likelihood of each symbol at individual receive node can be inferred from the quantized/unquantized observations and the channel transition probability so that correct decision statistics can be formed to decode the combined information. Based on this idea, a general framework for information combining with 8PSK, 4PAM and 16QAM forward link modulations is presented which turns out to be optimal in the outage probability sense. We also studied the quantizer design for 4PAM and 16QAM and showed that by choosing the proper quantizer amplitude threshold can greatly improve the outage probability. Simulation showed that by using 2-bit per observation for 4PAM and 4-bit per observation for 16QAM typically results in outage probability performance within 1 dB of ideal receive beamforming, while 3-bit/6-bit for 4PAM and 16QAM respectively performs within 0.5 dB of ideal receive beamforming.

The simulations of an LDPC coded system showed that achievable performance with real block codes can be close to the information-theoretic predictions.

Chapter 5

Conclusions and Future Research

5.1 Summary

The idea of cooperative communication, which typically refers to a system where users share and coordinate their resources to enhance the quality of transmission and reception is particularly attractive in wireless environments due to the diverse channel quality and the limited energy and bandwidth resources. As a cooperative distributed transmission technique, interference alignment has been shown to achieve the maximum capacity scaling, which is known as the degrees of freedom, of K-user interference channels with perfect channel state information and thus promises substantial theoretic gain in interference channels. It is of our interest to investigate its performance compared with the conventional interference management approach, i.e., opportunistic transmission under imperfect CSI assumption. On the receiver side, we developed and tested a belief combining distributed reception technique based on the exchange of coarsely-quantized observations among the nodes in the receive cluster.

The contributions of Chapter 2 of this dissertation present analytical and numerical results on the average sum rate performance of opportunistic transmission and SISO IA. In Chapter 3, we proposed and tested the performance of the belief combining technique with BPSK forward link modulation and showed that the performance penalty due to coarse quantization is small in the low SNR regimes enabled by cooperative distributed reception. In Chapter 4 we extended the idea

of belief combining with BPSK to a more general framework which works for more spectrally efficient forward link modulation schemes and demonstrated that with even 1-bit finer quantized observation, near beamforming outage probability performance can be achieved. We summarize our results by chapter below.

Chapter 2. In this chapter, we compared opportunistic transmission and interference alignment for a 3-user SISO interference channel in terms of average sum rate in the presence of channel estimation errors. In the case of interference alignment, channel estimation errors cause interference leakage which consequently results in a loss of achievable rate whereas in the case of opportunistic transmission, channel estimation errors result in a non-zero probability of incorrectly choosing the node with the best channel. Simulation results show that opportunistic transmission tends to outperform SISO IA in low SNR conditions and/or when channel estimates are poor whereas the SISO IA can achieve better average sum rate with good channel estimates and at high SNR.

Chapter 3. Unlike the majority of recent distributed reception techniques which are based on iterative transmission and decoding, this chapter analyzed an approximate distributed receive beamforming algorithm based on the exchange of coarsely-quantized observations among some or all of the nodes in the receive cluster. The numerical results from information-theoretic analysis, as well as simulations of an LDPC coded system, showed that exchanging just one bit per forward-link coded bit (i.e., hard decisions based on the sign of the observation) typically results in outage probability performance within 1.5 dB of ideal receive beamforming, while two bits per coded bit (one sign and one amplitude bit) performs within 0.5 dB

of ideal receive beamforming. Our results lead to the intuitively pleasing observation that the low (per node) SNR regimes enabled by cooperative distributed reception limit the performance loss caused by coarse quantization. We also provided explicit estimates of backhaul throughput requirements as a function of the forward information rate, and demonstrate the efficacy of the technique with full and limited receiver participation.

Chapter 4. This chapter considered extending the idea in Chapter 3 to a more general framework with higher forward link modulation schemes. We first proposed a suboptimal approximate distributed receive beamforming algorithm, i.e., pseudobeamforming for 8PSK based on the exchange of the hard decisions of the observations and fed it to a customerized demodulator based on the statistics of the aggregate quantization error after combining. Then a general framework for information combining with 8PSK, 4PAM and 16QAM forward link modulations is presented which turns out to be optimal in the outage probability sense. We also studied the quantizer design for 4PAM and 16QAM and showed that by choosing the proper quantizer amplitude threshold can greatly improve the outage probability. Simulation showed that by using 2-bit per observation for 4PAM and 4-bit per observation for 16QAM typically results in outage probability performance within 1 dB of ideal receive beamforming, while 3-bit/6-bit for 4PAM and 16QAM respectively performs within 0.5 dB of ideal receive beamforming. The simulations of an LDPC coded system showed that achievable performance with real block codes can be close to the information-theoretic predictions.

5.2 Future Research Directions

Future investigation on cooperative distributed transmission and reception could take several directions. The following is a list of possible research topics that can be pursued as an extension of this dissertation:

- In Chapter 2, we focused on a closed-form SISO IA solution particularly for 3-user SISO systems. IA solutions of K-user systems based on the structure of this closed-form solution turns out to be computationally expensive as the number of users increases. It is of interest to develop an efficient IA solution for K-user cases.

  While in this dissertation we mainly focused on theoretical issues, there is an increasing amount of work that explores practical challenges faced in the implementation of available IA schemes. For example, the overhead for acquiring CSI, impact of channel correlations, etc.

- While full knowledge of CSI is assumed in Chapter 3, it is important to investigate the effect of channel estimation errors, which may become a significant bottleneck at the low per-node receive SNRs of interest. It is also of interest to extend the simple frequency non-selective fading model here to more complex propagation environments. We are also interested in exploring the requirements on quantizer precision for distributed reception of spatially multiplexed data streams, which is a key concept in hierarchical cooperation for scaling ad hoc networks.

  Another important topic for future work is to apply the idea of space-time block code, i.e., Alamouti, to the distributed reception technique so that

spatial diversity can be explored. Similar bound approximations on such system can be applied so that quick performance evaluation can be done.

- In Chapter 4, a comprehensive bound or bound approximation analysis of the distributed reception technique with higher order forward link modulations is of great interest as a direction for future work. This is because given a LAN throughput requirement, it can quickly provide the best strategy of information combining in the outage probability sense with the most spectrally efficient forward link modulation schemes. We would also like to study the partial participation and bits allocation problems of distributed reception which are of particular interest in many practical conditions.

Appendices

Appendix A

Solution for Decoding Vectors U_k

Given the channel state information and precoding vectors V_k, the decoding vectors U_k can usually be obtained by using Gram-Schmidt process. For example, if CJ scheme is applied for a three-user SISO IA system, the corresponding $N \times l_k$ decoding vectors U_k, $k = \{1, 2, 3\}$ can be written as

$$\begin{aligned} U_1 &= \begin{bmatrix} \boldsymbol{u}_{1,1} & \boldsymbol{u}_{1,2} & \cdots & \boldsymbol{u}_{1,l_1} \end{bmatrix} \\ U_2 &= \begin{bmatrix} \boldsymbol{u}_{2,1} & \boldsymbol{u}_{2,2} & \cdots & \boldsymbol{u}_{2,l_2} \end{bmatrix} \\ U_3 &= \begin{bmatrix} \boldsymbol{u}_{3,1} & \boldsymbol{u}_{3,2} & \cdots & \boldsymbol{u}_{3,l_3} \end{bmatrix} \end{aligned} \tag{A.1}$$

where $\boldsymbol{u}_{k,i}$ denotes the i^{th} column of U_k. Since ideally we have

$$U_k^\dagger H_{kj} V_j = 0$$

$$\text{rank}(U_k^\dagger H_{kk} V_k) = l_k.$$

where $j \neq k$ which implies

$$U_k^\dagger H_{kj} V_j = 0 \Rightarrow U_k \perp H_{kj} V_j.$$

Let $H_{kj} V_j = A$ and $b = H_{kk} V_k$. Then by Gram-Schmidt, we have

$$U_k = b - A(A^\dagger A)^{-1} A^\dagger b.$$

However, ill-conditioning problem arises when the number of extensions or the number of users is large. In other words, we will run into the case where $|A^\dagger A| \approx 0$ which makes $A^\dagger A$ close to singular.

The simplest ill-conditioning problem arises in a three-user SISO system with $N = 7$ extensions. According to the CJ scheme, the DoFs are assigned as $(\frac{4}{7}, \frac{3}{7}, \frac{3}{7})$. Table A.1 shows the changes in rank in the process of computing decoding vectors U_k if normal Gram-Schmidt orthogonalization is applied. Let $H_{kj}V_j = A$, so at receiver 1, i.e., Rx 1, $A = H_{12}V_2$ or $A = H_{13}V_3$ since interference is aligned.

	rank(A)	rank($A^\dagger A$)	rank(V_i)	rank($V_i^\dagger V_i$)
Rx 1	3	3	3	3
Rx k	4	1	4	1

Table A.1: An example of rank deficient in computing U_k.

Hence $A^\dagger A$ at receiver k, where $k \neq 1$ is not invertible. Direct use of the Gram-Schmidt process might lead to inaccurate results. This phenomenon can be interpreted as the interference subspace spanned by transmitter 1 has redundant dimensions so that the solution to the decoding vectors at receiver k is not unique. In the specific example shown in table A.1, U_2 needs to satisfy

$$A^\dagger U_2 = \mathbf{0}_{3\times 3} \tag{A.2}$$

$$\text{rank}(b^\dagger U_2) = l_2 \tag{A.3}$$

where $A = H_{21}V_1$, $b = H_{22}V_2$ and U_2 is a 7×3 matrix with $l_1 = 3$. In other words, the columns of $U_2 \in \text{null}(A)$. Therefore, a small modification is made on the Gram-Schmidt process

$$U_k = b - A\text{pinv}(A^\dagger A)A^\dagger b. \tag{A.4}$$

where psuedo-inverse is applied instead of direct inverse of the $A^\dagger A$ matrix.

Appendix B

Solutions for K-user SISO IA ($K > 3$)

The idea of the CJ scheme for three-user interference alignment can be extended for K user. Recall *Theorem 1* in [104]: The number of degrees of freedom per user for the K-user interference channel is $K/2$

$$\max_{\mathcal{D}} d_1 + d_2 \cdots + d_K = K/2 \tag{B.1}$$

and a constructive proof of this achievability is provided in the appendix in [1]. The procedure is briefly summarized as follows:

Let $L = (K-1)(K-2)-1$ where L is the number of distinct ancillary matrices $T_j^{[i]}$, $i, j = \{2, 3, \cdots, K\}, i \neq j$. They show that $(d_1(n), d_2(n), \cdots, d_K(n))$ lies in the degrees of freedom region of the K-user interference channel for any $n \in \mathbb{N}$ where

$$d_1(n) = \frac{(n+1)^L}{(n+1)^L + n^L} \tag{B.2}$$

$$d_i(n) = \frac{n^L}{(n+1)^L + n^L}, \ i = 2, 3, \cdots, K. \tag{B.3}$$

The interference alignment scheme uses $(n+1)^L+n^L$ time slots and the $(n+1)^L+n^L$ symbols transmitted over these time slots are denoted as supersymbols. We call $N = (n+1)^L + n^L$ the symbol extension of the original channel.

As in the $K = 3$ user case, receiver 1 has to extract $(n+1)^L$ interference free dimensions from a total of $N = (n+1)^L + n^L$-dimensional received signal vector. Hence the dimension of the interference should be no more than n^L. Similarly, receiver 2 to K have to extract n^L out of N from each of their received signal

vectors leaving them $(n+1)^L$-dimensional interference space. Hence we have

$$\text{At receiver 1, } H_{12}V_2 = H_{13}V_3 = H_{14}V_4 = \cdots = H_{1K}V_K \tag{B.4}$$

$$\text{At receiver 2,} \begin{cases} H_{23}V_3 \prec H_{21}V_1 \\ H_{24}V_4 \prec H_{21}V_1 \\ \vdots \\ H_{2K}V_K \prec H_{21}V_1 \end{cases} \tag{B.5}$$

$$\text{At receiver } i,\ H_{ij}V_j \prec H_{i1}V_1 \tag{B.6}$$

where $i = \{3, \cdots, K\}$ and $j \notin \{1, i\}$.

Since H_{ij} are diagonal matrices and have full rank almost surely, (B.4)-(B.6) can be equivalently expressed as

$$\text{At receiver } 1, V_j = S_j B, \quad j = \{2, 3, 4, \cdots, K\} \tag{B.7}$$

$$\text{At receiver 2,} \begin{cases} T_3^{[2]}B = B \prec V_1 \\ T_4^{[2]}B \prec V_1 \\ \vdots \\ T_K^{[2]}B \prec V_1 \end{cases} \tag{B.8}$$

$$\text{At receiver } i, T_j^{[i]}B \prec V_1$$

where $i, j = \{3, \cdots, K\}, i \neq j$ and

$$B = (H_{31})^{-1}H_{32}V_2 \tag{B.9}$$

$$S_j = (H_{1j})^{-1}H_{12}(H_{32})^{-1}H_{31}, j = \{2, 3, \cdots, K\} \tag{B.10}$$

$$T_j^{[i]} = (H_{i1})^{-1}H_{ij}S_j \tag{B.11}$$

where $i, j = 2, 3, \cdots, K, j \neq i$. Note that $T_2^{[3]} = \boldsymbol{I}_{N\times N}$. The things left to be determined are B and V_1 so that (B.8)-(B.9) can be satisfied, i.e.,

$$T_j^{[i]} B \prec V_1 \tag{B.12}$$

for all $i, j = \{2, 3, \cdots, K\}, i \neq j$. Assuming that $\boldsymbol{\omega} = \begin{bmatrix} 1 \cdots 1 \end{bmatrix}^{\top}_{N\times 1}$, the $B_{N\times n^L}$ vector and $V_{1_{N\times(n+1)^L}}$ are as follows

$$B = \left[\left(\prod_{\substack{m,k \in \{2,3,\cdots,K\}, \\ m \neq k, (m,k) \neq (3,2)}} (T_k^{[m]})^{\alpha_{mk}} \right) \boldsymbol{\omega} : \forall \alpha_{mk} \in \{0, 1, 2, \cdots, n-1\} \right] \tag{B.13}$$

$$V_1 = \left[\left(\prod_{\substack{m,k \in \{2,3,\cdots,K\}, \\ m \neq k, (m,k) \neq (3,2)}} (T_k^{[m]})^{\alpha_{mk}} \right) \boldsymbol{\omega} : \forall \alpha_{mk} \in \{0, 1, 2, \cdots, n\} \right]. \tag{B.14}$$

Two examples are shown to illustrate this general procedure of computing precoding vetors and its corresponding average sum rate performance.

Example 1: When $K = 3, n = 1, L = 1$. B and V_1 are chosen as

$$B = \begin{bmatrix} \boldsymbol{\omega} & T_3^{[2]}\boldsymbol{\omega} & \cdots & (T_3^{[2]})^{n-1}\omega \end{bmatrix} \tag{B.15}$$

$$= \boldsymbol{\omega} \tag{B.16}$$

$$V_1 = \begin{bmatrix} \boldsymbol{\omega} & T_3^{[2]}\boldsymbol{\omega} & \cdots & (T_3^{[2]})^{n}\boldsymbol{\omega} \end{bmatrix} \tag{B.17}$$

$$= \begin{bmatrix} \boldsymbol{\omega} & T_3^{[2]}\boldsymbol{\omega} \end{bmatrix} \tag{B.18}$$

where according to equation (B.10), (B.11) $T_3^{[2]}$ is defined as

$$T_3^{[2]} = (H_{21})^{-1}H_{23}S_3 \tag{B.19}$$

$$= (H_{21})^{-1}H_{23}(H_{13})^{-1}H_{12}(H_{32})^{-1}H_{31} \tag{B.20}$$

$$= H_{12}(H_{21})^{-1}H_{23}(H_{32})^{-1}H_{31}(H_{13})^{-1}. \tag{B.21}$$

Recall T equation (4) in [84] which is $T := H_{12}(H_{21})^{-1}H_{23}(H_{32})^{-1}H_{31}(H_{13})^{-1}$. Hence the T matrices obtained by the general scheme when $K = 3$ (base case) agrees with that in [84], i.e. T: $T = T_3^{[2]}$.

Hence we have

$$V_1 = \begin{bmatrix} \boldsymbol{\omega} & T_3^{[2]}\boldsymbol{\omega} \end{bmatrix} \tag{B.22}$$

$$V_2 = S_2B \tag{B.23}$$

$$= (H_{12})^{-1}H_{12}(H_{32})^{-1}H_{31}\boldsymbol{\omega} \tag{B.24}$$

$$= (H_{32})^{-1}H_{31}\boldsymbol{\omega} \tag{B.25}$$

$$V_3 = S_3B \tag{B.26}$$

$$= (H_{13})^{-1}H_{12}(H_{32})^{-1}H_{31}\boldsymbol{\omega} \tag{B.27}$$

$$= (H_{23})^{-1}H_{21}T_3^{[2]} \tag{B.28}$$

$$= (H_{13})^{-1}H_{12}(H_{32})^{-1}H_{31}\boldsymbol{\omega} \tag{B.29}$$

Example 2: When $K = 4, n = 1$, we have $L = (K-1)(K-2) - 1 = 5, N = (n+1)^L + n^L = 33$. Hence

$$B = [\boldsymbol{\omega}]_{N \times n^L = 33 \times 1} \tag{B.30}$$

$$V_1 = \left[\boldsymbol{\omega} \quad \beta_1 \boldsymbol{\omega} \quad \cdots \quad \beta_{(n+1)^L} \boldsymbol{\omega}\right]_{N \times (n+1)^L} \tag{B.31}$$

where $\beta_i = (T_3^{[2]})^{\alpha_{23}} (T_4^{[2]})^{\alpha_{24}} (T_4^{[3]})^{\alpha_{34}} (T_2^{[4]})^{\alpha_{42}} (T_3^{[4]})^{\alpha_{43}}$ in which $\alpha_{23}, \alpha_{24}, \alpha_{34}, \alpha_{42}, \alpha_{43}$ take values 0,1. Hence there are 2^5 combinations. β_is are defined in Table B.1.

i	α_{43}	α_{42}	α_{34}	α_{24}	α_{23}	β_i
1	0	0	0	0	0	$\mathbf{1}$
2	0	0	0	0	1	$T_3^{[2]}$
3	0	0	0	1	0	$T_4^{[2]}$
4	0	0	0	1	1	$T_3^{[2]} T_4^{[2]}$
$\vdots$						$\vdots$
32	1	1	1	1	1	$T_3^{[2]} T_4^{[2]} T_4^{[3]} T_2^{[4]} T_3^{[4]}$

Table B.1: β_i where $i = \{1, 2, \cdots 32\}$.

Therefore, V_1 can be written as

$$V_1 = \left[\boldsymbol{\omega} \quad T_3^{[2]}\boldsymbol{\omega} \quad T_4^{[2]}\boldsymbol{\omega} \quad T_3^{[2]}T_4^{[2]}\boldsymbol{\omega} \quad \cdots \quad T_3^{[2]}T_4^{[2]}T_4^{[3]}T_2^{[4]}T_3^{[4]}\boldsymbol{\omega}\right]. \tag{B.32}$$

Use equation (B.7), (B.9), (B.10) and (B.30) , $V_i, i = \{2, 3, \cdots, K\}$ can be deter-

mined as

$$
\begin{aligned}
V_2 &= S_2 B \\
&= (H_{12})^{-1} H_{12} (H_{32})^{-1} H_{31} B \\
&= (H_{32})^{-1} H_{31} B \\
&= (H_{32})^{-1} H_{31} \boldsymbol{\omega} \\
V_3 &= S_3 B \\
&= (H_{13})^{-1} H_{12} (H_{32})^{-1} H_{31} B \\
&= (H_{13})^{-1} H_{12} (H_{32})^{-1} H_{31} \boldsymbol{\omega} \\
V_4 &= S_4 B \\
&= (H_{14})^{-1} H_{12} (H_{32})^{-1} H_{31} B \\
&= (H_{14})^{-1} H_{12} (H_{32})^{-1} H_{31} \boldsymbol{\omega}.
\end{aligned}
$$

Since the dimension of the solution goes exponentially with the number of users, the CJ scheme quickly becomes computationally impossible. The significance of this scheme is mainly theoretical.

Appendix C

Summing LLRs of Unquantized Observations Is Equivalent to Ideal Beamforming for BPSK

In this appendix, we show that the log-likelihood ratio of the ideal receive beamformer decision statistic is equivalent to the sum of the log-likelihood ratios of the unquantized decision statistics at each node in the receive cluster. Given the individual unquantized decision statistics Z_i for $i = 1, \ldots, N$, the ideal receive beamformer decision statistic can be written as

$$Z_{bf} = \frac{1}{\|\boldsymbol{h}\|} \sum_{i=1}^{N} |h_i| Z_i = \|\boldsymbol{h}\| \sqrt{2\mathcal{E}_s/N_0} X + W'$$

where $W' \sim \mathcal{N}(0, 1)$. Hence, given the realization $Z_{bf} = z$, the LLR is $\ell(z) = 2z\|\boldsymbol{h}\| \sqrt{2\mathcal{E}_s/N_0}$. But since $z = \frac{1}{\|\boldsymbol{h}\|} \sum_{i=1}^{N} |h_i| z_i$, this can be written as

$$\ell(z) = 2\sqrt{2\mathcal{E}_s/N_0} \sum_{i=1}^{N} |h_i| z_i = \sum_{i=1}^{N} 2z_i \sqrt{\rho_i} = \sum_{i=1}^{N} \ell_i(z_i).$$

Hence, the LLR of the ideal receive beamformer decision statistic is equivalent to the sum of the individual LLRs of the unquantized decision statistics at each receive node.

Appendix D

Summing LLRs of Unquantized Observations Is Not Equivalent to Ideal Beamforming for 8PSK

In this appendix, we show that for 8PSK, however, summing LLRs of unquantized observations is not equivalent to beamforming. To see this, recall that the log-likelihood ratio (LLR) is the logarithm of the ratio of probabilities of a 0 bit being transmitted versus a 1 bit being transmitted for a received signal. The LLR for a bit x conditioned on the received signal z is defined as

$$\ell(x|z) = \log\left\{\frac{\text{Prob}(X=+1|Z=z_i)}{\text{Prob}(X=-1|Z=z_i)}\right\}. \tag{D.1}$$

Given the 8PSK Gray constellation in Figure D.1 and let $\ell(x_{ki}|z_i)$ indicate the LLR of the k^{th} bit x_{ki} given z_i, the LLR based on the unquantized observation can be written as

$$L(x_{ki}|z_i) = \frac{\text{Prob}(x_{ki}=+1|Z=z_i)}{\text{Prob}(x_{ki}=-1|Z=z_i)} \tag{D.2}$$

where

$$\text{Prob}(x_{ki}=+1|Z=z_i) = \sum_{q\in S(x_{ki}=+1)} \text{Prob}(s_i = s^{(q)}|z_i) \tag{D.3}$$

$$\text{Prob}(x_{ki}=-1|Z=z_i) = \sum_{q\in S(x_{ki}=-1)} \text{Prob}(s_i = s^{(q)}|z_i) \tag{D.4}$$

where $S(x_{ki}=+1)$ and $S(x_{ki}=-1)$ are the subsets of symbol indexes corresponding to $x_i=+1$ and $x_i=-1$ respectively.

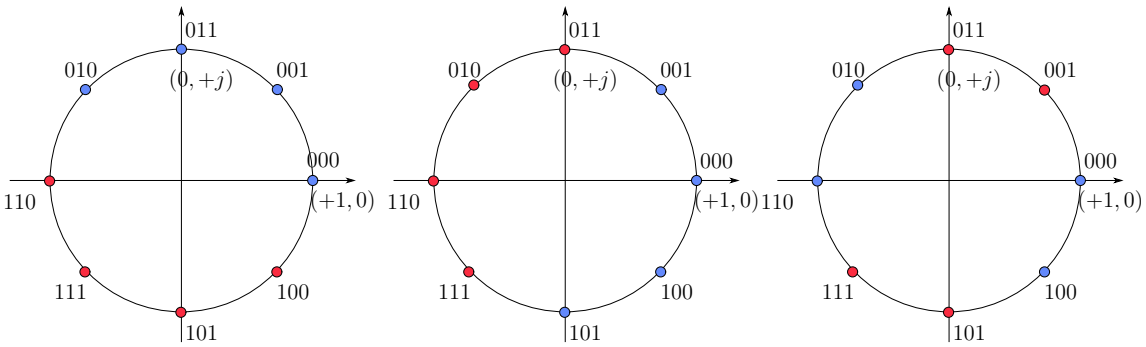

Figure D.1: Symbol set partitioning for each bit in 8PSK Gray constellation where the red dot indicates $-1(1)$ and blue dot indicates $+1(0)$.

In the case of equiprobable symbols, we have

$$\begin{aligned}\ell(x_{ki}|z_i) &= \ln \frac{\sum\limits_{q\in S(x_{ki}=+1)} \text{Prob}(s_i = s^{(q)}|z_i)}{\sum\limits_{q\in S(x_{ki}=-1)} \text{Prob}(s_i = s^{(q)}|z_i)} \\ &= \ln \frac{\sum\limits_{q\in S(x_{ki}=+1)} p(z_i|s^{(q)})}{\sum\limits_{q\in S(x_{ki}=-1)} p(z_i|s^{(q)})}. \end{aligned} \tag{D.5}$$

From the assumption on the noise, we have

$$\begin{aligned} p(z_i|s^{(q)}) &= \frac{1}{\sqrt{2\pi}}\exp\left\{-\frac{(z_i - \sqrt{2E_s/N_o}|h_i|s^{(q)})^2}{2}\right\} \qquad \text{(D.6)} \\ &= \frac{1}{\sqrt{2\pi}}\exp\left\{-\frac{(\text{Re}(z_i) - \sqrt{2E_s/N_o}|h_i|\text{Re}(s^{(q)}))^2 + (\text{Im}(z_i) - \sqrt{2E_s/N_o}|h_i|\text{Im}(s^{(q)}))^2}{2}\right\}. \end{aligned}$$

Therefore the straightforward calculation gives

$$\begin{aligned}
\ell(x_{1i}|z_i) \quad = \log \Bigg\{ \Bigg[& \exp\left(-\frac{(\mathrm{Re}(z_i)+\sqrt{2E_s/N_o}|h_i|\frac{\sqrt{2}}{2})^2+(\mathrm{Im}(z_i)-\sqrt{2E_s/N_o}|h_i|\frac{\sqrt{2}}{2})^2}{2} \right) \\
& + \exp\left(-\frac{(\mathrm{Re}(z_i))^2+(\mathrm{Im}(z_i)-\sqrt{2E_s/N_o}|h_i|)^2}{2} \right) \\
& + \exp\left(-\frac{(\mathrm{Re}(z_i)-\sqrt{2E_s/N_o}|h_i|\frac{\sqrt{2}}{2})^2+(\mathrm{Im}(z_i)-\sqrt{2E_s/N_o}|h_i|\frac{\sqrt{2}}{2})^2}{2} \right) \\
& + \exp\left(-\frac{(\mathrm{Re}(z_i)-\sqrt{2E_s/N_o}|h_i|)^2+(\mathrm{Im}(z_i))^2}{2} \right) \Bigg] / \\
& \Bigg[\exp\left(-\frac{(\mathrm{Re}(z_i)+\sqrt{2E_s/N_o}|h_i|\frac{\sqrt{2}}{2})^2+(\mathrm{Im}(z_i)+\sqrt{2E_s/N_o}|h_i|\frac{\sqrt{2}}{2})^2}{2} \right) \\
& + \exp\left(-\frac{(\mathrm{Re}(z_i))^2+(\mathrm{Im}(z_i)+\sqrt{2E_s/N_o}|h_i|)^2}{2} \right) \\
& + \exp\left(-\frac{(\mathrm{Re}(z_i)-\sqrt{2E_s/N_o}|h_i|\frac{\sqrt{2}}{2})^2+(\mathrm{Im}(z_i)+\sqrt{2E_s/N_o}|h_i|\frac{\sqrt{2}}{2})^2}{2} \right) \\
& + \exp\left(-\frac{(\mathrm{Re}(z_i)+\sqrt{2E_s/N_o}|h_i|)^2+(\mathrm{Im}(z_i))^2}{2} \right) \Bigg] \Bigg\}. \qquad \text{(D.7)}
\end{aligned}$$

Similarly we can write the expression for $\ell(x_{2i}|z_i)$ and $\ell(x_{3i}|z_i)$.

Since $Z_i = Y_i$ for unquantized output, i.e. receive beamforming outputs, $\ell_{\text{unquantized}}(x_{ki}|y_i) = \ell(x_{ki}|z_i)$. An ideal receive beamformer generates the decision statistic $Z = \sum_{i=1}^{N} |h_i| Y_i$. It can be shown that the LLR of the beamformer output realization $Z = z$ is

$$\begin{aligned}
\ell_{\text{bf}}(x_{ki}|z) &= \ln \left\{ \frac{\text{Prob}(x_{ki} = +1|Z = z)}{\text{Prob}(x_{ki} = -1|Z = z)} \right\} \\
&= \ell(x_{ki}|z)
\end{aligned}$$

where the expression for $\ell_{\text{bf}}(x_{ki}|z)$ is similar to equation (D.7) except that now the LLR is conditioned on $Z = \sum_{i=1}^{N} |h_i| Y_i$ instead of $Z_i = Y_i$ and $\sqrt{2E_s/N_o}|h_i|$ becomes

$\sqrt{2E_s/N_o}\sum_{i=1}^{N}|h_i|$, i.e.,

$$p(z_i|s^{(q)}) = \frac{1}{\sqrt{2\pi}}\exp\left\{-\frac{(z-\sqrt{2E_s/N_o}\sum_{i=1}^{N}|h_i|s^{(q)})^2}{2}\right\} \tag{D.8}$$

$$= \frac{1}{\sqrt{2\pi}}\exp\left\{-\frac{1}{2}\left[(\mathrm{Re}(\sum_{i=1}^{N}z_i) - \sqrt{2E_s/N_o}\sum_{i=1}^{N}|h_i|\mathrm{Re}(s^{(q)}))^2 + \right.\right.$$
$$\left.\left.(\mathrm{Im}(\sum_{i=1}^{N}z_i) - \sqrt{2E_s/N_o}\sum_{i=1}^{N}|h_i|\mathrm{Im}(s^{(q)}))^2\right]\right\}. \tag{D.9}$$

It is obvious that $\ell_{\mathrm{bf}}(x_{ki}|z) \neq \sum_{i=1}^{N}\ell_{\mathrm{unquantized}}(x_{ki}|z_i)$.

BIBLIOGRAPHY

[1] V. Cadambe and S. Jafar, "Interference alignment and spatial degrees of freedom for the k user interference channel," in *Communications, 2008. ICC '08. IEEE International Conference on*, 2008, pp. 971–975.

[2] M. Shen, A. Host-Madsen, and J. Vidal, "An improved interference alignment scheme for frequency selective channels," in *Information Theory, 2008. ISIT 2008. IEEE International Symposium on*, July 2008, pp. 559 –563.

[3] D. Kim and M. Torlak, "Interference alignment via improved subspace conditioning," in *Global Telecommunications Conference (GLOBECOM 2010), 2010 IEEE*, December 2010, pp. 1 –5.

[4] L. Dong, T. Li, and Y.-F. Huang, "Opportunistic transmission scheduling for multiuser mimo systems," in *Acoustics, Speech, and Signal Processing, 2003. Proceedings. (ICASSP '03). 2003 IEEE International Conference on*, vol. 5, April 2003, pp. V – 65–8 vol.5.

[5] Y.-W. Hong, W.-J. Huang, F.-H. Chiu, and C.-C. Kuo, "Cooperative communications in resource-constrained wireless networks," *Signal Processing Magazine, IEEE*, vol. 24, no. 3, pp. 47–57, 2007.

[6] J. N. Laneman, "Cooperative communications in mobile ad hoc networks," *IEEE Signal Processing Magazine*, vol. 1053, no. 5888/06, 2006.

[7] A. Sendonaris, E. Erkip, and B. Aazhang, "User cooperation diversity. part i. system description," *Communications, IEEE Transactions on*, vol. 51, no. 11, pp. 1927–1938, 2003.

[8] . A. Sendonaris, E. Erkip, and B. Aazhang, "User cooperation diversity. part ii. implementation aspects and performance analysis," *Communications, IEEE Transactions on*, vol. 51, no. 11, pp. 1939–1948, 2003.

[9] J. Laneman, D. Tse, and G. W. Wornell, "Cooperative diversity in wireless networks: Efficient protocols and outage behavior," *Information Theory, IEEE Transactions on*, vol. 50, no. 12, pp. 3062–3080, 2004.

[10] V. Chandrasekhar, J. Andrews, and A. Gatherer, "Femtocell networks: a survey," *Communications Magazine, IEEE*, vol. 46, no. 9, pp. 59–67, 2008.

[11] M. Catedra, J. Perez, F. Saez de Adana, and O. Gutierrez, "Efficient ray-tracing techniques for three-dimensional analyses of propagation in mobile communications: application to picocell and microcell scenarios," *Antennas and Propagation Magazine, IEEE*, vol. 40, no. 2, pp. 15–28, 1998.

[12] C.-L. I, L. Greenstein, and R. Gitlin, "A microcell/macrocell cellular architecture for low- and high-mobility wireless users," *Selected Areas in Communications, IEEE Journal on*, vol. 11, no. 6, pp. 885–891, 1993.

[13] R. Etkin, D. Tse, and H. Wang, "Gaussian interference channel capacity to within one bit: the symmetric case," in *Information Theory Workshop, 2006. ITW '06 Chengdu. IEEE*, 2006, pp. 601–605.

[14] A. Motahari and A. Khandani, "Capacity bounds for the gaussian interference channel," *Information Theory, IEEE Transactions on*, vol. 55, no. 2, pp. 620–643, 2009.

[15] G. Abhinav and B. Rajan, "Two-user gaussian interference channel with finite constellation input and fdma," in *Wireless Communications and Networking Conference (WCNC), 2011 IEEE*, 2011, pp. 25–30.

[16] J. Andrews, "Interference cancellation for cellular systems: a contemporary overview," *Wireless Communications, IEEE*, vol. 12, no. 2, pp. 19–29, 2005.

[17] M. Yavuz, F. Meshkati, S. Nanda, A. Pokhariyal, N. Johnson, B. Raghothaman, and A. Richardson, "Interference management and performance analysis of umts/hspa+ femtocells," *Communications Magazine, IEEE*, vol. 47, no. 9, pp. 102–109, 2009.

[18] D. Lopez-Perez, A. Valcarce, G. de la Roche, and J. Zhang, "Ofdma femtocells: A roadmap on interference avoidance," *Communications Magazine, IEEE*, vol. 47, no. 9, pp. 41–48, 2009.

[19] C. E. Shannon, "Two-way communication channels," in *Proc. 4th Berkeley Symp. Math. Stat. Prob*, vol. 1, 1961, pp. 611–644.

[20] H. Sato, "The capacity of the gaussian interference channel under strong interference (corresp.)," *Information Theory, IEEE Transactions on*, vol. 27, no. 6, pp. 786–788, 1981.

[21] T. Cover and A. Gamal, "Capacity theorems for the relay channel," *Information Theory, IEEE Transactions on*, vol. 25, no. 5, pp. 572–584, 1979.

[22] T. Han and K. Kobayashi, "A new achievable rate region for the interference channel," *Information Theory, IEEE Transactions on*, vol. 27, no. 1, pp. 49–60, 1981.

[23] S. Jafar, *Interference Alignment*. Now Publishers Inc, 2011.

[24] S. A. Jafar and S. Shamai, "Degrees of freedom region of the mimo x channel," *Information Theory, IEEE Transactions on*, vol. 54, no. 1, pp. 151–170, 2008.

[25] S. Peters and R. Heath, "Cooperative algorithms for mimo interference channels," *Vehicular Technology, IEEE Transactions on*, vol. 60, no. 1, pp. 206 –218, Janurary 2011.

[26] M. Medard, "The effect upon channel capacity in wireless communications of perfect and imperfect knowledge of the channel," *Information Theory, IEEE Transactions on*, vol. 46, no. 3, pp. 933–946, 2000.

[27] T. Yoo and A. Goldsmith, "Capacity of fading mimo channels with channel estimation error," in *Communications, 2004 IEEE International Conference on*, vol. 2, 2004, pp. 808–813 Vol.2.

[28] A. Lapidoth and S. Shamai, "Fading channels: how perfect need "perfect side information" be?" *Information Theory, IEEE Transactions on*, vol. 48, no. 5, pp. 1118–1134, 2002.

[29] B. Hassibi and B. Hochwald, "How much training is needed in multiple-antenna wireless links?" *Information Theory, IEEE Transactions on*, vol. 49, no. 4, pp. 951–963, 2003.

[30] C. Suh and D. Tse, "Interference alignment for cellular networks," in *Communication, Control, and Computing, 2008 46th Annual Allerton Conference on*, 2008, pp. 1037–1044.

[31] C. Suh, M. Ho, and D. Tse, "Downlink interference alignment," in *Global Telecommunications Conference (GLOBECOM 2010), 2010 IEEE*, 2010, pp. 1–5.

[32] D. G. Brennan, "Linear diversity combining techniques," *Proceedings of the IRE*, vol. 47, no. 6, pp. 1075–1102, 1959.

[33] U. Madhow, *Fundamentals of digital communication.* Cambridge University Press, 2008.

[34] F. Adachi and K. Ohno, "Ber performance of qdpsk with postdetection diversity reception in mobile radio channels," *Vehicular Technology, IEEE Transactions on*, vol. 40, no. 1, pp. 237–249, 1991.

[35] P.-Y. Kam, "Bit error probabilities mdpsk over the nonselective rayleigh fading channel with diversity reception," *Communications, IEEE Transactions on*, vol. 39, no. 2, pp. 220–224, 1991.

[36] C. Tellambura, A. Mueller, and V. Bhargawa, "Analysis of m-ary phase-shift keying with diversity reception for land-mobile satellite channels," *Vehicular Technology, IEEE Transactions on*, vol. 46, no. 4, pp. 910–922, 1997.

[37] L. Zheng and D. Tse, "Diversity and multiplexing: a fundamental tradeoff in multiple-antenna channels," *Information Theory, IEEE Transactions on*, vol. 49, no. 5, pp. 1073–1096, 2003.

[38] S. Sanayei and A. Nosratinia, "Antenna selection in mimo systems," *Communications Magazine, IEEE*, vol. 42, no. 10, pp. 68–73, 2004.

[39] P. Napier, A. Thompson, and R. Ekers, "The very large array: design and performance of a modern synthesis radio telescope," *Proceedings of the IEEE*, vol. 71, no. 11, pp. 1295–1320, 1983.

[40] A. Viterbi, A. Viterbi, K. Gilhousen, and E. Zehavi, "Soft handoff extends cdma cell coverage and increases reverse link capacity," *Selected Areas in Communications, IEEE Journal on*, vol. 12, no. 8, pp. 1281–1288, 1994.

[41] R. Narrainen and F. Takawira, "Performance analysis of soft handoff in cdma cellular networks," *Vehicular Technology, IEEE Transactions on*, vol. 50, no. 6, pp. 1507–1517, 2001.

[42] G. Kramer, M. Gastpar, and P. Gupta, "Cooperative strategies and capacity theorems for relay networks," *Information Theory, IEEE Transactions on*, vol. 51, no. 9, pp. 3037 – 3063, September 2005.

[43] E. Aktas, J. Evans, and S. Hanly, "Distributed decoding in a cellular multiple-access channel," *Wireless Communications, IEEE Transactions on*, vol. 7, no. 1, pp. 241 –250, Janurary 2008.

[44] A. Sanderovich, S. Shamai, Y. Steinberg, and G. Kramer, "Communication via decentralized processing," *Information Theory, IEEE Transactions on*, vol. 54, no. 7, pp. 3008 –3023, July 2008.

[45] I.-H. Wang and D. Tse, "Interference mitigation through limited receiver cooperation: Symmetric case," in *Information Theory Workshop, 2009. ITW 2009. IEEE*, October 2009, pp. 579 –583.

[46] S. Yi, B. Azimi-Sadjadit, S. Kalyanaraman, and V. Subramanian, "Error control code combining techniques in cluster-based cooperative wireless networks," in *Communications, 2005. ICC 2005. 2005 IEEE International Conference on*, vol. 5, May 2005, pp. 3510 – 3514 Vol. 5.

[47] S. Yi, S. Kalyanaraman, B. Azimi-Sadjadi, and H. Shen, "Energy-efficient cluster-based cooperative fec in wireless networks," *Wireless Networks*, vol. 15, no. 8, pp. 965–977, November 2009.

[48] H. Zhu, G. Giannakis, and A. Cano, "Distributed in-network channel decoding," *Signal Processing, IEEE Transactions on*, vol. 57, no. 10, pp. 3970–3983, 2009.

[49] J. Choi and S. Choi, "Cooperative and distributed receiver processing based on message passing," *Vehicular Technology, IEEE Transactions on*, vol. 60, no. 7, pp. 3066 –3075, September 2011.

[50] T. Wong, X. Li, and J. Shea, "Distributed decoding of rectangular parity-check code," *Electronics Letters*, vol. 38, no. 22, pp. 1364 – 1365, October 2002.

[51] T. Wong, X. Li, and . J. Shea, "Iterative decoding in a two-node distributed array," in *MILCOM 2002. Proceedings*, vol. 2, October 2002, pp. 1320 – 1324 vol.2.

[52] X. Li, T. Wong, and J. Shea, "Bit-interleaved rectangular parity-check coded modulation with iterative demodulation in a two-node distributed array," in *Communications, 2003. ICC '03. IEEE International Conference on*, vol. 4, May 2003, pp. 2812 – 2816 vol.4.

[53] A. Avudainayagam, J. Shea, T. Wong, and X. Li, "Reliability exchange schemes for iterative packet combining in distributed arrays," in *Wireless Communications and Networking, 2003. WCNC 2003. 2003 IEEE*, vol. 2, March 2003, pp. 832 –837 vol.2.

[54] A. Nayagam, J. Shea, and T. Wong, "Collaborative decoding in bandwidth-constrained environments," *Selected Areas in Communications, IEEE Journal on*, vol. 25, no. 2, pp. 434 –446, February 2007.

[55] X. Li, T. Wong, and J. Shea, "Performance analysis for collaborative decoding with least-reliable-bits exchange on awgn channels," *Communications, IEEE Transactions on*, vol. 56, no. 1, pp. 58 –69, January 2008.

[56] J. Choi and S. Choi "Cooperative and distributed receiver processing based on message passing," *Vehicular Technology, IEEE Transactions on*, vol. 60, no. 7, pp. 3066 –3075, September 2011.

[57] X. Liu, E. K. P. Chong, and N. Shroff, "Opportunistic transmission scheduling with resource-sharing constraints in wireless networks," *Selected Areas in Communications, IEEE Journal on*, vol. 19, no. 10, pp. 2053–2064, 2001.

[58] S. Sanayei and A. Nosratinia, "Opportunistic downlink transmission with limited feedback," *Information Theory, IEEE Transactions on*, vol. 53, no. 11, pp. 4363–4372, 2007.

[59] M. Ni and D. R. Brown III, "A performance comparison of interference alignment and opportunistic transmission with channel estimation errors."

[60] D. R. Brown III, M. Ni, U. Madhow, and P. Bidigare, "Distributed reception with coarsely-quantized observation exchanges," *Conference on Information Sciences and Systems (CISS 2013)*, March 2013.

[61] G. Boudreau, J. Panicker, N. Guo, R. Chang, N. Wang, and S. Vrzic, "Interference coordination and cancellation for 4g networks," *Communications Magazine, IEEE*, vol. 47, no. 4, pp. 74 –81, April 2009.

[62] Q. Zhang, Q. Chen, F. Yang, X. Shen, and Z. Niu, "Cooperative and opportunistic transmission for wireless ad hoc networks," *Network, IEEE*, vol. 21, no. 1, pp. 14 –20, Janurary 2007.

[63] A. Scaglione and Y.-W. Hong, "Opportunistic large arrays: cooperative transmission in wireless multihop ad hoc networks to reach far distances," *Signal Processing, IEEE Transactions on*, vol. 51, no. 8, pp. 2082–2092, 2003.

[64] A. Bletsas, H. Shin, M. Win, and A. Lippman, "Cooperative diversity with opportunistic relaying," in *Wireless Communications and Networking Conference, 2006. WCNC 2006. IEEE*, vol. 2, 2006, pp. 1034–1039.

[65] X. Liu, E. Chong, and N. Shroff, "Opportunistic transmission scheduling with resource-sharing constraints in wireless networks," *Selected Areas in Communications, IEEE Journal on*, vol. 19, no. 10, pp. 2053 –2064, October 2001.

[66] A. Vakili, M. Sharif, and B. Hassibi, "The effect of channel estimation error on the throughput of broadcast channels," in *Acoustics, Speech and Signal Processing, 2006. ICASSP 2006 Proceedings. 2006 IEEE International Conference on*, vol. 4, May 2006, p. IV.

[67] S. Liu and Y. Du, "A general closed-form solution to achieve interference alignment along spatial domain," in *Global Telecommunications Conference (GLOBECOM 2010), 2010 IEEE*, December 2010, pp. 1 –5.

[68] R. Tresch, M. Guillaud, and E. Riegler, "On the achievability of interference alignment in the k-user constant mimo interference channel," in *Statistical Signal Processing, 2009. SSP '09. IEEE/SP 15th Workshop on*, 2009, pp. 277–280.

[69] C. Yetis, T. Gou, S. Jafar, and A. Kayran, "Feasibility conditions for interference alignment," in *Global Telecommunications Conference, 2009. GLOBECOM 2009. IEEE*, 2009, pp. 1–6.

[70] C. Yetis, T. Gou, S. Jafar, and . A. Kayran, "On feasibility of interference alignment in mimo interference networks," *Signal Processing, IEEE Transactions on*, vol. 58, no. 9, pp. 4771–4782, 2010.

[71] K. Gomadam, V. Cadambe, and S. Jafar, "Approaching the capacity of wireless networks through distributed interference alignment," in *Global Telecommunications Conference, 2008. IEEE GLOBECOM 2008. IEEE*, December 2008, pp. 1 –6.

[72] S. Peters and R. Heath, "Interference alignment via alternating minimization," in *Acoustics, Speech and Signal Processing, 2009. ICASSP 2009. IEEE International Conference on*, April 2009, pp. 2445 –2448.

[73] D. Schmidt, C. Shi, R. Berry, M. Honig, and W. Utschick, "Minimum mean squared error interference alignment," in *Signals, Systems and Computers, 2009 Conference Record of the Forty-Third Asilomar Conference on*, 2009, pp. 1106–1110.

[74] K. Raj Kumar and F. Xue, "An iterative algorithm for joint signal and interference alignment," in *Information Theory Proceedings (ISIT), 2010 IEEE International Symposium on*, 2010, pp. 2293–2297.

[75] I. Santamaria, O. Gonzalez, R. Heath, and S. Peters, "Maximum sum-rate interference alignment algorithms for mimo channels," in *Global Telecommunications Conference (GLOBECOM 2010), 2010 IEEE*, 2010, pp. 1–6.

[76] D. Papailiopoulos and A. Dimakis, "Interference alignment as a rank constrained rank minimization," *Signal Processing, IEEE Transactions on*, vol. 60, no. 8, pp. 4278–4288, 2012.

[77] K. Gomadam, V. Cadambe, and S. Jafar, "A distributed numerical approach to interference alignment and applications to wireless interference networks," *Information Theory, IEEE Transactions on*, vol. 57, no. 6, pp. 3309 –3322, June 2011.

[78] R. Tresch and M. Guillaud, "Cellular interference alignment with imperfect channel knowledge," in *Communications Workshops, 2009. ICC Workshops 2009. IEEE International Conference on*, June 2009, pp. 1 –5.

[79] B. Nosrat-Makouei, J. Andrews, and R. Heath, "Mimo interference alignment over correlated channels with imperfect csi," *Signal Processing, IEEE Transactions on*, vol. 59, no. 6, pp. 2783 –2794, June 2011.

[80] S. Gollakota, S. D. Perli, and D. Katabi, "Interference alignment and cancellation," in *ACM SIGCOMM Computer Communication Review*, vol. 39, no. 4. ACM, 2009, pp. 159–170.

[81] O. El Ayach, S. Peters, and R. Heath, "Real world feasibility of interference alignment using mimo-ofdm channel measurements," in *Military Communications Conference, 2009. MILCOM 2009. IEEE*, 2009, pp. 1–6.

[82] P. Zetterberg and N. Moghadam, "An experimental investigation of simo, mimo, interference-alignment (ia) and coordinated multi-point (comp)," in *Systems, Signals and Image Processing (IWSSIP), 2012 19th International Conference on*, 2012, pp. 211–216.

[83] G. Casella and R. Berger, "Statistical inference," 2001.

[84] D. Kim and M. Torlak, "Optimization of interference alignment beamforming vectors," *Selected Areas in Communications, IEEE Journal on*, vol. 28, no. 9, pp. 1425 –1434, December 2010.

[85] M.-S. Alouini and A. Goldsmith, "Capacity of rayleigh fading channels under different adaptive transmission and diversity-combining techniques," *Vehicular Technology, IEEE Transactions on*, vol. 48, no. 4, pp. 1165–1181, 1999.

[86] T. Eng, N. Kong, and L. Milstein, "Comparison of diversity combining techniques for rayleigh-fading channels," *Communications, IEEE Transactions on*, vol. 44, no. 9, pp. 1117–1129, 1996.

[87] T. Eng and L. Ning Kong and Milstein, "Correction to "comparison of diversity combining techniques for rayleigh-fading channels"," *Communications, IEEE Transactions on*, vol. 46, no. 9, pp. 1111–, 1998.

[88] A. del Coso, U. Spagnolini, and C. Ibars, "Cooperative distributed mimo channels in wireless sensor networks," *Selected Areas in Communications, IEEE Journal on*, vol. 25, no. 2, pp. 402–414, 2007.

[89] Y. Xiao and K. Kim, "Alternative good ldpc codes for dvb-s2," in *Signal Processing, 2008. ICSP 2008. 9th International Conference on*, oct. 2008, pp. 1959 –1962.

[90] X. Huang, J. Fan, Y. Xiao, and K. Kim, "Girth 4 and low minimum weights' problems of ldpc codes in dvb-s2 and solutions," in *Wireless Communications, Networking and Mobile Computing, 2009. WiCom '09. 5th International Conference on*, sept. 2009, pp. 1 –4.

[91] I. Land, S. Huettinger, P. Hoeher, and J. Huber, "Bounds on information combining," *Information Theory, IEEE Transactions on*, vol. 51, no. 2, pp. 612–619, 2005.

[92] S. Huettinger, J. Huber, R. Johannesson, and R. Fischer, "Information processing in soft-output decoding," in *PROCEEDINGS OF THE ANNUAL ALLERTON CONFERENCE ON COMMUNICATION CONTROL AND COMPUTING*, vol. 39, no. 1. Citeseer, 2001, pp. 301–310.

[93] S. Huttinger, J. Huber, R. Fischer, and R. Johannesson, "Soft-output-decoding: Some aspects from information theory," *ITG FACHBERICHT*, pp. 81–90, 2002.

[94] J. Huber and S. Huettinger, "Information processing and combining in channel coding," in *3rd International Symposium on Turbo Codes & Related Topics*, 2003, pp. 95–102.

[95] Y. Li, S. Lee, Y. Fong, F. Pan, T.-C. Kuo, J. Park, T. Samaddar, H. Nguyen, M. Mui, K. Htoo, T. Kamei, M. Higashitani, E. Yero, G. Kwon, P. Kliza, J. Wan, T. Kaneko, H. Maejima, H. Shiga, M. Hamada, N. Fujita, K. Kanebako, E. Tarn, A. Koh, I. Lu, C. Kuo, T. Pham, J. Huynh, Q. Nguyen, H. Chibvongodze, M. Watanabe, K. Oowada, G. Shah, B. Woo, R. Gao, J. Chan, J. Lan, P. Hong, L. Peng, D. Das, D. Ghosh, V. Kalluru, S. Kulkarni, R. Cernea, S. Huynh, D. Pantelakis, C.-M. Wang, and K. Quader, "A 16gb 3b/ cell nand flash memory in 56nm with 8mb/s write rate," in *Solid-State Circuits Conference, 2008. ISSCC 2008. Digest of Technical Papers. IEEE International*, 2008, pp. 506–632.

[96] D. B. III, U. Madhow, R. W. M. Ni, and P. Bidigare, "Distributed reception with hard decision exchanges: Performance bounds," in *Asilomar Conference on Signals, Systems, and Computers (Asilomar 2013)*, November 2013.

[97] V. Kuhn, *Wireless communications over MIMO channels: applications to CDMA and multiple antenna systems.* John Wiley & Sons, 2006.

[98] B. Smith, "Instantaneous companding of quantized signals," *Bell Syst. Tech. J*, vol. 36, no. 3, pp. 653–709, 1957.

[99] J. Max, "Quantizing for minimum distortion," *Information Theory, IRE Transactions on*, vol. 6, no. 1, pp. 7–12, 1960.

[100] B. Chen and G. W. Wornell, "Quantization index modulation: a class of provably good methods for digital watermarking and information embedding," *Information Theory, IEEE Transactions on*, vol. 47, no. 4, pp. 1423–1443, 2001.

[101] R. Gray, "Vector quantization," *ASSP Magazine, IEEE*, vol. 1, no. 2, pp. 4–29, 1984.

[102] X. Shao and H. S. Cronie, "Modulation and coding for quantized channels," October 2007.

[103] J. Wang, T. Courtade, H. Shankar, and R. D. Wesel, "Soft information for ldpc decoding in flash: Mutual-information optimized quantization," in *Global Telecommunications Conference (GLOBECOM 2011), 2011 IEEE*, August 2011.

[104] V. Cadambe and S. Jafar, "Can feedback, cooperation, relays and full duplex operation increase the degrees of freedom of wireless networks?" in *Information Theory, 2008. ISIT 2008. IEEE International Symposium on*, July 2008, pp. 1263 –1267.